Diffusion along mean motion resonance in the restricted planar three-body problem

Jacques Féjoz*, Marcel Guàrdia†, Vadim Kaloshin‡ and Pablo Roldán§

September 12, 2011

Abstract

We study the dynamics of the restricted planar three-body problem near a mean motion resonance, i.e. a resonance involving the Keplerian periods of the two lighter bodies revolving around the most massive one. This problem is often used to model Sun–Jupiter–asteroid systems. For the primaries (Sun and Jupiter), we pick a realistic mass ratio $\mu = 10^{-3}$ and a small eccentricity $e_0 > 0$. The main result is a construction of a variety of diffusing orbits which show a drastic change of the osculating eccentricity of the asteroid, while the osculating semi major axis is kept almost constant. The proof relies on the careful analysis of the circular problem, which has a hyperbolic structure, but for which diffusion is prevented by KAM tori. In the proof we verify certain non-degeneracy conditions numerically.

Based on the work of Treschev, it is natural to conjecture that the time of diffusion for this problem is at least $\sim -\ln(\mu e_0)/(\mu^{3/2} e_0)$. We expect our instability mechanism to apply to realistic values of e_0 and we give heuristic arguments in its favor. If so, the applicability of Nekhoroshev theory to the three-body problem as well as the long time stability become questionable.

It is well known that, in the Asteroid Belt, located between the orbits of Mars and Jupiter, the distribution of asteroids has the so-called *Kirkwood gaps* exactly at mean motion resonances of low order. Our mechanism gives a possible explanation of their existence. To relate the existence of Kirkwood gaps with Arnold diffusion, we also state a conjecture on its existence for a typical ε-perturbation of the product of the pendulum and the rotator. Namely, we predict that a positive conditional measure of initial conditions concentrated in the main resonance exhibits Arnold diffusion on time scales $-\ln \varepsilon/\varepsilon^2$.

*Université Paris-Dauphine and Observatoire de Paris (fejoz@imcce.fr)
†University of Maryland at College Park (marcel.guardia@upc.edu)
‡University of Maryland at College Park (kaloshin@math.umd.edu)
§Universitat Politècnica de Catalunya (pablo.roldan@upc.edu)

Contents

1 Introduction and main result **3**
- 1.1 The problem of the stability of gravitating bodies . . . 3
- 1.2 Relevance in astronomy . . . 4
- 1.3 Main theorem . . . 6
- 1.4 Refinements and comments . . . 8
- 1.5 Mechanism of instability . . . 10
- 1.6 Sketch of the proof . . . 10
- 1.7 Nature of numerics . . . 13

2 Setting of and notations **13**

3 The circular problem **16**
- 3.1 Invariant cylinder . . . 16
- 3.2 The inner map . . . 19
- 3.3 Outer map . . . 19

4 The elliptic problem **23**
- 4.1 The specific form of the inner and outer maps . . . 24
- 4.2 The e_0-expansion of the elliptic Hamiltonian . . . 26
- 4.3 Perturbative analysis of the flow . . . 28
- 4.4 Perturbative analysis of an invariant cylinder and its inner map . . . 29
- 4.5 The outer map . . . 32

5 Existence of diffusing orbits **34**

A Numerical study of the hyperbolic cylinder of the circular problem. **39**
- A.1 Computation of the periodic orbits . . . 39
- A.2 Computation of invariant manifolds . . . 44
- A.3 Computation of transversal homoclinic points and splitting angle . . . 46
- A.4 Accuracy of computations . . . 50

B The resonance in Delaunay coordinates **52**
- B.1 From Cartesian to Delaunay and computation of $\partial_G \Delta H_{\mathrm{circ}}$ . . . 52

C Numerical study of the inner and outer dynamics **54**
- C.1 Inner and outer dynamics of the circular problem . . . 54
- C.2 Inner and outer dynamics of the elliptic problem . . . 57
- C.3 Comparison of the inner and outer dynamics of the elliptic problem . . . 59

D Conjectures on the speed of diffusion **60**
- D.1 Speed of diffusion for a priori unstable systems and Positive measure . . . 60
- D.2 Structure of the restricted planar elliptic three-body problem . . . 61
- D.3 The Mather accelerating problem and its speed of diffusion . . . 62
- D.4 Modified positive measure conjecture . . . 63

1 Introduction and main result

1.1 The problem of the stability of gravitating bodies

The stability of the Solar System is a longstanding problem. Over the centuries, mathematicians and astronomers have spent an inordinate amount of energy proving stronger and stronger stability theorems for dynamical systems closely related to the Solar System, generally within the frame of the Newtonian N-body problem:

$$\ddot{q}_i = \sum_{j \neq i} m_j \frac{q_j - q_i}{\|q_j - q_i\|^3}, \quad q_i \in \mathbf{R}^2, \quad i = 0, 1, ..., N-1, \tag{1}$$

and its planetary subproblem, where m_0 (thought of as that of the Sun) is much larger than the other masses m_i.

A famous theorem of Lagrange entails that the observed variations in the motion of Jupiter and Saturn come from resonant terms of large amplitude and long period, but with zero average (see [Las06] and references therein, or [AKN88, Example 6.16]). Yet it is a mistake, which Laplace made, to infer the topological stability of the planetary system, since the theorem deals only with an approximation of the first order with respect to the masses, eccentricities and inclinations of the planets [Lap89, p. 296]. Another key result is Arnold's theorem, which proves the existence of a set of positive Lebesgue measure filled by invariant tori in planetary systems, provided that the masses of the planets are small [Arn63, Féj04]. However, in the phase space the gaps left by the invariant tori leave room for instability.

It was a big surprise when the numerical computations of Sussman, Wisdom and Laskar showed that over the life span of the Sun, or even over a few million years, collisions and ejections of inner planets are probable (because of the exponential divergence of solutions, only a probabilistic result seems within the reach of numerical experiments); see for example [SW92, Las94], or [Las10] for a recent account. Our Solar System, as well as newly discovered extra-solar systems, are now widely believed to be unstable, and the general conjecture about the N-body problem is quite the opposite of what it used to be:

Conjecture 1.1 (Global instability of the N-body problem)**.** *In restriction to any energy level of the N-body problem, the non-wandering set is nowhere dense. (One can reparameterize orbits so as to have a complete flow, despite collisions.)*

According to Herman [Her98], this is the oldest open problem in dynamical systems (see also [Kol57]). This conjecture would imply that bounded orbits form a *nowhere dense set* and that no topological stability whatsoever holds, in a very strong sense. It is largely confirmed by numerical experiments. In our Solar System, Laskar for instance has shown that collisions between Mars and Venus could occur within a few billion years. The coexistence of a nowhere dense set of positive measure of bounded quasiperiodic motions with an open and dense set of initial conditions with unbounded orbits is a remarkable conjecture.

Currently the above conjecture is largely out of reach. A more modest but still much challenging goal is a local version of the conjecture:

Conjecture 1.2 (Instability of the planetary problem)**.** *If the masses of the planets are small enough, the wandering set accumulates on the set of circular, coplanar, Keplerian motions.*

There have been some prior attempts to prove such a conjecture. For instance, Moeckel discovered an instability mechanism in a special configuration of the 5-body problem [Moe96].

His proof of diffusion was limited by the so-called big gaps problem between hyperbolic invariant tori; this problem was later solved in this setting by Zheng [Zhe10]. A somewhat opposite strategy was developed by Bolotin and McKay, using the Poincaré orbits of the second species to show the existence of symbolic dynamics in the three-body problem, hence of chaotic orbits, but considering far from integrable, non-planetary conditions; see for example [Bol06]. Also, Delshams, Gidea and Roldán have shown an instability mechanism in the spatial restricted three-body problem, but only locally around the equilibrium point L_1 (see [DGR11]).

In this paper we prove the existence of large instabilities in a realistic planetary system and describe the associated instability mechanism. We thus provide a step towards the proof of Conjecture 1.2. The instability mechanism shown in this paper is related to a generalized version of the Mather mechanism [Mat96, BT99, DdlLS00, GT08, Kal03, Pif06]. Some parts of the proof rely on numerical computations, but our strategy allows us to keep these computations to the simplest and, hopefully, most convincing.

More specifically, consider the planetary problem (1), with one planet mass (say, m_1), larger than the others small masses: $m_0 \gg m_1 \gg m_2, ..., m_{N-1}$. The equations of motion of lighter objects ($i = 2, ..., N-1$) can advantageously be written as

$$\ddot{q}_i = m_0 \frac{q_0 - q_i}{\|q_0 - q_i\|^3} + m_1 \frac{q_1 - q_i}{\|q_1 - q_i\|^3} + \sum_{j \neq i, j>1} m_j \frac{q_j - q_i}{\|q_j - q_i\|^3}. \tag{2}$$

Letting the masses m_j tend to 0 for $j = 2, ..., N-1$, we obtain a collection of $(N-2)$ independent *restricted problems*:

$$\ddot{q}_i = m_0 \frac{q_0 - q_i}{\|q_0 - q_i\|^3} + m_1 \frac{q_1 - q_i}{\|q_1 - q_i\|^3}, \tag{3}$$

where the massless bodies are influenced by, without themselves influencing the *primaries* of masses m_0 and m_1.

For $N = 3$, this model is often used to approximate the dynamics of Sun-Jupiter-asteroid or other Sun-planet-object problems and it is the simplest one conjectured to have a wide range of instabilities.

1.2 Relevance in astronomy

1.2.1 The Asteroid Belt

One place in the Solar system where the dynamics is well described by the restricted three-body problem, is the Asteroid Belt. The Asteroid Belt is located between the orbits of Mars and Jupiter and consists of 1.7 million objects ranging from asteroids of 950 kilometers to dust particles. Since the mass of Jupiter is approximately 2960 masses of Mars, away from close encounters with Mars, one can neglect the influence of Mars on the asteroids and focus on the influence of Jupiter. We also omit interactions with the second biggest planet in the Solar System, namely Saturn, which actually is not so small. Indeed, its mass is about a third of the mass of Jupiter and its semi major axis is about 1.83 times the semi major axis of Jupiter. This implies that the strength of interaction with Saturn is around 10% of the strength of interaction with Jupiter. However, instabilities discussed in this paper are fairly robust and we believe that they are not destroyed by the interaction with Saturn (or other celestial bodies), which, to some degree averages out.

With these assumptions one can model the motion of the objects in the Asteroid Belt by the restricted problem. Denote by $\mu = m_1/(m_0 + m_1)$ the mass ratio, where m_0 is the mass of

the Sun and m_1 is the mass of Jupiter. For $\mu = 0$ (namely, neglecting the influence of Jupiter) bounded orbits of the asteroids are ellipses. Up to orientation the ellipses are characterized by their semi major axis a and eccentricity e.

The aforementioned theorem of Lagrange asserts that, for $\mu > 0$ small, the semi major axis $a(t)$ of an asteroid satisfies $|a(t)-a(0)| \lesssim \mu$ for all $|t| \lesssim 1/\mu$. For very small μ the time of stability was greatly improved by Niederman [Nie96] using Nekhoroshev theory (see the discussion in the next section). Nevertheless, if one looks at the asteroid distribution in terms of their semi major axis, one encounters several gaps, the so-called *Kirkwood gaps*. It is believed that the existence of these gaps is due to instability mechanisms.

1.2.2 Kirkwood gaps and Wisdom's ejection mechanism

The *mean motion resonances* appear when the ratio between the period of Jupiter and the period of the asteroid is rational. The Kirkwood gaps correspond to the ratios $3:1,\ 5:2,\ 7:3$.

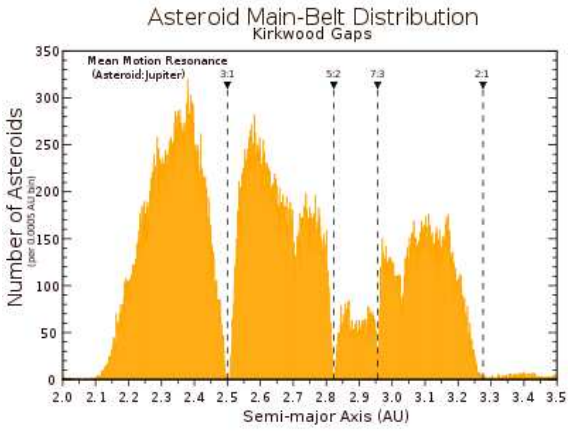

Figure 1: Kirkwood gaps

In this section we present a heuristic explanation of why these gaps exist.

It is conjectured and confirmed by numerical data [Wis82], that eccentricities of the asteroids appropriately placed in the Kirkwood gaps change by a magnitude of order of one. Notice that in the real data eccentricities of most asteroids in the Asteroid Belt are between 0 and 0.25 (see e.g. `http://en.wikipedia.org/wiki/File:Mainbeltevsa.png`).

As the eccentricity of the asteroid grows while its semi major axis is nearly constant, its perihelion gets closer and closer to the origin, namely at the distance $a(t)[1 - e(t)]$, where $a(t)$ and $e(t)$ are the semi major axis and eccentricity of the asteroid respectively (see Figure 2, where the inner circle is the orbit of Mars). In particular, a close encounter with Mars becomes increasingly probable. Eventually at some point Mars and the asteroid come close to one another and the asteroid most probably gets ejected from the Asteroid Belt.

A surprising fact is that *the change of eccentricity of the asteroid is only possible due to the ellipticity of the motion of Jupiter*, due to the following count of dimensions. For circular motions of Jupiter the problem reduces to two degrees of freedom (see Section 2) and plausibly there are invariant two-dimensional tori separating the three dimensional energy surfaces (see

e.g. [GDF$^+$89, CC07]). If the eccentricity of Jupiter is positive, the system has two and a half degrees of freedom and then KAM tori do not prevent drastic changes in the eccentricity.

Heuristically, the conclusion is that, if the eccentricity of the asteroid changes by a magnitude of order one in the Sun-Jupiter-asteroid restricted problem, then the asteroid might come into zones where the restricted problem does not describe dynamics appropriately, due to the influence of Mars.

The main result of the paper is that in a certain mean motion resonance there are unstable motions which lead to significant changes in the eccentricity. In this paper we only present results for one particular resonance, the resonance $1 : 7$, because the proof relies on numerical computations. This resonance is different from the ones in the Kirkwood gaps. It was initially chosen for reasons which turned out to be incidental (however, see the speculative remark in Section 1.4.3 about the speed of diffusion). Thus we are confident that our mechanism of instability applies to other resonances as long as the orbits of the unperturbed problem stay away from collisions. Thus, the instability mechanism showed in this paper gives an insight into the existence of the Kirkwood gaps. Another instability mechanism, using the adiabatic invariant theory, can be seen in [NS04] and applies to different ranges of mass ratio and Jupiter's eccentricity.

1.2.3 Capture in resonance of other objects

There are many known light objects in the Solar System which display a mean motion resonance of low order with Jupiter or some other planet. Some of them are: Trojan satellites (which librate around one of the two Lagrangian points of a planet, hence in $1 : 1$ mean motion resonance with the planet), Uranus (which is close to the $7 : 1$ mean motion resonance with Jupiter, thus giving an example of an "outer" restricted problem, close in phase space to the solutions we are studying), or the Kuiper Belt beyond Neptune (whose objects, behaving in the exact opposite manner to the thoses of the Asteroid Belt, seem to *concentrate* close to mean motion resonances; in particular, the Keplerian ellipse of the dwarf planet Pluto notoriously meets the ellipse of Neptune). The current existence of these resonant objects, and thus their relative stability, seemingly contradicts the above mechanism. This calls at least for a short explanation, although there are many effects at work here.

The main point is that in the eye of a resonance lies an elliptic island, where some kind of long term stability prevails. Besides, the geometry often prevents the ejection mechanism described in Section 1.2.2 to occur in a straightforward manner (or to lead to a spectacular ejection), because there is no such body as Mars to kick the asteroid through a close encounter. In many cases, the mean motion resonance itself precludes collisions with the main planet (e.g. for Trojan asteroids with respect to Jupiter, obviously, or for Pluto with respect to Neptune; for a discussion of this effect in the Asteroid Belt, see [Rob05]). One should add that the complete picture certainly includes secular resonances, close encounters between asteroids themselves, as well as more complicated kinds of resonance involving sometimes more bodies (e.g. the second Kirkwood gap, where a four-body problem resonance seems to play a crucial role). We refer to [Mor02, Rob05] for further astronomical details.

1.3 Main theorem

Let us consider the three-body problem and let us assume that the massless body moves in the same plane as the pair of primaries. Normalize the total mass to one and call the three bodies

the Sun (mass $1-\mu$), Jupiter (mass $0<\mu\ll 1$) and the asteroid (zero mass). If the energy of the primaries is negative, their orbits describe two ellipses with the same eccentricity, say $e_0 \geq 0$. For the sake of later simplicity, we will change notations here, as we will denote by $q_0(t)$ the normalized position of the primaries ("fictitious body"), so that the Sun and Jupiter have respective positions $-\mu q_0(t)$ and $(1-\mu)q_0(t)$. The Hamiltonian of the asteroid is

$$K(q,p,t) = \frac{\|p\|^2}{2} - \frac{1-\mu}{\|q+\mu q_0(t)\|} - \frac{\mu}{\|q-(1-\mu)q_0(t)\|} \tag{4}$$

where $q,p \in \mathbb{R}^2$. Without loss of generality one can assume that $q_0(t)$ has semi major axis equal to 1 and period 2π. For $e_0 \geq 0$ this system has two and a half degrees of freedom.

When $e_0 = 0$, the primaries describe uniform circular motions aroung their center of mass (restricted planar circular three-body problem). Hence, in a frame rotating with the primaries, the system becomes autonomous and thus has only 2 degrees of freedom. Its energy in the rotating frame is a first integral, called *the Jacobi constant*. It is defined by

$$J = \frac{\|p\|^2}{2} - \frac{1-\mu}{\|q+\mu q_0(t)\|} - \frac{\mu}{\|q-(1-\mu)q_0(t)\|} - \frac{\|q\|^2}{2}. \tag{5}$$

The aforementioned KAM theory applies to both the circular and the elliptic problems [Arn63, SM95] and asserts that if the mass of Jupiter is small enough, there is a set of initial conditions of positive Lebesgue measure leading to quasiperiodic motions, in the neighborhood of circular motions of the asteroid.

If Jupiter has a circular motion, since the system has only 2 degrees of freedom, KAM invariant tori are 2-dimensional and separate the 3-dimensional energy surfaces. But in the elliptic problem, 3-dimensional KAM tori do not prevent orbits to wander on a 5-dimensional phase space. In this paper we prove the existence of a wide enough set of wandering orbits in the elliptic planar restricted three-body problem.

Let us write the Hamiltonian (4) as

$$K(q,p,t) = K_0(q,p) + K_1(q,p,t,\mu)$$

with

$$\begin{aligned} K_0(q,p) &= \frac{\|p\|^2}{2} - \frac{1}{\|q\|} \\ K_1(q,p,t,\mu) &= \frac{1}{\|q\|} - \frac{1-\mu}{\|q+\mu q_0(t)\|} - \frac{\mu}{\|q-(1-\mu)q_0(t)\|}. \end{aligned}$$

One can see that $K_1 = \mathcal{O}(\mu)$ uniformly away from collisions. Then, notice that there is a competition between the integrability K_0 and the non-integrability K_1, without which there would be no wandering. In this present work we consider a realistic value of the mass ratio, $\mu = 10^{-3}$. For brevity in what follows we abbreviate *the restricted planar circular (resp. elliptic) three-body problem to the circular (resp. elliptic) problem.*

Here is the main result of this paper.

Theorem 1. *Let us consider the elliptic problem with mass ratio $\mu = 10^{-3}$ and the eccentricity of Jupiter $e_0 > 0$. Then, for e_0 small enough, there exist $T > 0$ and a trajectory whose eccentricity $e(t)$ satisfies that*

$$e(0) < 0.48 \quad \text{and} \quad e(T) > 0.67.$$

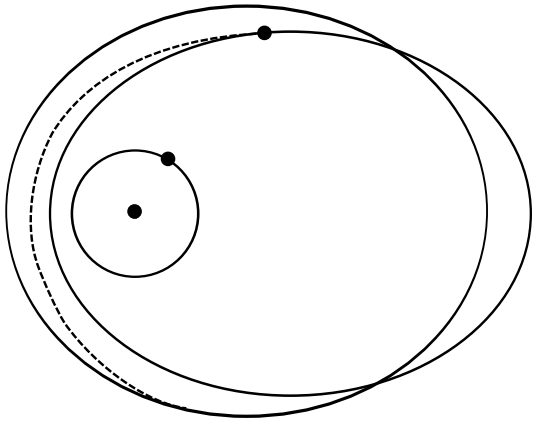

Figure 2: Transition from the instant ellipse of eccentricty $e = 0.48$ to the ellipse of eccentricty $e = 0.67$. The dashed line schematically shows the transition. Nevertheless, the actual diffusing orbit is very complicated and diffusion is very slow.

There is a more precise result, which is more difficult to state at this stage (see Theorem 2). Let us say that along the above trajectory, the semi major axis $a(t)$ remains almost constant, and, more precisely,

$$\left| a(t) - 7^{2/3} \right| \leq 14\mu \quad \text{for } t \in [0, T],$$

and that

$$|J(T) - J(0)| > 0.1,$$

where J is the Jacobi constant defined in (5). Now we discuss the main result from different perspectives.

1.4 Refinements and comments

1.4.1 Smallness of the eccentricity of Jupiter

When Jupiter describes a circular motion, the Jacobi constant is an integral of motion and then KAM theory prevents global instabilities. We consider the eccentricity e_0 as a small parameter so that we can compare the dynamics of the elliptic problem with the dynamics of the circular one.

It turns out that the difference between the elliptic and circular Hamiltonians is $\mathcal{O}(\mu e_0)$. The analysis of the difference, performed later in the paper (see Section 4.2), shows that using averaging one can reduce the difference to $\mathcal{O}(\mu e_0^5)$ (or even smaller). This makes us believe that e_0 should not be infinitesimally small for our mechanism to work. Even the actual value $e_0 \approx 0.048$ is not out of question. However, having realistic e_0, to a large extend, becomes a matter of numerical experiment, not of mathematical proof –it is the limit and the interest of perturbation theory, to describe some dynamical behavior in terms of asymptotic models. See Appendix D.2 for more details.

1.4.2 On infinitesimally small μ's

In Theorem 1, we do not know what would happen asymptotically if we let $\mu \to 0$ (our estimates worsen). Indeed, one of the crucial steps of the proof is to study the transversality of certain invariant manifolds (see Section 1.6) and this transversality becomes exponentially small with respect to μ as $\mu \to 0$. On the other hand, Theorem 1 holds for realistic values of μ, which is out of reach of many qualitative results of perturbation theory where parameters are conveniently assumed to be as small as needed. See Appendix D for more details.

1.4.3 Speed of diffusion

In Appendix D we discuss the relation of this problem with a priori unstable systems and the Mather accelerating problem. This leads us to conjecture that, for orbits constructed in this paper, the diffusion time T can be chosen

$$T \sim -\frac{\ln(\mu e_0)}{\mu^{3/2} e_0}. \tag{6}$$

De la Llave [dlL04], Gelfreich-Turaev [GT08], and Piftankin [Pif06], using Treschev's techniques of separatrix maps (see e.g. [PT07]), proved linear diffusion for the Mather acceleration problem. This might lead to possibility of linear diffusion after a smart choice of diffusing orbits, i.e. $T \sim -\ln \mu (\mu^{3/2} e_0)^{-1}$ (see Appendix D for more details) [1].

We emphasize that an analytic proof might well require restrictive conditions between μ and e_0. However, for realistic values of μ and e_0 or smaller, i.e. $0 < \mu \leq 10^{-3}$ and $0 < e_0 < 0.048$, we expect that the speed of our mechanism of diffusion should also obey the above heuristic formula.

On the other hand, the above asymptotics for the speed of diffusion probably does not hold in the neighborhood of circular motions of the masless body, which might be much more stable than more eccentric motions. This fact could give an explanation of the fact that Uranus, whose eccentricity of 0.04 is significantly smaller than most asteriods from the asteriod belt, and which is roughly in 7 : 1-resonance with Jupiter (its period is 7.11 times larger than that of Jupiter) has not been expelled yet (see also Section 1.2.3). However, a deeper analysis would require to compare the distances of the various celestial bodies to the mean motion resonance, as well as the splitting of their invariant manifolds.

1.4.4 On Nekhoroshev's stability

Consider an analytic nearly integrable system of the form $H_\varepsilon(\theta, I) = H_0(I) + \varepsilon H_1(\theta, I)$ with $\theta \in \mathbb{T}^n$ and I in the unit ball B^n. Suppose H_0 is *convex* (or even weaker so-called *steep*). [2] Then a famous result of Nekhoroshev (see e.g. [Nie96] for the history and precise references and [Xue10] for the estimate on the involved constant c) states that for some $c > 0$ independent of ε we have

$$|I(t) - I(0)| \lesssim \varepsilon^{1/2n} \qquad \text{for} \qquad |t| \lesssim \exp(c\,\varepsilon^{-1/2n}).$$

Niederman [Nie96] applied Nekhoroshev theory to the planetary N-body problem. He showed that the semi major axis obey the above estimate for exponentially long time $\exp(c\,\varepsilon^{-1/2n})$ with ε

[1] This does not seem crucial, since the real value e_0 is not smaller than μ

[2] Recall that H_0 is called *steep* if for any affine subspace L of $\mathbb{R}^n$ the restriction $H_0|_L$ has only isolated critical points

being the smallness of the planetary masses. However, the constant c along with other constants involved in the proof are not so good. In particular, in order to have stability time comparable to the age of the Solar system ε needs to be $3 \cdot 10^{-24}$. Moreover, having stability of semi major axis does not provide stability of the eccentricity, which we claim can have substantial deviations in polynomially long time.

With $\varepsilon \sim \mu$, there was a hope that this result could be applied to long stability of e.g. the Sun-Jupiter-Saturn system (see e.g. [GG85]). However, (6) indicates absence of even $\mathcal{O}(\varepsilon^{-2})$-stability. Indeed, the unperturbed Hamiltonian of the three body problem is neither convex, nor steep. This turns out to be not only a technical problem but a true obstruction to exponentially long stability, since Nekhoroshev's theory does not to apply to this kind of systems. See Appendix D for more details.

1.5 Mechanism of instability

The result obtained in Theorem 1 gives an example of large instability for this mechanical system. It can be interpreted as an example of Arnold diffusion (see [Arn64]). Nevertheless, Arnold diffusion usually refers to nearly integrable systems whereas Hamiltonian (4) cannot be considered as close to integrable since $\mu = 10^{-3}$ is fixed. The mechanism of diffusion used in this paper is somewhat similar to the so-called Mather accelerating problem ([Mat96, BT99, DdlLS00, GT08, Kal03, Pif06]). This analogy will be specified in Section 3.3.

Arguably, the main source of the existence of instabilities are *resonances*. One of the most natural resonances in the elliptic problem (even a three-body problem) are the *mean motion orbital resonances*[3]. Along such a resonance, Jupiter and the asteroid will regularly be in the same relative position. Over a long time interval, Jupiter's influence could thus a priori pile up and, despite its small amplitude due to the small mass of Jupiter, could modify the eccentricity of the asteroid, instead of averaging out. According to Kepler's third Law, these resonances take place when $a^{3/2}$ is close to a rational, where a is the semi major axis of instant ellipse of the asteroid. In our case we consider $a^{3/2}$ *close to 7*. Nevertheless, one should expect that the same mechanism takes place for a large number of mean motion orbital resonances.

The semi major axis a and the eccentricity e describe completely an instant ellipse of the asteroid (up to orientation). Therefore, geometrically Theorem 1 says that the asteroid evolves from a Keplerian ellipse of eccentricity $e = 0.48$ to one of eccentricity $e = 0.67$, without changing much its semi major axis (see Figure 2). In Figure 3 we consider the plane (a, e), which describes the ellipse of the asteroid. Then diffusing orbits given by Theorem 1 correspond to a nearly horizontal line.

A qualitative description of such a diffusing orbit is outlined at the end of section 5.

1.6 Sketch of the proof

The diffusing orbit of the elliptic problem we are looking for lies in a neighborhood of a (3-dimensional) normally hyperbolic invariant cylinder Λ and its local invariant manifolds, which exist near our mean motion resonance. The vertical component of the cylinder can be parameterized by the eccentricity of the asteroid and the horizontal ones by its mean longitude and time.

[3]The mean motions are the frequencies of the Keplerian revolution of Jupiter and the asteroid around the Sun: in our case the asteroid makes one full revolution while Jupiter makes seven revolutions.

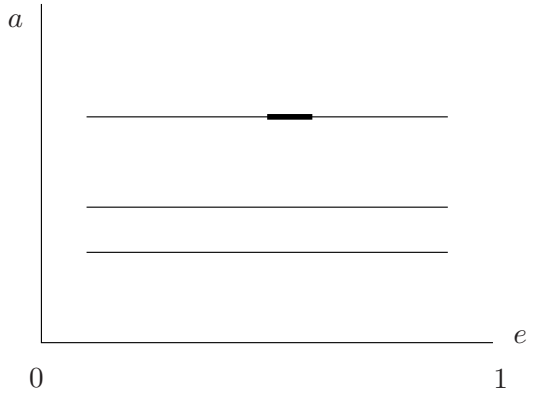

Figure 3: In this graphic we show the diffusion path that we study in the (a, e) plane. The horizontal lines represent the resonances along which we drift. The thicker line is the diffusion path whose existence we are able to prove in this paper.

If the stable and unstable invariant manifolds of Λ intersect transversally, the elliptic problem induces two different dynamics on the cylinder (see Sections 4.4 and 4.5): *the inner and the outer ones*. The inner dynamics is simply the restriction of the Newtonian flow to Λ. The outer dynamics is obtained by a limiting process: it can be observed asymptotically by starting very close to the cylinder and to its unstable manifold, traveling all the way up to a homoclinic intersection, and coming back close to the cylinder and along its stable manifold. Since the system has different homoclinic orbits to the cylinder, one can define several different outer dynamics. In our diffusing mechanism we use two different outer maps. The reason is that each of the outer maps are not defined in the whole cylinder and then we need the two of them to achieve diffusion (see Section 3).

The proof consists in the following four steps:

1. Prove existence of the normally hyperbolic invariant cylinder Λ.
2. Establish transversality of the stable and unstable invariant manifolds of this cylinder.
3. Compare the inner and outer dynamics on Λ and, in particular, check that they do not have common invariant circles.
4. Construct diffusing orbits by shadowing a carefully chosen composition of the outer and inner maps.

This program faces difficulties at every step.

1.6.1 Existence of a normally hyperbolic invariant cylinder Λ

The first difficulty comes from the proper degeneracy of the Newtonian potential: at the limit $\mu = 0$ (no Jupiter), the asteroid has a one-frequency, Keplerian motion, whereas symplectic geometry would allow for a three-frequency motion (as with any potential other than the Newtonian potential $1/r$ and the elastic potential r^2). Due to this degeneracy, switching to $\mu > 0$ (even with $e_0 = 0$) is a singular perturbation.

1.6.2 Transversality of invariant manifolds

The second step, establishing the transversality of the invariant manifolds of Λ, even for $e_0 = 0$, is a delicate problem. Asymptotically when $\mu \ll 1$, the difference (splitting) between the invariant manifolds becomes exponentially small with respect to μ, that is of order $\exp(-c/\sqrt{\mu})$ for some constant $c > 0$. Despite inordinate efforts of specialists, all the known techniques fail to estimate this splitting, because the relevant Poincaré-Melnikov integral is not algebraic. Note that this step simplifies dramatically when people study generic systems.

At the expense of creating other difficulties, setting $\mu = 10^{-3}$ avoids this splitting problem, since for this value of the parameter one can see that the splitting of separatrices is not extremely small and therefore, can be detected by means of a computer with convincing accuracy. Besides, $\mu = 10^{-3}$ is a realistic value of the mass ratio for the Sun-Jupiter model. Since the splitting of the separatrices varies smoothly with respect to the eccentricity e_0 of the primaries, it suffices to estimate the splitting numerically for $e_0 = 0$, i.e. in the circular problem. *This is a key point for the numerical computation*, which thus remains relatively simple. On the other hand, in the following two steps it will be crucial to have $e_0 > 0$, without which the KAM tori would separate energy levels.

Finally, recall that the cylinder Λ has two branches of both stable and unstable invariant manifolds. In certain regions the intersections between one of the branches of the stable and unstable invariant manifolds is tangential, which does not allow to define the outer map. Nevertheless, then one can check that the other two branches intersect transversally so that we can define a different outer map. Thus, we will combine the two outer maps depending which branches of the invariant manifolds intersect transversally.

1.6.3 Asymptotic formulas for the outer and inner maps

Now we turn to the third step. Using classical perturbation theory and the specific properties of the underlying system one can reduce the inner and (the two different) outer dynamics to three two-dimensional symplectic smooth maps of the form

$$\mathcal{F}^{\text{in}}_{e_0} : \begin{pmatrix} I \\ t \end{pmatrix} \mapsto \begin{pmatrix} I + e_0 \left(A^+(I,\mu) e^{it} + A^-(I,\mu) e^{-it} \right) + \mathcal{O}\left(\mu e_0^2\right) \\ t + \mu \mathcal{T}_0(I,\mu) + \mathcal{O}(\mu e_0) \end{pmatrix} \tag{7}$$

and

$$\mathcal{F}^{\text{out},*}_{e_0} : \begin{pmatrix} I \\ t \end{pmatrix} \mapsto \begin{pmatrix} I + e_0 \left(B^{*,+}(I,\mu) e^{it} + B^{*,-}(I,\mu) e^{-it} \right) + \mathcal{O}\left(\mu e_0^2\right) \\ t + \mu \omega^*(I,\mu) + \mathcal{O}(\mu e_0) \end{pmatrix}, \quad * = \text{f}, \text{b}, \tag{8}$$

where (I, t) are conjugate variables which parameterize a certain connected component of the 3-dimensional normally hyperbolic invariant cylinder Λ intersected with a certain transversal Poincaré section and $A^{\pm}, \mathcal{T}_0, B^{*,\pm}, \omega^*$ are smooth functions. The superindexes f and b stand for the forward and backward heteroclinic orbits that are used to define the outer maps. The choice of this notation will be clear later on in Section 3. Note that these maps are real and therefore A^- and $B^{*,-}$ are complex conjugate to A^+ and $B^{*,+}$ respectively.

1.6.4 Non-degeneracy implies the existence of diffusing orbits

As we will see in Section 5, the existence of diffusing orbits can be established provided the smooth functions

$$\mathcal{K}^{*,+}(I,\mu) = B^{*,+}(I,\mu) - \frac{e^{i\mu\omega^*(I,\mu)} - 1}{e^{i\mu\mathcal{T}_0(I,\mu)} - 1} A^+(I,\mu) \quad * = \text{f}, \text{b} \tag{9}$$

do not vanish for all $I \in [I_-, I_+]$ for which the corresponding outer map is defined. Since $A^{\pm}$ and $B^{*,\pm}$ are complex conjugate, we do not write the complex conjugate $\mathcal{K}^{*,-}(I,\mu)$. Numerically, one can check that $\mathcal{K}^{*,+}(I,\mu) \neq 0$ in their domain of definition. It turns out that $\mathcal{K}^{*,+}(I,\mu) \neq 0$ implies absence of common invariant curves for the inner and outer maps. This reduces the proof of Theorem 1 to shadowing, made in step 4, and thus it leads to the existence of diffusing orbits. Moreover, it turns out that for this problem *no large gaps* appear. This fact is not so surprising taking into account that the elliptic problem has three time scales.

Finally, let us point out that the complex functions $\mathcal{K}^{*,+}(I,\mu)$ can be regarded as a 2-dimensional real-valued function depending smoothly on (I,μ). If the dependence in μ is non-trivial, a complex valued function $\mathcal{K}^{*,+}(I,\mu)$ does not vanish at any point of their domain of definition except for a finite number of μ's.

1.7 Nature of numerics

In this section we outline which parts of the mechanism are based on numerics.

- On each 3-dimensional energy surface the circular problem has a well-defined Poincaré map $F_J : \Sigma_J \to \Sigma_J$ of a 2-dimensional cylinder Σ_J for a range of J's. For each J in some interval $[J_-, J_+]$ we establish the existence of a saddle periodic orbit $F_J^7(p_J) = p_J$.
- We show that for all $J \in [J_-, J_+]$ we have two intersections of $W^s(p_J)$ and $W^u(p_J)$. Each intersection is transversal for almost all values of J, but it becomes tangent at an exceptional (discrete) set of J's. Nevertheless, we check that at least one of the two intersections is transversal for each $J \in [J_-, J_+]$. See figure 15.
- Each transversal intersection q_J gives rise to a homoclinic orbit, denoted γ_J. For each $J \in [J_-, J_+]$ we compute several Melnikov integrals of certain quantities related to ΔH_{ell} along γ_J and p_J. Out of these integrals we compute the leading terms of the dynamics of the elliptic problem and verify a necessary condition for diffusion.

As seen in the Appendixes A-C, the numerical values that we deal with are several orders of magnitude larger than the estimated error of our computations, and therefore these computations are reliable. Moreover, all the computations that we handle are standard and low-dimensional.

2 Setting of and notations

The model of the Sun, Jupiter and a massless asteroid in Cartesian coordinates is given by the Hamiltonian (4). First, let us consider the case $\mu = 0$, that is, we consider Jupiter with zero mass. In that case, Jupiter and the asteroid do not make influence on each other and therefore the system is reduced to two uncoupled 2-body problems, the Sun-Jupiter and the Sun-asteroid, which are integrable.

We want to study the existence of instability in one particular resonance of this system, which appears when the period of the asteroid is seven times the period of Jupiter. One can consider the so-called Delaunay variables, which we denote by $(\ell, L, \hat{g}, G)$, which are angle-action coordinates of the Sun-asteroid system. The variable ℓ is the mean anomaly, L is the square of the semi major axis, $\hat{g}$ is the argument of the perihelion and G is the angular momentum. These variables can be obtained from the Cartesian coordinates as follows (see [AKN88] for more

details and background, or [Féj10, Appendix] for a straightforward definition). First define polar coordinates for the position:

$$q = (r\cos\phi, r\sin\phi).$$

Then, the actions of the Delaunay coordinates are defined by

$$-\frac{1}{2L^2} = \frac{\|p\|^2}{2} - \frac{1}{\|q\|} \tag{10}$$

$$G = -J - \frac{1}{2L^2} \tag{11}$$

(recall that $\mu = 0$ for these definitions). Using these actions, the eccentricity of the asteroid can be expressed as

$$e = \sqrt{1 - \frac{G^2}{L^2}}. \tag{12}$$

To define the angles, let v and $\hat{g}$ be the true anomaly and the argument of the perihelion, so that

$$\phi = v + \hat{g}. \tag{13}$$

Then, from v one can obtain the eccentric anomaly u using

$$\tan\frac{v}{2} = \sqrt{\frac{1+e}{1-e}}\tan\frac{u}{2}. \tag{14}$$

From the eccentric anomaly, the mean anomaly is given by Kepler's equation

$$u - e\sin u = \ell. \tag{15}$$

In Delaunay coordinates, the Hamiltonian (4) can be split into the Keplerian part $-1/2L^2$, the circular part of the perturbing function $\mu\Delta H_{circ}$ and the remainder which vanishes when $e_0 = 0$:

$$\hat{H}(L,\ell,G,\hat{g}-t,t) = -\frac{1}{2L^2} + \mu\Delta H_{\text{circ}}(L,\ell,G,\hat{g}-t,\mu) + \mu e_0\Delta H_{\text{ell}}(L,\ell,G,\hat{g}-t,t,\mu,e_0). \tag{16}$$

For $e_0 = 0$, the circular problem only depends on $\hat{g} - t$. To simplify the comparison with the circular problem, we consider rotating Delaunay coordinates, in which ΔH_{circ} is autonomous. Define the new angle $g = \hat{g} - t$ (the argument of the pericenter, measured in the rotating frame) and a new variable I conjugate to time t. Then, we have

$$H(L,\ell,G,g,I,t) = -\frac{1}{2L^2} - G + \mu\Delta H_{\text{circ}}(L,\ell,G,g,\mu) + \mu e_0\Delta H_{\text{ell}}(L,\ell,G,g,t,\mu,e_0) + I. \tag{17}$$

In these new variables, the difference of number of degrees of freedom of the elliptic and circular problems becomes more apparent. When $e_0 = 0$ the system is autonomous and then I is constant, which corresponds to the conservation of the Jacobi constant (5). Therefore, the circular problem reduces to 2 degrees of freedom. Moreover, it will later be crucial to see the circular problem as an approximation of the elliptic one, in order to reduce the Herculean (and more doubtful) numerical computations of a direct approach to the corresponding lower dimensional, and thus simpler, computations of the circular problem.

Recall that we consider the $1:7$ mean motion orbit resonance between Jupiter and the asteroid. That is, the period of the asteroid being approximately seven times the period of Jupiter. In rotating Delaunay variables, this corresponds to

$$\dot{\ell} \sim \frac{1}{7} \quad \text{and} \quad \dot{g} \sim -1. \tag{18}$$

A nearby resonance is

$$\dot{\ell} \sim \frac{1}{7} \quad \text{and} \quad \dot{t} \sim 1,$$

but we will stick to the previous one.

The resonance takes place when $L \sim 7^{1/3}$. We will study the dynamics in a large neighborhood of this resonance and we will see that one can drift along it. Namely, we will find trajectories that keep L close to $7^{1/3}$ while the G-component changes noticeably. Using (12), one can see that e also changes by an order of one. In this setting, Theorem 1 can be rephrased as follows.

Theorem 2. *There exist $e_0^* > 0$ such that for $0 < e_0 < e_0^*$, there exist $T > 0$ and an orbit of the Hamiltonian System with Hamiltonian* (17) *which satisfies*

$$G(0) < G_0 \text{ and } G(T) > G_1$$

whereas

$$\left| L(t) - 7^{1/3} \right| \leq 7\mu,$$

By definition the Hamiltonian (17) is autonomous and thus preserved. Therefore, we will restrict ourselves to a level of energy which, without loss of generality, can be taken as $H = 0$. Therefore, since $|I - G| = \mathcal{O}(\mu)$, for orbits satisfying $\left|L(t) - 7^{1/3}\right| \leq 7\mu$, drift in G is equivalent to drift in I.

The proof of this theorem is structured as follows.

In Section 3, we study the dynamics in the circular problem, that is $e_0 = 0$ and the underlying Hamiltonian (17) becomes

$$H_{\text{circ}}(L, \ell, G, g) = -\frac{1}{2L^2} - G + \mu \Delta H_{\text{circ}}(L, \ell, G, g, \mu). \tag{19}$$

Theorem 3 says that for an interval of Jacobi energies $[J_-, J_+]$ the circular problem has a smooth family of hyperbolic periodic orbits λ_J, whose stable and unstable manifolds intersect transversally for each $J \in [J_-, J_+]$. This theorem implies (Corollary 3.1) existence of a normally hyperbolic invariant cylinder. Later in the section (Subsections 3.2 and 3.3) we calculate the aforementioned outer and inner maps for the circular problem (see (7) and (8)).

Then in Section 4 we consider the elliptic case $e_0 > 0$ as a perturbation of the circular case.

Theorem 4 says that the family of periodic orbits $\{\lambda_J\}_{J \in [J_-.J_+]}$ give rise to a normally hyperbolic invariant cylinder Λ_{e_0} whose stable and unstable manifolds intersect transversally for each $J \in [J_- + \delta, J_+ - \delta]$ with small $\delta > 0$. These objects give rise to the inner and outer maps for the elliptic problem. *Theorem* 5 provides expansions for the inner and outer maps (see formulas (46) and (49) respectively).

Finally, in Section 5 in *Theorem* 6 we complete the proof of Theorem 2. This is done by comparing the inner and the two outer maps in Lemma 5.2 and constructing a transition chain of tori. It turns out that there are **no large gaps**, due to the specific structure of times scales and the Fourier series involved. This a priori contrasts with the typical situation of dynamics near a resonance (see e.g. [DdlLS06]).

Notation 2.1. *From now on, we will omit the dependence on μ (keeping in mind at various points the question of what would happen if we let μ vary). Recall that we are taking a realistic value of $\mu = 10^{-3}$.*

3 The circular problem

3.1 Invariant cylinder

The circular problem is given by the Hamiltonian (17) with $e_0 = 0$. Since it does not depend on t, I is an integral of motion. Moreover, since we are studying the dynamics in the energy surface $H = 0$, we have $I = -H_{\text{circ}}(\ell, L, g, G)$. Therefore, the variable I equals the opposite of the Jacobi constant (5). For each level $I =$ constant, one can study the dynamics close to the resonance $7\dot{\ell} + \dot{g} \sim 0$. Since t is a cyclic variable, one can consider the two degree of freedom Hamiltonian of the circular problem for which the conservation of energy corresponds to the conservation of the Jacobi constant (5). Moreover, one can see that the circular problem is reversible with respect to the involution

$$\Psi(L, \ell, G, g, I, t) = (L, -\ell, G, -g, I, -t). \tag{20}$$

This symmetry will facilitate several numerical computations.

Theorem 3. *Consider the Hamiltonian* (19) *with $\mu = 10^{-3}$. Then, in each energy level $J \in [J_-, J_+] = [-1.81, -1.56]$, there exists a hyperbolic periodic orbit $\lambda_J = (L_J(t), \ell_J(t), G_J(t), g_J(t))$ of period T_J which satisfies*

$$|T_J - 14\pi| < 60\mu,$$

and is smooth with respect to J, and

$$\left| L_J(t) - 7^{1/3} \right| < 7\mu$$

for all $t \in \mathbb{R}$.

Each λ_J has two branches of stable and unstable invariant manifolds $W^{s,j}(\lambda_J)$ and $W^{u,j}(\lambda_J)$, $j = 1, 2$. Then, for each $J \in [J_-, J_+]$ either $W^{s,1}(\lambda_J)$ and $W^{u,1}(\lambda_J)$ or $W^{s,2}(\lambda_J)$ and $W^{u,2}(\lambda_J)$ intersect transversally.

Proof. Based on convincing numerical data. See Appendix A. □

We will study the elliptic problem as a perturbation of the circular one. Therefore we do not reduce the dimension of the phase space while studying the inner and outer dynamics of the circular problem. Namely, we consider the *Extended Circular Problem* given by the Hamiltonian (17) with $e_0 = 0$. In other words, we keep the conjugate variables (I, t) even if t is a cyclic variable. Consider the energy level $H = 0$. In this setting the conservation of the Jacobi constant corresponds to the conservation of I. Therefore, the periodic orbits obtained in Theorem 3 become invariant two-dimensional tori which belong to hyperplanes $I =$ constant for any

$$I \in [I_-, I_+] = [-J_+, -J_-] = [1.56, 1.81]. \tag{21}$$

Moreover, the union of these 2-dimensional invariant tori form a normally hyperbolic invariant 3-dimensional manifold.

Corollary 3.1. *The Hamiltonian* (17) *with* $\mu = 10^{-3}$ *and* $e_0 = 0$ *has an analytic normally hyperbolic invariant* 3*-dimensional manifold* Λ_0*, which is foliated by two-dimensional invariant tori.*

Moreover, Λ_0 *has two branches of stable and unstable invariant manifolds, which we call* $W^{s,j}(\Lambda_0)$ *and* $W^{u,j}(\Lambda_0)$*,* $j = 1, 2$*. Then, in the invariant planes* $I =$ *constant, for each* $I \in [I_-, I_+]$ *either* $W^{s,1}(\Lambda_0)$ *and* $W^{u,1}(\Lambda_0)$ *or* $W^{s,2}(\Lambda_0)$ *and* $W^{u,2}(\Lambda_0)$ *intersect transversally.*

It follows from the implicit function theorem applied with the energy as a parameter (the nondegeneracy of the hyperbolic periodic orbits being observed numerically) that the cylinder Λ_0 is analytic.

We define a global Poincaré section and deal with maps to reduce the dimension by one. There are two natural choices: $\{t = 0\}$ and $\{g = 0\}$, since both variables satisfy $\dot{t} \neq 0$ and $\dot{g} \neq 0$. We choose the section $\{g = 0\}$ and call

$$\mathcal{P}_0 : \{g = 0\} \longrightarrow \{g = 0\} \tag{22}$$

this Poincaré map. Since we are studying the resonance (18), the intersection of the cylinder Λ_0 with the section $\{g = 0\}$ is formed by seven cylinders (see Figure 4). We denote them by $\widetilde{\Lambda}_0^j$, $j = 0, \ldots, 6$. Namely,

$$\Lambda_0 \cap \{g = 0\} = \widetilde{\Lambda}_0 = \bigcup_{j=0}^{6} \widetilde{\Lambda}_0^j. \tag{23}$$

As a whole $\cup_{j=0}^{6} \widetilde{\Lambda}_0^j$ is a normally hyperbolic invariant manifold for the Poincaré map $\mathcal{P}_0$. One can also consider the Poincaré map $\mathcal{P}_0^7$, namely iterate seven times $\mathcal{P}_0$. Then, for this map, each $\widetilde{\Lambda}_0^j$ is a normally hyperbolic invariant manifold (of course, their union is also a normally hyperbolic invariant manifold for $\mathcal{P}_0^7$). We work with the cylinders $\widetilde{\Lambda}_0^j$ since they have the advantage of having a natural system of coordinates. This system of coordinates will be used later on to study the inner and outer dynamics on them. In particular, we will work with $\widetilde{\Lambda}_0^3$ and $\widetilde{\Lambda}_0^4$. The reason is that in each invariant plane $I =$ constant they are connected by at least one heteroclinic connection (of $\mathcal{P}_0^7$) which is symmetric with respect to the involution (20). We call it a forward heteroclinic orbit if it is asymptotic to $\widetilde{\Lambda}_0^3$ in the past and $\widetilde{\Lambda}_0^4$ in the future and a backward heteroclinic orbit if it is asymptotic to $\widetilde{\Lambda}_0^4$ in the past and to $\widetilde{\Lambda}_0^3$ in the future. We denote by $\mathcal{D}^{\mathrm{f}} \subset [I_-, I_+]$, where f stands for forward, the subset of $[I_-, I_+]$ where $W^u(\widetilde{\Lambda}_0^3)$ and $W^s(\widetilde{\Lambda}_0^4)$ intersect transversally and by $\mathcal{D}^{\mathrm{b}} \subset [I_-, I_+]$, where b stands for backward, the subset of $[I_-, I_+]$ where $W^s(\widetilde{\Lambda}_0^3)$ and $W^u(\widetilde{\Lambda}_0^4)$ intersect transversally. By Corollary 3.1 we have that $\mathcal{D}^{\mathrm{f}} \cup \mathcal{D}^{\mathrm{b}} = [I_-, I_+]$.

Corollary 3.2. *The Poincaré map* $\mathcal{P}_0^7$ *defined in* (22)*, which is induced by the Hamiltonian* (17) *with* $\mu = 10^{-3}$ *and* $e_0 = 0$*, has seven analytic normally hyperbolic invariant manifolds* $\widetilde{\Lambda}_0^j$*,* $j = 0, \ldots, 6$*. They are foliated by one-dimensional invariant curves. Moreover, there exist analytic functions* $\mathcal{G}_0^j : [I_-, I_+] \times \mathbb{T} \to (\mathbb{R} \times \mathbb{T})^3$*,*

$$\mathcal{G}_0^j(I, t) = \left(\widetilde{\mathcal{G}}_0^j(I), 0, I, t\right) = \left(\mathcal{G}_0^{j,L}(I), \mathcal{G}_0^{j,\ell}(I), \mathcal{G}_0^{j,G}(I), 0, I, t\right), \tag{24}$$

that parameterize $\widetilde{\Lambda}_0^j$*, namely,*

$$\widetilde{\Lambda}_0^j = \left\{\mathcal{G}_0^j(I, t) : (I, t) \in [I_-, I_+] \times \mathbb{T}\right\}.$$

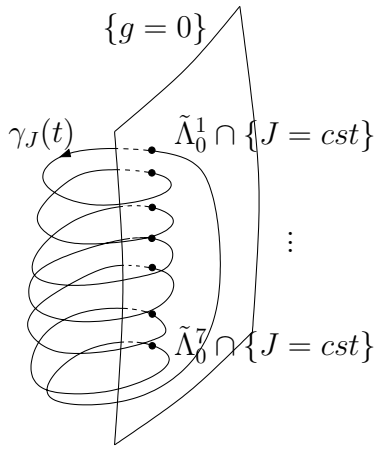

Figure 4: The periodic orbit obtained at each energy level intersects seven times the Poincaré section $\{g = 0\}$, as it is shown schematically in this picture. Then, when one considers the Poincaré map $\mathcal{P}_0$, the normally hyperbolic invariant manifold $\widetilde{\Lambda}_0$ has seven connected components $\widetilde{\Lambda}_0^0, \dots, \widetilde{\Lambda}_0^6$.

The associated invariant manifolds $W^u(\widetilde{\Lambda}_0^3)$ and $W^s(\widetilde{\Lambda}_0^4)$ intersect transversally provided $I \in \mathcal{D}^{\mathrm{f}}$; and $W^s(\widetilde{\Lambda}_0^3)$ and $W^u(\widetilde{\Lambda}_0^4)$ intersect transversally provided $I \in \mathcal{D}^{\mathrm{b}}$. Moreover, one of the points of these intersections belongs to the symmetry axis of (20)*. Let us denote by Γ_0^*, $* = \mathrm{f}, \mathrm{b}$, these intersections. Then, there exist analytic functions*

$$\mathcal{C}_0^* : \mathcal{D}^j \times \mathbb{R} \to (\mathbb{R} \times \mathbb{T})^3, \quad (I,t) \mapsto \mathcal{C}_0^*(I,t), \ \ * = \mathrm{f}, \mathrm{b}$$

which parameterize them:

$$\Gamma_0^* = \left\{ \mathcal{C}_0^*(I,t) = (\mathcal{C}_0^{*,L}(I), \mathcal{C}_0^{*,\ell}(I), \mathcal{C}_0^{*,G}(I), 0, I, t) : (I,t) \in \mathcal{D}^* \times \mathbb{T} \right\}, \ \ * = \mathrm{f}, \mathrm{b}.$$

The zero which appears in the parameterizations $\mathcal{G}$ and $\mathcal{C}$ is just the g-coordinate. We keep it although we are in the Poincaré section because later on we will use these parameterizations in the full phase space.

Again, it follows from the implicit function theorem that $W^s(\tilde{\Lambda}_0^3)$ and $W^u(\tilde{\Lambda}_0^4)$ are analytic (taking the distance from the cylinder $\tilde{\Lambda}_0^3$ or $\tilde{\Lambda}_0^4$ as a small parameter, as in [Mey75] with the cylinder as factor variable).

Corollary 3.1 gives global coordinates (I,t) for each cylinder $\widetilde{\Lambda}_0^j$. These coordinates are symplectic with respect to the canonical symplectic form

$$\Omega_0 = dI \wedge dt, \tag{25}$$

Indeed, one has to consider the pullback of the canonical form $dL \wedge d\ell + dG \wedge dg + dI \wedge dt$ to the cylinders $\widetilde{\Lambda}_0^j$. By Corollary 3.2 we have that in the cylinders: $g = 0$, $\ell = \mathcal{G}_0^{j,\ell}(I)$ and $L = \mathcal{G}_0^{j,L}(I)$. Then, it is easy to see that the pullback of $dL \wedge d\ell + dG \wedge dg + dI \wedge dt$ is just Ω_0.

We consider the inner and the two outer maps in one of these cylinders. We choose $\widetilde{\Lambda}_0^3$. As we have explained before, the reason is that the heteroclinic connections with the following cylinder $\widetilde{\Lambda}_0^4$ intersect the symmetry axis of the involution (20) and therefore they are easier to be studied numerically (see Figure 11). Since I is conserved by the inner and outer maps, these maps are integrable and the variables (I,t) are the action-angle variables. In this way, it will be easier to understand the influence of ellipticity.

3.2 The inner map

We first define the inner map. One could take the Poincaré map $\mathcal{P}_0$ restricted to the whole normally hyperbolic invariant manifold (23). Nevertheless, in order to study the diffusion mechanism it is more convenient to consider just one of the cylinders that form (23), for instance $\widetilde{\Lambda}_0^3$. To this end, we can define the inner map $\mathcal{F}_0^{\text{in}} : \widetilde{\Lambda}_0^3 \to \widetilde{\Lambda}_0^3$ as the analytic Poincaré map $\mathcal{P}_0^7$ restricted to the symplectic invariant submanifold $\widetilde{\Lambda}_0^3$. We can express $\mathcal{F}_0^{\text{in}}$ using the global coordinates (I, t) of $\widetilde{\Lambda}_0^3$.

Since I is an integral of motion, this inner map is of the form

$$\mathcal{F}_0^{\text{in}} : \begin{pmatrix} I \\ t \end{pmatrix} \mapsto \begin{pmatrix} I \\ t + \mu \mathcal{T}_0(I) \end{pmatrix}, \tag{26}$$

where the function $\mathcal{T}_0$ is independent of t due to the fact that the inner map preserves the differential form (25), which does not depend on t, and that I is a first integral. In fact, $14\pi + \mu\mathcal{T}_0(I)$ is the period of the periodic orbit obtained in Theorem 3 on the corresponding energy surface. It can be seen numerically that this map is twist.

Lemma 3.3. *The analytic symplectic inner map $\mathcal{F}_0^{\text{in}}$ defined in* (26) *is twist, that is*

$$\partial_I \mathcal{T}_0(I) \neq 0 \qquad \text{for } I \in [I_-, I_+].$$

Moreover, the function $\mathcal{T}_0(I)$ satisfies

$$0 < \mu \mathcal{T}_0(I) < \pi. \tag{27}$$

Proof. Based on convincing numerical data. See Appendix A. □

In Section 3.3, the function $\mathcal{T}_0(I)$ will be written by means of an integral (see (39)).

The information contained in this lemma will be crucial in Section 5 to prove the existence of a transition chain of invariant tori.

3.3 Outer map

Sometimes the outer map is called scattering map (see for instance [Tre04, DdlLS08]). We first recall the construction in a general perturbative setting, which we apply next to the circular problem, and in section 4.1 to the elliptic problem.

Let $\mathcal{P}_0$ be a map of a compact manifold M. Let $\Lambda_0 \subset M$ be a normally hyperbolic invariant manifold of $\mathcal{P}_0$, whose inner map $\mathcal{P}_0|_{\Lambda_0}$ has zero Lyapunov exponents: $\lim_{n\to+\infty} \ln \|d\mathcal{P}_0^n(z)v\|/n = 0$ for any $z \in \Lambda_0$ and $v \in T_z\Lambda_0$ (where $\|\cdot\|$ is some smooth Riemannian norm on M). Further assume that the stable and unstable invariant manifolds of Λ_0 intersect transversally.

Let $\mathcal{P}$ be a small perturbation of $\mathcal{P}_0$. Since Λ_0 is normally hyperbolic it persists under small perturbation of $\mathcal{P}_0$. Let $\Lambda \subset M$ be a normally hyperbolic invariant manifold of $\mathcal{P}$.

Then, the outer map associated to $\mathcal{P}$ and Λ (a particular case being $\mathcal{P} = \mathcal{P}_0$ and $\Lambda = \Lambda_0$) is defined over some domain as follows.

Definition 3.4. *Assume that $\gamma \subset W_\Lambda^s \cap W_\Lambda^u$ is a homoclinic orbit and that the intersection of W_Λ^s and W_Λ^u is transversal along γ, that is*

$$T_z W_\Lambda^s + T_z W_\Lambda^u = T_z M \quad \text{and} \quad T_z W_\Lambda^s \cap T_z W_\Lambda^u = T_z\gamma \quad \text{for } z \in \gamma.$$

Then, we say that $\mathcal{S}(x_-) = x_+$, if there exists a point $z \in \gamma$ such that for some $C > 0$ we have

$$\operatorname{dist}(\mathcal{P}^n(z), \mathcal{P}^n(x_\pm)) < C\lambda^{-|n|} \qquad \text{for all } n \in \mathbb{Z}^\pm. \tag{28}$$

That condition (28) indeed defines a map $x_- \mapsto x_+$ locally uniquely, is justified in [DdlLS08].

Remark 3.5. Since Λ is normally hyperbolic, for each point $x \in \Lambda$ there are strong stable and unstable manifolds $W^{ss}(x)$ and $W^{su}(x)$. Then $\mathcal{S}(x_-) = x_+$ holds only if $W^{su}(x_-) \cap W^{ss}(x_+) \neq \emptyset$ and the intersection occurs on γ.

In the case when the Lyapunov exponents of the inner dynamics $\mathcal{P}|_\Lambda$ are positive, for the points x_- and x_+ to be still uniquely defined given $z \in \gamma$, λ must exceed the maximal Lyapunov exponent i.e., the convergence towards Λ must dominate the motion inside of Λ. Otherwise, one cannot distinguish if the orbit of z is (backward- or forward-) asymptotic to a point of Λ or to the stable manifold of this point.

Remark 3.6. If the Lyapunov exponents of the inner map $\mathcal{P}|_\Lambda$ are zero (thus in particular for the unperturbed map $\mathcal{P}_0$), the outer map $\mathcal{S}$ is C^∞.

On the other hand, if the Lyapunov exponents of the inner map are small (thus in particular for a map $\mathcal{P}$ close enough to $\mathcal{P}_0$), the outer map is C^k, and k tends to infinity as the Lyapunov exponents tend to 0.

Strictly speaking, there is hardly any published regularity theorem from which these assertions follow directly. In order to prove them, one can first localize in the neighborhood of a small continuous set of hyperbolic periodic orbits of $\mathcal{P}_0$, modify $\mathcal{P}$ outside this neighborhood in order to embed the periodic orbits into a compact *invariant* normally hyperbolic cylinder, and characterize for the stable and unstable manifolds of the modified system in terms of an equation of class C^k, the perturbative parameter being the distance from the invariant cylinder. Such arguments belong to well understood hyperbolic theory, and we will omit further details, refering to the techniques developped in [Fen72, Cha04] or [BKZ11, Appendix B] for a closer context.

We now intend to apply a variant of this definition, in the unperturbed case, to the dynamics of the circular problem. One could consider the normally hyperbolic invariant manifold $\cup_{j=1}^7 \widetilde{\Lambda}_0^j$. Nevertheless, since it is not connected, it is more convenient to proceed as we have done for the inner map in the previous section. Namely, we look for an outer map which sends $\widetilde{\Lambda}_0^3$ to itself. Now one has to be more careful since one cannot consider the outer maps induced by the Poincaré map $\mathcal{P}_0^7$. Indeed, for $\mathcal{P}_0^7$, the cylinder $\widetilde{\Lambda}_0^3$ is a normally hyperbolic invariant manifold but the homoclinic points obtained in Theorem 3.1 now correspond to heteroclinic connections between $\widetilde{\Lambda}_0^3$ and $\widetilde{\Lambda}_0^4$ and between $\widetilde{\Lambda}_0^4$ and $\widetilde{\Lambda}_0^3$. To overcome this problem we will compose the heteroclinic outer maps $\mathcal{S}^*$, $* = \mathrm{f}, \mathrm{b}$ with the Poincaré map $\mathcal{P}_0$ as many times as necessary so that the composition sends $\widetilde{\Lambda}_0^3$ to itself.

Therefore, the smooth outer maps $\mathcal{F}_0^{\mathrm{out},\pm}$ that we consider connect $\widetilde{\Lambda}_0^3$ to itself and are defined as

$$\begin{aligned} \mathcal{F}_0^{\mathrm{out,f}} &= \mathcal{P}_0^6 \circ \mathcal{S}^{\mathrm{f}} : \widetilde{\Lambda}_0^3 \longrightarrow \widetilde{\Lambda}_0^3 \\ \mathcal{F}_0^{\mathrm{out,b}} &= \mathcal{S}^{\mathrm{b}} \circ \mathcal{P}_0 : \widetilde{\Lambda}_0^3 \longrightarrow \widetilde{\Lambda}_0^3, \end{aligned} \tag{29}$$

where $\mathcal{S}^{\mathrm{f}}$ is the outer map which connects $\widetilde{\Lambda}_0^3$ and $\widetilde{\Lambda}_0^4$ through $W^u(\widetilde{\Lambda}_0^3) \cap W^s(\widetilde{\Lambda}_0^4)$ and $\mathcal{S}^{\mathrm{b}}$ is the outer map which connects $\widetilde{\Lambda}_0^4$ and $\widetilde{\Lambda}_0^3$ through $W^u(\widetilde{\Lambda}_0^4) \cap W^s(\widetilde{\Lambda}_0^3)$. Note that here we are abusing notation since the forward and backwards outer maps are only defined provided $I \in \mathcal{D}^{\mathrm{f}}$ and $I \in \mathcal{D}^{\mathrm{b}}$ respectively and not in the whole cylinder $\widetilde{\Lambda}_0^3$.

The outer map is always exact symplectic (see [DdlLS08]). So, in the circular problem, since I is preserved, the outer maps must be of the form

$$\mathcal{F}_0^{\mathrm{out},*} : \begin{pmatrix} I \\ t \end{pmatrix} \mapsto \begin{pmatrix} I \\ t + \mu\omega^*(I) \end{pmatrix}, \quad * = \mathrm{f}, \mathrm{b}. \tag{30}$$

Outer maps can be defined with either discrete or continuous time. Since the Poincaré-Melnikov theory is considerably simpler for flows than for maps, we compute $\mathcal{F}_0^{\text{out},*}$ using continuous time. Moreover, in Section 4.5 we will use also flows to study the outer map of the elliptic problem as a perturbation of (30). The outer map given by the Hamiltonian (17) with $e_0 = 0$ does not preserve the section $\{g = 0\}$ but the inner map does. In order to fix this problem, we reparameterize the flow so that the inner and outer map preserve this section.

This reparameterization corresponds to identifying the variable g with time and is given by,

$$\begin{array}{llll} \frac{d}{ds}\ell = & \frac{\partial_L H}{-1+\mu\partial_G \Delta H_{\text{circ}}} & \frac{d}{ds}L = & -\frac{\partial_\ell H}{-1+\mu\partial_G \Delta H_{\text{circ}}} \\ \frac{d}{ds}g = & 1 & \frac{d}{ds}G = & -\frac{\partial_g H}{-1+\mu\partial_G \Delta H_{\text{circ}}} \\ \frac{d}{ds}t = & \frac{1}{-1+\mu\partial_G \Delta H_{\text{circ}}} & \frac{d}{ds}I = & 0 \end{array} \tag{31}$$

where H is Hamiltonian (17) with $e_0 = 0$. Notice that this reparameterization implies the change of direction of time. However, the geometric objects stay the same. In particular, the new flow still possesses the normally invariant cylinder obtained in Corollary 3.1 and its invariant manifolds.

We will refer to this system as a *reduced circular problem*. We call it reduced because we identify g with the time s. Moreover, the t-component (and in fact, all the others) only depends on the other coordinates. Denote by Φ_0^{circ} the flow associated to the (L, ℓ, G, g) components of equation (31) (which are independent of t and I). Componentwise it can be written as

$$\Phi_0^{\text{circ}}\{s, (L, \ell, G, g)\} = \left(\Phi_0^L\{s, (L, \ell, G, g)\}, \Phi_0^\ell\{s, (L, \ell, G, g)\}, \Phi_0^G\{s, (L, \ell, G, g)\}, g + s\right). \tag{32}$$

Then, the outer map can be computed as follows.

Let

$$\begin{aligned} \gamma_I^*(\sigma) &= \Phi_0^{\text{circ}}\{\sigma, (\mathcal{C}_0^{*,L}(I), \mathcal{C}_0^{*,\ell}(I), \mathcal{C}_0^{*,G}(I), 0)\}, \quad * = \text{f}, \text{b} \\ \lambda_I^j(\sigma) &= \Phi_0^{\text{circ}}\{\sigma, (\mathcal{G}_0^{j,L}(I), \mathcal{G}_0^{j,\ell}(I), \mathcal{G}_0^{j,G}(I), 0)\} \end{aligned} \tag{33}$$

be trajectories of the circular problem. The first ones have the initial conditions at the homoclinic points obtained in Theorem 3 with action I since $\mathcal{C}_0^{\text{f,b}}$ are the parameterizations of the intersections of the invariant manifolds of $\widetilde{\Lambda}_0^3$ and $\widetilde{\Lambda}_0^4$, given in Corollary 3.2. The second ones have the initial condition in the fixed points of the Poincaré map $\mathcal{P}_0^7$, which are parameterized by $\mathcal{G}_0^3$ and $\mathcal{G}_0^4$ given in Corollary 3.2.

Lemma 3.7. *The functions $\omega^{\text{f,b}}(I)$ involved in the definition of the outer maps in* (30) *can be defined as*

$$\omega^*(I) = \omega_{\text{out}}^*(I) + \omega_{\text{in}}^*(I),$$

where

$$\omega_{\text{out}}^*(I) = \omega_+^*(I) - \omega_-^*(I) \tag{34}$$

with

$$\begin{aligned} \omega_+^*(I) &= \lim_{N\to+\infty}\left(\int_0^{14N\pi} \frac{(\partial_G \Delta H_{\text{circ}}) \circ \gamma_I^*(\sigma)}{-1+\mu(\partial_G \Delta H_{\text{circ}}) \circ \gamma_I^*(\sigma)}\, d\sigma + N\mathcal{T}_0(I)\right) \\ \omega_-^*(I) &= \lim_{N\to-\infty}\left(\int_0^{14N\pi} \frac{(\partial_G \Delta H_{\text{circ}}) \circ \gamma_I^*(\sigma)}{-1+\mu(\partial_G \Delta H_{\text{circ}}) \circ \gamma_I^*(\sigma)}\, d\sigma + N\mathcal{T}_0(I)\right), \quad * = \text{f}, \text{b} \end{aligned} \tag{35}$$

and

$$\begin{aligned}\omega_{\rm in}^{\rm f}(I) &= \int_0^{-12\pi} \frac{(\partial_G \Delta H_{\rm circ}) \circ \lambda_I^4(\sigma)}{-1+\mu(\partial_G \Delta H_{\rm circ}) \circ \lambda_I^4(\sigma)}\, d\sigma \\ \omega_{\rm in}^{\rm b}(I) &= \int_0^{-2\pi} \frac{(\partial_G \Delta H_{\rm circ}) \circ \lambda_I^3(\sigma)}{-1+\mu(\partial_G \Delta H_{\rm circ}) \circ \lambda_I^3(\sigma)}\, d\sigma,\end{aligned} \tag{36}$$

where $\mathcal{T}_0(I)$ is the function in (26)*.*

Note that the minus sign that appears in the limits of integration of the integrals involved in the definition of functions $\omega_{\rm in}^*(I)$ is due to the fact that the reparameterized flow (31) reverses time. Using that the circular problem is symmetric with respect to (20) and that the homoclinic points $\mathcal{C}_0^{\rm f}$ and $\mathcal{C}_0^{\rm b}$ belong to the symmetry axis, one can easily see that $\omega_-^* = -\omega_+^*$, $* = {\rm f}, {\rm b}$.

The geometric interpretation of $\omega^{\rm f,b}(I)$ is that the t-shift occurs since the homoclinic orbits approach different points of the same invariant curve in the future and in the past. This shift is equivalent to the shift in t that appears in the Mather Problem [Mat96]. See, for instance, formula (2.1) in Theorem 2.1 of [DdlLS00] and the constants a and b used in formula (1.4) of [BT99].

Proof. We compute $\omega^{\rm f}(I)$. The other case can be done analogously. Since the t-component of the reduced circular system (31) does not depend on t, its behavior is given by

$$\begin{aligned}\Phi_0^t\{s,(L,\ell,G,g,t)\} &= t + \widetilde{\Phi}_0\{s,(L,\ell,G,g)\} \\ &= t + \int_0^s \frac{1}{-1+\mu\partial_G \Delta H_{\rm circ}\left(\Phi_0^{\rm circ}\{\sigma,(L,\ell,G,g)\}\right)}\, d\sigma\end{aligned} \tag{37}$$

Note that, using this flow, the inner map on (26) is just the (-14π)-time map in the time s. Then, the original period of the periodic orbits obtained in Theorem 3, can be expressed using this new flow as

$$14\pi + \mu\mathcal{T}_0(I) = \int_0^{-14\pi} \frac{1}{-1+\mu(\partial_G \Delta H_{\rm circ}) \circ \lambda_I^3(\sigma)}\, d\sigma. \tag{38}$$

This allows us to define the function $\mathcal{T}_0(I)$ in (26) through integrals as

$$\mathcal{T}_0(I) = \int_0^{-14\pi} \frac{(\partial_G \Delta H_{\rm circ}) \circ \lambda_I^3(\sigma)}{-1+\mu(\partial_G \Delta H_{\rm circ}) \circ \lambda_I^3(\sigma)}\, d\sigma. \tag{39}$$

Consider now a point $(\mathcal{C}_0^{{\rm f},L}(I), \mathcal{C}_0^{{\rm f},\ell}(I), \mathcal{C}_0^{{\rm f},G}(I), 0, I, t)$ in $W^u(\widetilde{\Lambda}_0^3) \cap W^s(\widetilde{\Lambda}_0^4) \cap \{g=0\}$. Since the first four components are independent of t, $(\mathcal{C}_0^{{\rm f},L}(I), \mathcal{C}_0^{{\rm f},\ell}(I), \mathcal{C}_0^{{\rm f},G}(I), 0, I, t)$ is forward asymptotic (in the reparameterized time) to a point

$$\left(\mathcal{G}_0^{3,L}(I), \mathcal{G}_0^{3,\ell}(I), \mathcal{G}_0^{3,G}(I), 0, I, t + \mu\omega_+^{\rm f}(I)\right)$$

and backward asymptotic (in the reparameterized time) to a point

$$\left(\mathcal{G}_0^{4,L}(I), \mathcal{G}_0^{4,\ell}(I), \mathcal{G}_0^{4,G}(I), 0, I, t + \mu\omega_-^{\rm f}(I)\right).$$

Using (37), the functions $\omega^{\rm f}_{\pm}(I)$ can be defined as

$$\begin{aligned}\omega^{\rm f}_{+}(I) &= \lim_{T\to+\infty}\int_0^T\left(\frac{1}{-1+\mu(\partial_G\Delta H_{\rm circ})\circ\gamma^{\rm f}_I(\sigma)}-\frac{1}{-1+\mu(\partial_G\Delta H_{\rm circ})\circ\lambda^3_I(\sigma)}\right)d\sigma\\ \omega^{\rm f}_{-}(I) &= \lim_{T\to-\infty}\int_0^T\left(\frac{1}{-1+\mu(\partial_G\Delta H_{\rm circ})\circ\gamma^{\rm f}_I(\sigma)}-\frac{1}{-1+\mu(\partial_G\Delta H_{\rm circ})\circ\lambda^4_I(\sigma)}\right)d\sigma.\end{aligned}\tag{40}$$

Moreover, since the system is 14π-periodic in the time s due to the identification of s with g, it is more convenient to write these in integrals as

$$\begin{aligned}\omega^{\rm f}_{+}(I) &= \lim_{N\to+\infty}\int_0^{14N\pi}\left(\frac{1}{-1+\mu(\partial_G\Delta H_{\rm circ})\circ\gamma^{\rm f}_I(\sigma)}-\frac{1}{-1+\mu(\partial_G\Delta H_{\rm circ})\circ\lambda^3_I(\sigma)}\right)d\sigma.\\ \omega^{\rm f}_{-}(I) &= \lim_{N\to-\infty}\int_0^{14N\pi}\left(\frac{1}{-1+\mu(\partial_G\Delta H_{\rm circ})\circ\gamma^{\rm f}_I(\sigma)}-\frac{1}{-1+\mu(\partial_G\Delta H_{\rm circ})\circ\lambda^4_I(\sigma)}\right)d\sigma.\end{aligned}$$

Then, taking (38) into account, one obtains

$$\omega^{\rm f}_{\pm}(I) = \lim_{N\to\pm\infty}\left(\int_0^{14N\pi}\frac{1}{-1+\mu(\partial_G\Delta H_{\rm circ})\circ\gamma^{\rm f}_I(\sigma)}\,d\sigma + N(14\pi+\mathcal{T}_0(I))\right),$$

from which the formulas for $\omega^{\rm f}_{\pm}$ in (35) follow.

Finally we have to compute $\omega^{\rm f}_{\rm in}(I)$. This term corresponds to the contribution of $\mathcal{P}^6_0$ to the outer map in formula (29). Then, taking into account that t is defined modulo 2π is straightforward to obtain $\omega^{\rm f}_{\rm in}(I)$ in (35). □

4 The elliptic problem

We can eventually study the elliptic problem. We will obtain perturbative expansions of the inner and outer maps. To this end, we use Poincaré-Melnikov techniques applied to the reduced elliptic problem, which is given by

$$\begin{aligned}\tfrac{d}{ds}\ell &= \frac{\partial_L H}{-1+\mu\partial_G\Delta H_{\rm circ}+\mu e_0\partial_G\Delta H_{\rm ell}} & \tfrac{d}{ds}L &= -\frac{\partial_\ell H}{-1+\mu\partial_G\Delta H_{\rm circ}+\mu e_0\partial_G\Delta H_{\rm ell}}\\ \tfrac{d}{ds}g &= 1 & \tfrac{d}{ds}G &= -\frac{\partial_g H}{-1+\mu\partial_G\Delta H_{\rm circ}+\mu e_0\partial_G\Delta H_{\rm ell}}\\ \tfrac{d}{ds}t &= \frac{1}{-1+\mu\partial_G\Delta H_{\rm circ}+\mu e_0\partial_G\Delta H_{\rm ell}} & \tfrac{d}{ds}I &= -\frac{\mu e_0\partial_t\Delta H_{\rm ell}}{-1+\mu\partial_G\Delta H_{\rm circ}+\mu e_0\partial_G\Delta H_{\rm ell}}.\end{aligned}\tag{41}$$

This system is a perturbation of (31). The study of the inner map can be done both dealing with this system or the system associated to the Hamiltonian (16). Nevertheless, to simplify the exposition we use only (41) for both the inner and outer maps. We also consider the Poincaré map associated with this system and the section $\{g=0\}$,

$$\mathcal{P}_{e_0}:\{g=0\}\longrightarrow\{g=0\},\tag{42}$$

which is a perturbation of (22).

There are two main results in this section:

- Existence of a normally hyperbolic invariant manifold with transversal intersections of its invariant manifolds for the elliptic problem (Theorem 4)
- Computation of the e_0-expansions of the inner and outer maps associated to it (Theorem 5).

The above theorems are stated in the next section. Theorem 4 relies on Corollary 3.2, because we study the elliptic problem as a perturbation of the circular one. The proof of Theorem 5 consists of several steps. In Section 4.2 we analyze the e_0-expansion of the elliptic Hamiltonian, and from it, in Section 4.3, we deduce properties of the e_0-expansion of the flow associated to system (41). In Section 4.4 we do perturbative analysis of the normally hyperbolic invariant cylinders $\widetilde{\Lambda}^j_{e_0}$, which are the perturbation of the cylinders $\widetilde{\Lambda}^j_0$ obtained in Corollary 3.2. This analysis allow us to obtain perturbative in e_0 formulas for the inner map derived. Finally, in Section 4.5 we use the above expansions and compute the outer maps using Poincaré-Melnikov techniques. These expansions allows us to give perturbative formulas of the inner and outer maps of the elliptic problem, which are defined in $\widetilde{\Lambda}^3_{e_0}$, which is e_0-close to the cylinder $\widetilde{\Lambda}^3_0$ obtained in Corollary 3.2.

4.1 The specific form of the inner and outer maps

For e_0 small enough the system associated to the Hamiltonian (17) has a normally hyperbolic invariant cylinder Λ_{e_0}, which is e_0-close to Λ_0 given in Corollary 3.1. Analogously, the Poincaré map $\mathcal{P}_{e_0}$ associated to this system and the section $\{g = 0\}$ has a normally hyperbolic invariant cylinder $\widetilde{\Lambda}_{e_0} = \Lambda_{e_0} \cap \{g = 0\}$. Moreover, it is formed by seven connected components $\widetilde{\Lambda}^j_{e_0}$, $j = 0, \dots, 6$, which are e_0-close to the cylinders $\widetilde{\Lambda}^j_{e_0}$ obtained in Corollary 3.2.

Recall that in Corollary 3.2, we have seen that in the invariant planes $I =$ constant there where forward and backward transveral heteroclinic connections between $\widetilde{\Lambda}^3_0$ and $\widetilde{\Lambda}^4_0$ provided $I \in \mathcal{D}^{\mathrm{f}}$ and $I \in \mathcal{D}^{\mathrm{b}}$ respectively. For the elliptic problem and e_0 small enough we will have transversal heteroclinic connections in slightly smaller domains. To this end, we define

$$\mathcal{D}^*_\delta = \{I \in \mathcal{D}^* : \mathrm{dist}(I, \partial\mathcal{D}^*) > \delta\}, \quad * = \mathrm{f}, \mathrm{b}. \tag{43}$$

Theorem 4. *For any $\delta > 0$, there exists $e_0^* > 0$ such that for $0 < e_0 < e_0^*$ the map $\mathcal{P}^7_{e_0}$, where $\mathcal{P}_{e_0}$ is the Poincaré map associated to Hamiltonian (17) and section $\{g = 0\}$, has seven normally hyperbolic locally[4] invariant manifolds $\widetilde{\Lambda}^j_{e_0}$, which are e_0-close in the $\mathcal{C}^1$ sense to $\widetilde{\Lambda}^j_0$. Moreover, there exist functions $\mathcal{G}^j_{e_0} : [I_- + \delta, I_+ - \delta] \times \mathbb{T} \to (\mathbb{R} \times \mathbb{T})^3$, $j = 0, \dots, 6$ which can be expressed in coordinates as*

$$\mathcal{G}^j_{e_0}(I, t) = \left(\mathcal{G}^{j,L}_{e_0}(I, t), \mathcal{G}^{j,\ell}_{e_0}(I, t), \mathcal{G}^{j,G}_{e_0}(I, t), 0, I, t\right), \tag{44}$$

that parameterize $\widetilde{\Lambda}^j_{e_0}$. In other words $\widetilde{\Lambda}^j_{e_0}$ is a graph over (I, t) defined as

$$\widetilde{\Lambda}^j_{e_0} = \{\mathcal{G}_{e_0}(I, t) : (I, t) \in [I_- + \delta, I_+ - \delta] \times \mathbb{T}\}.$$

The invariant manifolds $W^u(\widetilde{\Lambda}^3_{e_0})$ and $W^s(\widetilde{\Lambda}^4_{e_0})$ intersect transversally provided $I \in \mathcal{D}^{\mathrm{f}}_\delta$ and the invariant manifolds $W^u(\widetilde{\Lambda}^4_{e_0})$ and $W^s(\widetilde{\Lambda}^3_{e_0})$ intersect transversally provided $I \in \mathcal{D}^{\mathrm{b}}_\delta$. Moreover, one of these intersections is e_0-close in the $\mathcal{C}^1$ sense to the manifolds $\Gamma^{\mathrm{f,b}}_0$ defined in Corollary 3.2. Denote $\Gamma^{\mathrm{f,b}}_{e_0}$ these intersections. There exist functions

$$\mathcal{C}^*_{e_0}(I, t) = \left(\mathcal{C}^{*,L}_{e_0}(I, t), \mathcal{C}^{*,\ell}_{e_0}(I, t), \mathcal{C}^{*,G}_{e_0}(I, t), 0, I, t\right), \quad * = \mathrm{f}, \mathrm{b}$$

[4] see remark right below

which parameterize them. Namely,

$$\Gamma^*_{e_0} = \left\{ \mathcal{C}^*_{e_0}(I,t) : (I,t) \in [I_- + \delta, I_+ - \delta] \times \mathbb{T} \right\}, \ \ * = \mathrm{f}, \mathrm{b}.$$

For the elliptic problem, the coordinates (I,t) are symplectic not with respect to the canonical symplectic form $dI \wedge dt$. Indeed, if we make the pullback of the canonical form $dL \wedge d\ell + dG \wedge dg + dI \wedge dt$ into the cylinders $\widetilde{\Lambda}^j_{e_0}$, we obtain the symplectic form

$$\Omega^j_{e_0} = \left(1 + e_0 a^j_1(I,t) + e_0^2 a^j_2(I,t) + e_0^3 a^j_{\geq}(I,t)\right) dI \wedge dt, \tag{45}$$

for certain functions $a^j_k : [I_-, I_+] \times \mathbb{T} \to \mathbb{R}$. The functions $a^j_{\geq}$ contain the e_0^3 remainder terms, and thus depend on e_0 even if we do not write explicitly this dependence to simplify notation.

Remark 4.1. Objects and maps of Theorem 4 have increasing regularity when e_0 tends to 0. Indeed, by Gronwall's inequality the Lyapunov exponents of Λ_{e_0} tend to zero with e_0. So for every $k \geq 1$, if e_0 is small enough, the invariant manifold Λ_{e_0} and the above subsequent objects are of class C^k (see Remark 3.6). For the sake of simplicity, we will not henceforth emphasize regularity issues. But the main point is that for e_0 small enough all objects of our construction are smooth enough, and in particular it will be possible below to apply the KAM theorem to the invariant manifolds $\tilde{\Lambda}^j_0$.

Remark 4.2. Theorem 4 only guarantees local invariance for $\widetilde{\Lambda}^j_{e_0}$. Namely, the boundary might not be invariant. Nevertheless, later in Section 5 we will show the existence of invariant tori in $\widetilde{\Lambda}^j_{e_0}$, which will play the role of boundaries of $\widetilde{\Lambda}^j_{e_0}$. Thanks to these tori, one can choose $\widetilde{\Lambda}^j_{e_0}$ to be invariant. For that reason, from now on we will refer $\widetilde{\Lambda}^j_{e_0}$ as a normally hyperbolic invariant manifold.

We introduce the following notation.

Notation 4.3. *For any function f with 2π-periodic dependence on t, $\mathcal{N}(f)$ is the subset of the integers corresponding to which t-harmonics of f (which may depend on other variables) are non-zero.*

In the invariant cylinder $\widetilde{\Lambda}^3_{e_0}$ given in Theorem 4 one can define inner and outer maps as we have done in $\widetilde{\Lambda}^3_0$ for the circular problem. Next sections are devoted to the perturbative analysis of these maps. We state here their main result.

Theorem 5. *The normally hyperbolic invariant manifold $\widetilde{\Lambda}^3_{e_0}$ given in Theorem 4 of the Poincaré map $\mathcal{P}^7_{e_0}$ in (42) has associated inner and outer maps. Moreover*

- *The inner map is of the form*

$$\mathcal{F}^{\mathrm{in}}_{e_0} : \begin{pmatrix} I \\ t \end{pmatrix} \mapsto \begin{pmatrix} I + e_0 A_1(I,t) + e_0^2 A_2(I,t) + \mathcal{O}\left(e_0^3\right) \\ t + \mu \mathcal{T}_0(I) + e_0 \mathcal{T}_1(I,t) + e_0^2 \mathcal{T}_2(I,t) + \mathcal{O}\left(e_0^3\right) \end{pmatrix}. \tag{46}$$

  and the functions A_1, A_2, $\mathcal{T}_1$, and $\mathcal{T}_2$ satisfy

$$\mathcal{N}(A_1) = \{\pm 1\}, \ \ \mathcal{N}(A_2) = \{0, \pm 1, \pm 2\} \tag{47}$$

$$\mathcal{N}(\mathcal{T}_1) = \{\pm 1\}, \ \ \mathcal{N}(\mathcal{T}_2) = \{0, \pm 1, \pm 2\}. \tag{48}$$

- *The outer maps are of the form*

$$\mathcal{F}^{\mathrm{out},*}_{e_0} : \begin{pmatrix} I \\ t \end{pmatrix} \mapsto \begin{pmatrix} I + e_0 B^*(I,t) + \mathcal{O}\left(e_0^2\right) \\ t + \mu \omega^*(I) + \mathcal{O}(e_0) \end{pmatrix}, \ \ * = \mathrm{f}, \mathrm{b}. \tag{49}$$

  and the functions B^* satisfy

$$\mathcal{N}(B^*) = \{\pm 1\}. \tag{50}$$

4.2 The e_0-expansion of the elliptic Hamiltonian

We obtain expansions of ΔH_{ell} in (17) with respect to e_0. These expansions will be used later in Sections 4.3, 4.4 and 4.5. The most important goal is to see which harmonics in t have the e_0 and e_0^2 terms of the elliptic perturbation in (17). Note that the circular problem is independent of t.

We define the function

$$\mathcal{B}(r,v,g,t)=\frac{1}{\left|re^{i(v+g-t)}-r_0(t)e^{iv_0(t)}\right|}. \tag{51}$$

This function is the potential

$$\frac{1}{|q-q_0(t)|}$$

expressed in terms of $g=\hat{g}-t$, where $\hat{g}$ is the argument of the perihelion, the true anomaly v of the asteroid defined in (13) and the radius r. The functions $r_0(t)$ and $v_0(t)$ are the radius and the true anomaly of Jupiter. The functions $r_0(t)$ and $v_0(t)$ are the only ones involved in the definition of $\mathcal{B}$ which depend on e_0.

Then, the perturbation in (16) can be expressed as

$$\begin{aligned}\mu\Delta H_{\text{circ}}(L,\ell,G,g)+\mu e_0\Delta H_{\text{ell}}(L,\ell,G,g,t)=&-\frac{1-\mu}{\mu}\mathcal{B}\left(-\frac{r}{\mu},v,g,t\right)\\&-\frac{\mu}{1-\mu}\mathcal{B}\left(\frac{r}{1-\mu},v,g-t,t\right)+\frac{1}{r}\Big|_{(r,v)=(r(L,\ell,G),v(L,\ell,G))}.\end{aligned}$$

First we study the expansion of $\mathcal{B}$, and from it, we deduce the one of ΔH_{ell}.

Lemma 4.4. *Consider the expansion*

$$\mathcal{B}(r,v,g,t)=\mathcal{B}_0(r,v,g)+e_0\mathcal{B}_1(r,v,g,t)+e_0^2\mathcal{B}_2(r,v,g,t)+\mathcal{O}\left(e_0^3\right) \tag{52}$$

of the function $\mathcal{B}$ defined in (51)*. Then,*

- $\mathcal{B}_0$ *satisfies* $\mathcal{N}(\mathcal{B}_0)=\{0\}$.
- $\mathcal{B}_1$ *satisfies* $\mathcal{N}(\mathcal{B}_1)=\{\pm1\}$ *and is given by*

$$\mathcal{B}_1(r,v,g,t)=-\frac{1}{2\Delta^3(r,v,g)}\left(2\cos t-3r\cos(v+g+t)+r\cos(v+g-t)\right), \tag{53}$$

  where

$$\Delta(r,v,g)=\left(r^2+1-2r\cos(v+g)\right)^{1/2}.$$

- $\mathcal{B}_2$ *satisfies* $\mathcal{N}(\mathcal{B}_2)=\{0,\pm1,\pm2\}$.

Note that the elliptic problem is a peculiar perturbation of the circular problem in the sense that the k-th e_0-order has t-harmonics up to order k. This fact will be crucial when we will compare the inner and outer dynamics in Section 5.

Proof. To prove this lemma we look for the e_0-expansions of the functions $r_0(t)$ and $v_0(t)$ involved in the definition of $\mathcal{B}$ in (51). We obtain them using the eccentric, true and mean anomalies of Jupiter.

From the relation $t = u_0 - e_0 \sin u_0$ (see (15)), one can obtain that

$$u_0(t) = t + e_0 \sin t + \frac{e_0^2}{2} \sin 2t + \mathcal{O}\left(e_0^3\right).$$

Then, using $r_0 = 1 - e_0 \cos u_0$,

$$r_0(t) = 1 - e_0 \cos t + e_0^2 \sin^2 t + \mathcal{O}\left(e_0^3\right).$$

For the eccentric anomaly we can use

$$\tan \frac{v_0}{2} = \sqrt{\frac{1+e_0}{1-e_0}} \tan \frac{u_0}{2}$$

(see (95)), to obtain

$$v_0 = u_0 + e_0 \sin u_0 + e_0^2 \left(\frac{9}{2} \sin u_0 - 2 \sin 2u_0\right) + \mathcal{O}\left(e_0^3\right)$$

and then

$$v_0(t) = t + 2e_0 \sin t + e_0^2 \left(\frac{9}{2} \sin t - \sin 2t\right) + \mathcal{O}\left(e_0^3\right).$$

Plugging $r_0(t)$ and $v_0(t)$ into (51), it can be easily seen that the expansion (52) satisfies all the properties of $\mathcal{B}_0$, $\mathcal{B}_1$ and $\mathcal{B}_2$ stated in the lemma. □

From the expansion of $\mathcal{B}$, one can easily deduce the expansion of ΔH_{ell} in (17).

Corollary 4.5. *Let us consider the e_0-expansion of the function ΔH_{ell} in* (17)*,*

$$\Delta H_{\text{ell}} = \Delta H_{\text{ell}}^1 + e_0 \Delta H_{\text{ell}}^2 + \mathcal{O}\left(e_0^2\right).$$

Then, the first order is given by

$$\begin{aligned} \Delta H_{\text{ell}}^1(L,\ell,G,g,t) = &- \frac{1-\mu}{\mu} \mathcal{B}_1 \left(-\frac{r(L,\ell,G)}{\mu}, v(L,\ell,G), g, t\right) \\ &- \frac{\mu}{1-\mu} \mathcal{B}_1 \left(\frac{r(L,\ell,G)}{1-\mu}, v(L,\ell,G), g, t\right). \end{aligned} \tag{54}$$

where $\mathcal{B}_1$ is the function defined in Lemma 4.4 and therefore it satisfies

$$\mathcal{N}\left(\Delta H_{\text{ell}}^1\right) = \{\pm 1\}.$$

The second order ΔH_{ell}^2 satisfies

$$\mathcal{N}\left(\Delta H_{\text{ell}}^2\right) = \{0, \pm 1, \pm 2\}.$$

4.3 Perturbative analysis of the flow

To study the inner and outer maps perturbatively, we need first to study the first orders with respect to e_0 of the flow $\Phi_{e_0}\{s,(g,I,t)\}$ associated to the vector field (41). Particularly, we want to know their dependence on the variable t. Recall that we already know the dependence on t of the 0-order thanks to formulas (32) and (37).

Lemma 4.6. *The flow $\Phi_{e_0}\{s,(L,\ell,G,g,I,t)\}$ has a perturbative expansion*

$$\begin{aligned}\Phi_{e_0}\{s,(L,\ell,G,g,I,t)\} =&\Phi_0\{s,(L,\ell,G,g,I,t)\} + e_0\Phi_1\{s,(L,\ell,G,g,I,t)\}\\ &+ e_0^2\Phi_2\{s,(L,\ell,G,g,I,t)\} + \mathcal{O}\left(e_0^3\right),\end{aligned}$$

which satisfies

$$\mathcal{N}\left(\Phi_1\{s,(L,\ell,G,g,I,t)\}\right) = \{\pm 1\} \tag{55}$$

$$\mathcal{N}\left(\Phi_2\{s,(L,\ell,G,g,I,t)\}\right) = \{0,\pm 1,\pm 2\}. \tag{56}$$

Proof. Let us denote $z=(L,\ell,G,g,I)$ and call $\mathcal{X}_{e_0}$ to the vector field (41), which has expansion

$$\mathcal{X}_{e_0} = \mathcal{X}_0 + e_0\mathcal{X}_1 + e_0^2\mathcal{X}_2 + \mathcal{O}\left(e_0^3\right).$$

We first prove (55). The e_0-order Φ_1 is a solution of the ordinary differential equation

$$\frac{d}{ds}\xi = D\mathcal{X}_0\left(\Phi_0\{s,(z,t)\}\right)\xi + \mathcal{X}_1\left(\Phi_0\{s,(z,t)\}\right)$$

with initial condition $\xi(0)=(0,0)$. By (31), $\mathcal{X}_0$ is independent of t and therefore,

$$D\mathcal{X}_0\left(\Phi_0\{s,(z,t)\}\right) = D\mathcal{X}_0\left(\Phi_0^{\text{circ}}(s,z)\right),$$

where Φ_0^{circ} has been defined in (32). Then, this term is also independent of t. From Corollary 4.5, one can deduce that $\mathcal{N}(\mathcal{X}_1)=\{\pm 1\}$ and therefore $\mathcal{X}_1$ can be written as

$$\mathcal{X}_1(z,t) = \mathcal{X}_1^+(z)e^{it} + \mathcal{X}_1^-(z)e^{-it},$$

Therefore, using formulas (32) and (37), one has that

$$\mathcal{X}_1\left(\Phi_0\{s,(z,t)\}\right) = \left(\mathcal{X}_1^+\left(\Phi_0^{\text{circ}}\{s,z\}\right)e^{i\widetilde{\Phi}_0\{s,z\}}\right)e^{it} + \left(\mathcal{X}_1^-\left(\Phi_0^{\text{circ}}\{s,z\}\right)e^{i\widetilde{\Phi}_0\{s,z\}}\right)e^{-it}.$$

To prove (55), it is enough to use variation of constants formula. Let us consider $M_z(s)$ the fundamental matrix of the linear equation

$$\frac{d}{ds}\xi = D\mathcal{X}_0\left(\Phi_0^{\text{circ}}(s,z)\right)\xi,$$

then

$$\Phi_1\{s,(z,t)\} = \Phi_1^+\{s,z\}e^{it} + \Phi_1^-\{s,z\}e^{-it}$$

with

$$\Phi_1^\pm\{s,z\} = M_z(s)\int_0^s M_z^{-1}(\sigma)\left(\mathcal{X}_1^\pm\left(\Phi_0^{\text{circ}}\{s,z\}\right)e^{\pm i\widetilde{\Phi}_0\{s,z\}\}}\right)d\sigma.$$

The proof of (56) follows the same lines. Indeed, Φ_2 is solution of an equation of the form

$$\frac{d}{ds}\xi = D\mathcal{X}_0\left(\Phi_0^{\rm circ}\{s,z\}\right)\xi + \Xi(s,g,I,t)$$

with initial condition $\xi(0)=(0,0,0)$. The function Ξ is given in terms of the previous orders of $\mathcal{X}_{e_0}$ and Φ_{e_0} as

$$\Xi = \frac{1}{2}D^2\mathcal{X}_0\left(\Phi_0^{\rm circ}\right)\left(\Phi_1\right)^{\otimes 2} + D\mathcal{X}_1\left(\Phi_0^{\rm circ}\right)\Phi_1^{\rm in} + \mathcal{X}_2\left(\Phi_0^{\rm circ}\right),$$

and then it satisfies $\mathcal{N}(\Xi)=\{0,\pm1,\pm2\}$.

Since the homogeneous linear equation is the same as for $\Phi_1^{\rm in}$ and does not depend on t, one can easily see that (56) is satisfied. □

4.4 Perturbative analysis of an invariant cylinder and its inner map

We devote this section to study the normally hyperbolic invariant manifold of the elliptic problem $\widetilde{\Lambda}^3_{e_0}$, given in Theorem 4, and the inner map associated to it. We study the inner map of the elliptic problem perturbatively from (26), taking e_0 as a small parameter. We call the inner map $\mathcal{F}^{\rm in}_{e_0}:\widetilde{\Lambda}^3_{e_0}\to\widetilde{\Lambda}^3_{e_0}$, which is defined as the (-14π)-Poincaré map of the flow Φ_{e_0}, defined in Lemma 4.6, restricted to $\widetilde{\Lambda}^3_{e_0}$.

We want to see which t-harmonics the first orders of the inner map has and also we want to compute the first order of the I-component. To this end we consider the classical theory of normally hyperbolic invariant manifolds [Fen74, Fen77]. This theory ensures the existence of the maps $\mathcal{G}^j_{e_0}$ parameterizing the normally hyperbolic manifolds $\widetilde{\Lambda}^j_0$ of the map $\mathcal{P}^7_{e_0}$. Moreover, they can be made unique imposing

$$\pi_I\mathcal{G}^j_{e_0}(I,t)=I,\ \pi_t\mathcal{G}^j_{e_0}(I,t)=t, \tag{57}$$

where π_* is the projection with respect to the corresponding component of the function. Since we only need properties of the parameterization of $\widetilde{\Lambda}^3_{e_0}$ and the dynamics on it, we just consider the case $j=3$. The map $\mathcal{G}^3_{e_0}$ satisfies the invariance equation

$$\widetilde{\mathcal{P}}_{e_0}\circ\mathcal{G}^3_{e_0} = \mathcal{G}^3_{e_0}\circ\mathcal{F}^{\rm in}_{e_0}, \tag{58}$$

where $\widetilde{\mathcal{P}}_{e_0}=\mathcal{P}^7_{e_0}$ and $\mathcal{F}^{\rm in}_{e_0}$ is the inner map of the elliptic problem, namely the Poincaré map $\mathcal{P}^7_{e_0}$ restricted to the cylinder $\widetilde{\Lambda}^3_{e_0}$.

Since we have regularity with respect to parameters, the invariance equation allows us to obtain expansions of both the parameterizations of $\widetilde{\Lambda}^3_{e_0}$ and the inner map $\mathcal{F}^{\rm in}_{e_0}$ with respect to e_0. Let us expand $\mathcal{G}^3_{e_0}$ and $\mathcal{F}^{\rm in}_{e_0}$ as

$$\mathcal{G}^3_{e_0} = \mathcal{G}^3_0 + e_0\mathcal{G}^3_1 + e_0^2\mathcal{G}^3_2 + \mathcal{O}\left(e_0^3\right) \tag{59}$$

$$\mathcal{F}^{\rm in}_{e_0} = \mathcal{F}^{\rm in}_0 + e_0\mathcal{F}^{\rm in}_1 + e_0^2\mathcal{F}^{\rm in}_2 + \mathcal{O}\left(e_0^3\right). \tag{60}$$

Then, $\mathcal{G}^3_0$ is the function defined in (24) and $\mathcal{F}^{\rm in}_0$ is the inner map of the circular problem obtained in (26), which is defined in $\widetilde{\Lambda}^3_0$. Recall that

$$\widetilde{\mathcal{P}}_{e_0}(L,\ell,G,0,I,t) = \mathcal{P}^7_{e_0}(L,\ell,G,0,I,t) = \Phi_{e_0}\{-14\pi,(L,\ell,G,0,I,t)\}, \tag{61}$$

where Φ_{e_0} is the flow considered in Lemma 4.6. Then, we have that

$$\mathcal{N}\left(\widetilde{\mathcal{P}}_1\right) = \{\pm 1\} \quad \text{and} \quad \mathcal{N}\left(\widetilde{\mathcal{P}}_2\right) = \{0, \pm 1, \pm 2\}.$$

Then, expanding equation (58) with respect to e_0 allows us to deduce the properties we need about the inner map. They are summarized in the next lemma, which reproduces the part of Theorem 5 referred to the inner dynamics.

Lemma 4.7. *The expansions of the functions $\mathcal{G}^3_{e_0}$ and $\mathcal{F}^{\rm in}_{e_0}$ in* (59) *and* (60) *satisfy that*

$$\mathcal{N}\left(\mathcal{G}^3_1\right) = \{\pm 1\} \quad \textit{and} \quad \mathcal{N}\left(\mathcal{G}^3_2\right) = \{0, \pm 1, \pm 2\}$$

and

$$\mathcal{N}(\mathcal{F}^{\rm in}_1) = \{\pm 1\} \quad \textit{and} \quad \mathcal{N}(\mathcal{F}^{\rm in}_2) = \{0, \pm 1, \pm 2\}.$$

Namely, the inner map is of the form,

$$\mathcal{F}^{\rm in}_{e_0} : \begin{pmatrix} I \\ t \end{pmatrix} \mapsto \begin{pmatrix} I + e_0 A_1(I,t) + e_0^2 A_2(I,t) + \mathcal{O}\left(\mu e_0^3\right) \\ t + \mu \mathcal{T}_0(I) + e_0 \mathcal{T}_1(I,t) + e_0^2 \mathcal{T}_2(I,t) + \mathcal{O}\left(\mu e_0^2\right) \end{pmatrix}, \tag{62}$$

and the functions A_1, A_2 $\mathcal{T}_1$ and $\mathcal{T}_2$ satisfy

$$\mathcal{N}(A_1) = \{\pm 1\}, \ \mathcal{N}(A_2) = \{0, \pm 1, \pm 2\} \tag{63}$$

$$\mathcal{N}(\mathcal{T}_1) = \{\pm 1\}, \ \mathcal{N}(\mathcal{T}_2) = \{0, \pm 1, \pm 2\}. \tag{64}$$

Moreover A_1 can be split as,

$$A_1(I,t) = A_1^+(I)e^{it} + A_1^-(I)e^{-it},$$

with

$$A_1^{\pm}(I) = \mp i\mu \int_0^{-14\pi} \frac{\Delta H^{1,\pm}_{\rm ell} \circ \lambda^3_I(\sigma)}{-1 + \mu \partial_G \Delta H_{\rm circ} \lambda^3_I(\sigma)} e^{\pm i \widetilde{\lambda}^3_I(\sigma)} d\sigma, \tag{65}$$

where the functions $\Delta H^{1,\pm}_{\rm ell}$ are defined as

$$\Delta H^1_{\rm ell}(L, \ell, G, g, t) = \Delta H^{1,+}_{\rm ell}(L, \ell, G, g)e^{it} + \Delta H^{1,\pm}_{\rm ell}(L, \ell, G, g)e^{-it},$$

$\lambda^3_I(\sigma)$ has been defined in (33) *and*

$$\widetilde{\lambda}^3_I(\sigma) = \widetilde{\Phi}_0\{\sigma, (\mathcal{G}^{3,L}_0(I), \mathcal{G}^{3,\ell}_0(I), \mathcal{G}^{3,G}_0(I), 0)\}, \tag{66}$$

where $\widetilde{\Phi}_0$ has been defined in (72) *and $\mathcal{G}^3_0$ in Corollary 3.2.*

From the properties of $\mathcal{G}^3_{e_0}$, we can deduce properties of the symplectic form $\Omega^3_{e_0}$ in (45), which is defined in the cylinder $\widetilde{\Lambda}^3_{e_0}$.

Corollary 4.8. *The functions a^3_1 and a^3_2 in the expansion of the symplectic form $\Omega^3_{e_0}$ in* (45)*, which is the pullback of the symplectic form $dL \wedge d\ell + dG \wedge dg + dI \wedge dt$ into the cylinder $\widetilde{\Lambda}^3_{e_0}$, satisfy*

$$\mathcal{N}\left(a^3_1\right) = \{\pm 1\} \quad \textit{and} \quad \mathcal{N}\left(a^3_2\right) = \{0, \pm 1, \pm 2\}.$$

Proof of Lemma 4.7. In the proof we omit the superscript 3 of the terms in the expansion of $\mathcal{G}^3_{e_0}$.

Expanding equation (58) with respect to e_0, we have that the first terms satisfy

$$\widetilde{\mathcal{P}}_0 \circ \mathcal{G}_0 = \mathcal{G}_0 \circ \mathcal{F}_0^{\text{in}} \tag{67}$$

$$\widetilde{\mathcal{P}}_1 \circ \mathcal{G}_0 + \left(D\widetilde{\mathcal{P}}_0 \circ \mathcal{G}_0\right) \mathcal{G}_1 = \mathcal{G}_1 \circ \mathcal{F}_0^{\text{in}} + \left(D\mathcal{G}_0 \circ \mathcal{F}_0^{\text{in}}\right) \mathcal{F}_1^{\text{in}} \tag{68}$$

$$\begin{aligned}\widetilde{\mathcal{P}}_2 \circ \mathcal{G}_0 + \left(D\widetilde{\mathcal{P}}_1 \circ \mathcal{G}_0\right) \mathcal{G}_1 + \frac{1}{2}\left(D^2\widetilde{\mathcal{P}}_0 \circ \mathcal{G}_0\right) \mathcal{G}_1^{\otimes 2} + \\ + \left(D\widetilde{\mathcal{P}}_0 \circ \mathcal{G}_0\right) \mathcal{G}_2 = \mathcal{G}_2 \circ \mathcal{F}_0^{\text{in}} + \left(D\mathcal{G}_1 \circ \mathcal{F}_0^{\text{in}}\right) \mathcal{F}_1^{\text{in}} \\ + \frac{1}{2}\left(D^2\mathcal{G}_0 \circ \mathcal{F}_0^{\text{in}}\right) (\mathcal{F}_1^{\text{in}})^{\otimes 2} + \left(D\mathcal{G}_0 \circ \mathcal{F}_0^{\text{in}}\right) \mathcal{F}_2^{\text{in}}.\end{aligned} \tag{69}$$

By the uniqueness condition (57), $\mathcal{G}_1$ is of the form

$$\mathcal{G}_1(g, I, t) = \left(\widetilde{\mathcal{G}}_1(g, I, t), 0, 0, 0\right)$$

with $\widetilde{\mathcal{G}}_1(g, I, t) = (\mathcal{G}_1^L(g, I, t), \mathcal{G}_1^\ell(g, I, t), \mathcal{G}_1^G(g, I, t))$.

Equation (67) corresponds to the inner dynamics of the circular problem. We use equations (68) and (69) to deduce the properties of $\mathcal{F}_1^{\text{in}}$ and $\mathcal{F}_2^{\text{in}}$ respectively. These equations can be solved iteratively and thus we start with (68). Since

$$D\mathcal{G}_0 = \begin{pmatrix} D\widetilde{\mathcal{G}}_0 \\ \text{Id} \end{pmatrix} \text{ and } D\mathcal{G}_i = \begin{pmatrix} D\widetilde{\mathcal{G}}_i \\ 0 \end{pmatrix} \text{ for } i \geq 1, \tag{70}$$

we have that

$$\mathcal{F}_1^{\text{in},*} = \pi_* \left(\widetilde{\mathcal{P}}_1 \circ \mathcal{G}_0 + \left(D\widetilde{\mathcal{P}}_0 \circ \mathcal{G}_0\right) \widetilde{\mathcal{G}}_1\right), \ * = I, t.$$

Replacing this into (68) we obtain an equation for $\mathcal{G}_1$. The equation for every Fourier t-coefficient is uncoupled, and therefore, using (61), that $\widetilde{\mathcal{P}}_0$ is independent of t and the uniqueness of $\mathcal{G}_1$, one can deduce that $\mathcal{N}(\mathcal{G}_1) = \{\pm 1\}$. As a consequence we have that $\mathcal{N}(\mathcal{F}_1^{\text{in}}) = \{\pm 1\}$.

Reasoning analogously and using (61) again, one can see that $\mathcal{N}(\mathcal{G}_2) = \{0, \pm 1, \pm 2\}$ and $\mathcal{N}(\mathcal{F}_2^{\text{in}}) = \{0, \pm 1, \pm 2\}$.

Now it only remains to prove formula (65). To this end, let us recall that one can write the I-component of the inner equation as

$$\mathcal{F}_{e_0}^{\text{in},I}(I, t) = \Phi_{e_0}^I \{-14\pi, \mathcal{G}_{e_0}(I, t)\}$$

since it is defined as the (-14π)-Poincaré map associated to the flow of system (41) restricted to the cylinder $\widetilde{\Lambda}^3_{e_0}$. Recall that the minus sign in the time appears due to the fact that system (41) has the time reversed with respect to the original one. Then, one can apply the Fundamental Theorem of Calculus and use (41) to obtain

$$\begin{aligned}\mathcal{F}_{e_0}^{\text{in},I}(I, t) &= \int_0^{-14\pi} \frac{d}{ds} \Phi_{e_0}^I \{s, \mathcal{G}_{e_0}(I, t)\}\, ds \\ &= -\int_0^{-14\pi} \frac{\mu e_0 \partial_t \Delta H_{\text{ell}} \circ \Phi_{e_0} \{s, \mathcal{G}_{e_0}(I, t)\}}{-1 + \mu \partial_G \Delta H_{\text{circ}} \circ \Phi_{e_0} \{s, \mathcal{G}_{e_0}(I, t)\} + \mu e_0 \partial_g \Delta H_{\text{ell}} \circ \Phi_{e_0} \{s, \mathcal{G}_{e_0}(I, t)\}} ds\end{aligned}$$

Then, using the expansions of the Hamiltonian $\Delta H_{\rm ell}$ in Corollary 4.5, of the flow Φ_{e_0} in Lemma 4.6 and of $\mathcal{G}_{e_0}$ just obtained,

$$\mathcal{F}^{{\rm in},I}_{e_0}(I,t) = -e_0 \int_0^{-14\pi} \frac{\mu\partial_t \Delta H^1_{\rm ell}\circ\Phi_0\left\{s,\mathcal{G}_0(I,t)\right\}}{-1+\mu\partial_G\Delta H_{\rm circ}\circ\Phi_0\left\{s,\mathcal{G}_0(I,t)\right\}} ds + \mathcal{O}\left(e_0^2\right)$$

Namely,

$$A_1(I,t) = -\int_0^{-14\pi} \frac{\mu\partial_t \Delta H^1_{\rm ell}\circ\Phi_0\left\{s,\mathcal{G}_0(I,t)\right\}}{-1+\mu\partial_G\Delta H_{\rm circ}\circ\Phi_0\left\{s,\mathcal{G}_0(I,t)\right\}} ds$$

To deduce the formulas for $A_1^{\pm}$ it is enough to split $\Delta H^1_{\rm ell}$ as

$$\Delta H^1_{\rm ell}(L,\ell,G,g,t) = \Delta H^{1,+}_{\rm ell}(L,\ell,G,g)e^{it} + \Delta H^{1,\pm}_{\rm ell}(L,\ell,G,g)e^{-it},$$

and recall that by formulas (32) and (37), Φ_0 can be written as

$$\Phi_0\left\{s,(L,\ell,G,g,I,t)\right\} = \left(\Phi_{\rm circ}\left\{s,(L,\ell,G,g,I)\right\},t+\widetilde{\Phi}_0\left\{s,(L,\ell,G,g,I)\right\}\right).$$

□

4.5 The outer map

We devote this section to study the outer maps

$$\mathcal{F}^{{\rm out},*}_{e_0} : \widetilde{\Lambda}^3_{e_0} \longrightarrow \widetilde{\Lambda}^3_{e_0},\ \ *={\rm f,b} \tag{71}$$

for $e_0>0$.

Theorem 4 gives the existence of $\mathcal{C}^*_{e_0}$, $*={\rm f,b}$, transversal intersections of the invariant manifolds of $\widetilde{\Lambda}^3_{e_0}$ and $\widetilde{\Lambda}^4_{e_0}$. The Poincaré map (42) possesses then also a normally hyperbolic invariant manifold $\widetilde{\Lambda}_{e_0}=\cup_{j=0}^6\widetilde{\Lambda}^j_{e_0}$ and its invariant manifolds intersect transversally at $\widetilde{\Gamma}_{e_0}$.

Then, we can proceed as in Section 3.3 to define the outer maps $\mathcal{F}^{\rm out}_{e_0}$. We want to study it as a perturbation of the outer map of the circular problem given in (30). To this end we use Poincaré-Melnikov techniques. As we have explained in Section 3.3, the original flow associated to Hamiltonian (16) does not allow us to study perturbatively $\mathcal{F}^{\rm out}_{e_0}$. Instead, we use the reduced elliptic problem defined in (41).

The results stated in Theorem 5 about the outer map are summarized in the next lemma. We also show how to compute the first order term. To this end, we use the notation used in Section 3.3. In particular, we will use the notation $\gamma^{\rm f,b}_I(\sigma)$ and $\lambda^{3,4}_I(\sigma)$ defined in (33). Analogously we define their corresponding t-component of the flow as

$$\begin{aligned}
\widetilde{\gamma}^*_I(\sigma) &= \widetilde{\Phi}_0\{\sigma,(\mathcal{C}^{*,L}_0(I),\mathcal{C}^{*,\ell}_0(I),\mathcal{C}^{*,G}_0(I),0)\},\ \ *={\rm f,b}\\
\widetilde{\lambda}^j_I(\sigma) &= \widetilde{\Phi}_0\{\sigma,(\mathcal{G}^{j,L}_0(I),\mathcal{G}^{j,\ell}_0(I),\mathcal{G}^{j,G}_0(I),0)\},\ \ j=3,4
\end{aligned} \tag{72}$$

where $\widetilde{\Phi}_0$ has been defined in (37) and $\mathcal{C}^*_0$ and $\mathcal{G}^j_0$ have been given in Corollary 3.2.

Lemma 4.9. *The outer map defined in* (71) *has the following expansion with respect to* e_0*,*

$$\mathcal{F}^{{\rm out},*}_{e_0} : \begin{pmatrix} I\\ t\end{pmatrix} \mapsto \begin{pmatrix} I+e_0\left(B^{*,+}(I)e^{it}+B^{*,-}(I)e^{-it}\right)+\mathcal{O}\left(e_0^2\right)\\ t+\mu\omega^*(I)+\mathcal{O}(e_0)\end{pmatrix},\ \ *={\rm f,b}. \tag{73}$$

Moreover, the functions $B^{*,\pm}(I)$ can be defined as

$$\begin{aligned} B^{\mathrm{f},\pm}(I) &= B^{\mathrm{f},\pm}_{\mathrm{out}}(I) + B^{\mathrm{f},\pm}_{\mathrm{in}}(I) e^{\pm i\mu\omega^{\mathrm{f}}_{\mathrm{out}}(I)} \\ B^{\mathrm{b},\pm}(I) &= B^{\mathrm{b},\pm}_{\mathrm{in}}(I) + B^{\mathrm{b},\pm}_{\mathrm{out}}(I) e^{\pm i\mu\omega^{\mathrm{b}}_{\mathrm{in}}(I)}, \end{aligned} \tag{74}$$

where $\omega^{\mathrm{f}}_{\mathrm{out}}(I)$ and $\omega^{\mathrm{b}}_{\mathrm{in}}(I)$ are the functions defined in (34) *and* (36) *respectively and*

$$\begin{aligned} B^{\mathrm{f},\pm}_{\mathrm{out}}(I) = \pm i\mu \lim_{T\to+\infty} \int_0^T \Bigg(& \frac{\Delta H^{1,\pm}_{\mathrm{ell}} \circ \gamma^{\mathrm{f}}_I(\sigma)}{-1+\mu\partial_G \Delta H_{\mathrm{circ}} \circ \gamma^{\mathrm{f}}_I(\sigma)} e^{\pm i\widetilde{\gamma}^{\mathrm{f}}_I(\sigma)} \\ & - \frac{\Delta H^{1,\pm}_{\mathrm{ell}} \circ \lambda^3_I(\sigma)}{-1+\mu\partial_G \Delta H_{\mathrm{circ}} \circ \lambda^3_I(\sigma)} e^{\pm i\left(\widetilde{\lambda}^3_I(\sigma)+\mu\omega^{\mathrm{f}}_+(I)\right)} \Bigg) d\sigma \\ \mp i\mu \lim_{T\to-\infty} \int_0^T \Bigg(& \frac{\Delta H^{1,\pm}_{\mathrm{ell}} \circ \gamma^{\mathrm{f}}_I(\sigma)}{-1+\mu\partial_G \Delta H_{\mathrm{circ}} \circ \gamma^{\mathrm{f}}_I(\sigma)} e^{\pm i\widetilde{\gamma}^{\mathrm{f}}_I(\sigma)} \\ & - \frac{\Delta H^{1,\pm}_{\mathrm{ell}} \circ \lambda^4_I(\sigma)}{-1+\mu\partial_G \Delta H_{\mathrm{circ}} \circ \lambda^4_I(\sigma)} e^{\pm i\left(\widetilde{\lambda}^4_I(\sigma)+\mu\omega^{\mathrm{f}}_-(I)\right)} \Bigg) d\sigma, \end{aligned} \tag{75}$$

$$\begin{aligned} B^{\mathrm{b},\pm}_{\mathrm{out}}(I) = \pm i\mu \lim_{T\to+\infty} \int_0^T \Bigg(& \frac{\Delta H^{1,\pm}_{\mathrm{ell}} \circ \gamma^{\mathrm{b}}_I(\sigma)}{-1+\mu\partial_G \Delta H_{\mathrm{circ}} \circ \gamma^{\mathrm{b}}_I(\sigma)} e^{\pm i\widetilde{\gamma}^{\mathrm{b}}_I(\sigma)} \\ & - \frac{\Delta H^{1,\pm}_{\mathrm{ell}} \circ \lambda^4_I(\sigma)}{-1+\mu\partial_G \Delta H_{\mathrm{circ}} \circ \lambda^4_I(\sigma)} e^{\pm i\left(\widetilde{\lambda}^4_I(\sigma)+\mu\omega^{\mathrm{b}}_+(I)\right)} \Bigg) d\sigma \\ \mp i\mu \lim_{T\to-\infty} \int_0^T \Bigg(& \frac{\Delta H^{1,\pm}_{\mathrm{ell}} \circ \gamma^{\mathrm{b}}_I(\sigma)}{-1+\mu\partial_G \Delta H_{\mathrm{circ}} \circ \gamma^{\mathrm{b}}_I(\sigma)} e^{\pm i\widetilde{\gamma}^{\mathrm{b}}_I(\sigma)} \\ & - \frac{\Delta H^{1,\pm}_{\mathrm{ell}} \circ \lambda^3_I(\sigma)}{-1+\mu\partial_G \Delta H_{\mathrm{circ}} \circ \lambda^3_I(\sigma)} e^{\pm i\left(\widetilde{\lambda}^3_I(\sigma)+\mu\omega^{\mathrm{b}}_-(I)\right)} \Bigg) d\sigma, \end{aligned} \tag{76}$$

$$\begin{aligned} B^{\mathrm{f},\pm}_{\mathrm{in}}(I) &= \mp i\mu \int_0^{-12\pi} \frac{\Delta H^{1,\pm}_{\mathrm{ell}} \circ \lambda^4_I(\sigma)}{-1+\mu\partial_G \Delta H_{\mathrm{circ}} \circ \lambda^4_I(\sigma)} e^{\pm i\widetilde{\lambda}^4_I(\sigma)} d\sigma \\ B^{\mathrm{b},\pm}_{\mathrm{in}}(I) &= \mp \int_0^{-2\pi} \frac{\Delta H^{1,\pm}_{\mathrm{ell}} \circ \lambda^3_I(\sigma)}{-1+\mu\partial_G \Delta H_{\mathrm{circ}} \circ \lambda^3_I(\sigma)} e^{\pm i\widetilde{\lambda}^3_I(\sigma)} d\sigma \end{aligned} \tag{77}$$

where

$$\Delta H^{1,\pm}_{\mathrm{ell}}(\ell, L, g, G, t) = \Delta H^{1,\pm}_{\mathrm{ell}}(\ell, L, g, G) e^{it} + \Delta H^{1,\pm}_{\mathrm{ell}}(\ell, L, g, G) e^{-it}$$

has been defined in Corollary 4.5 and $\omega^*_\pm$ have been defined in (35)*.*

Proof. To prove the lemma recall that the outer maps are the composition of two maps. Indeed, as we have explained in Section 3.3, they are defined as

$$\begin{aligned} \mathcal{F}^{\mathrm{out,f}}_{e_0} &= \mathcal{P}^6_{e_0} \circ \mathcal{S}^{\mathrm{f}}_{e_0} : \widetilde{\Lambda}^3_0 \longrightarrow \widetilde{\Lambda}^3_0 \\ \mathcal{F}^{\mathrm{out,b}}_{e_0} &= \mathcal{S}^{\mathrm{b}}_{e_0} \circ \mathcal{P}_{e_0} : \widetilde{\Lambda}^3_0 \longrightarrow \widetilde{\Lambda}^3_0. \end{aligned}$$

Thus, we will study both maps perturbatively and then the composition of them will lead to the proof of the lemma. We only deal with $\mathcal{F}^{\mathrm{out,f}}_{e_0}$ since the proof for $\mathcal{F}^{\mathrm{out,b}}_{e_0}$ can be done analogously.

To study $\mathcal{S}^{\rm f}_{e_0}:\widetilde{\Lambda}^3_0\longrightarrow\widetilde{\Lambda}^4_0$ we use the Definition 3.4 of the (heteroclinic) outer map. Let us consider points $z\in\widetilde{\Gamma}^*_{e_0}$, $x_+\in\widetilde{\Lambda}^4_{e_0}$ and $x_-\in\widetilde{\Lambda}^3_{e_0}$ such that

$$\operatorname{dist}\left(\mathcal{P}^n_{e_0}(z),\mathcal{P}^n_{e_0}(x_\pm)\right)<C\lambda^{-|n|}\qquad\text{for } n\in\mathbb{Z}^\pm$$

for certain constants $C>0$ and $\lambda>1$. Using the parameterizations of $\widetilde{\Gamma}^{\rm f}_{e_0}$ and $\widetilde{\Lambda}^j_{e_0}$, $j=3,4$, given in Theorem 4, we can write the points z and $x_\pm$ in coordinates as $z=\mathcal{C}_{e_0}(I_0,t_0)$, $x_+=\mathcal{G}^4_{e_0}(I_+,t_+)$ and $x_-=\mathcal{G}^3_{e_0}(I_-,t_-)$. Then, the I-component of the outer map is just given by the relation

$$\mathcal{F}^{{\rm out},I}_{e_0}(I_-,t_-)=I_+=I_-+(I_+-I_-).$$

To measure I_+-I_- we first deal with $I_0-I_\pm$. Consider the flow Φ_{e_0} associated to the reduced elliptic problem (41). Then, applying Fundamental Theorem of Calculus

$$\begin{aligned}
I_0-I_+&=\lim_{T\to-\infty}\int_T^0\left(\frac{d}{ds}\Phi_{e_0}\left\{s,\mathcal{C}^{\rm f}_{e_0}(I_0,t_0)\right\}-\frac{d}{ds}\Phi_{e_0}\left\{s,\mathcal{G}^4_{e_0}(I_+,t_+)\right\}\right)ds\\
I_0-I_-&=\lim_{T\to+\infty}\int_T^0\left(\frac{d}{ds}\Phi_{e_0}\left\{s,\mathcal{C}^{\rm f}_{e_0}(I_0,t_0)\right\}-\frac{d}{ds}\Phi_{e_0}\left\{s,\mathcal{G}^3_{e_0}(I_-,t_-)\right\}\right)ds
\end{aligned}$$

Note that the changed signs in the limits come from the fact that system (41) has the time reversed.

Using the perturbative expansions of $\mathcal{C}^{\rm f}_{e_0}$ and $\Lambda^j_{e_0}$ given in Theorem 4, equation (41), the perturbative expansion of the Hamiltonian (16) given in Corollary 4.5 and the perturbation of the flow Φ_{e_0} given in Lemma 4.6, one can see that

$$\begin{aligned}
I_0-I_+=-e_0\lim_{T\to-\infty}\int_T^0\Bigg(&\left.\frac{\mu\partial_t\Delta H^1_{\rm ell}(L,\ell,G,g,t)}{-1+\mu\partial_G\Delta H_{\rm circ}(L,\ell,G,g)}\right|_{(L,\ell,G,g,t)=(\Phi_0^{\rm circ},\Phi_0^t)\left\{s,\mathcal{C}^{\rm f}_0(I_0,t_0)\right\}}\\
&-\left.\frac{\mu\partial_t\Delta H^1_{\rm ell}(L,\ell,G,g,t)}{-1+\mu\partial_G\Delta H_{\rm circ}(L,\ell,G,g)}\right|_{(L,\ell,G,g,t)=(\Phi_0^{\rm circ},\Phi_0^t)\left\{s,\mathcal{G}^4_0(I_+,t_+)\right\}}\Bigg)ds+\mathcal{O}\left(e_0^2\right)\\
I_0-I_-=-e_0\lim_{T\to+\infty}\int_T^0\Bigg(&\left.\frac{\mu\partial_t\Delta H^1_{\rm ell}(L,\ell,G,g,t)}{-1+\mu\partial_G\Delta H_{\rm circ}(L,\ell,G,g)}\right|_{(L,\ell,G,g,t)=(\Phi_0^{\rm circ},\Phi_0^t)\left\{s,\mathcal{C}^{\rm f}_0(I_0,t_0)\right\}}\\
&-\left.\frac{\mu\partial_t\Delta H^1_{\rm ell}(L,\ell,G,g,t)}{-1+\mu\partial_G\Delta H_{\rm circ}(L,\ell,G,g)}\right|_{(L,\ell,G,g,t)=(\Phi_0^{\rm circ},\Phi_0^t)\left\{s,\mathcal{G}^3_0(I_-,t_-)\right\}}\Bigg)ds+\mathcal{O}\left(e_0^2\right).
\end{aligned}$$

where $\Phi_0^{\rm circ}$ and Φ_0^t have been defined in (32) and (37) respectively.

Taking into account that in Corollary 4.5 we have proved that $\Delta H^1_{\rm ell}$ satisfies $\mathcal{N}\left(\Delta H^1_{\rm ell}\right)=\{\pm1\}$, one can easily obtain the formula for $B^{{\rm f},\pm}_{\rm out}$ in (75).

To obtain the formula for $B^{{\rm f},\pm}_{\rm in}$ one can proceed as in the study of the inner map in Section 4.1. Finally, to obtain the formula for $B^{{\rm f},\pm}$ it is enough to compose both maps $\mathcal{P}^6_{e_0}$ and $\mathcal{S}^{\rm f}_{e_0}$. □

5 Existence of diffusing orbits

The main result of this section is the following.

Theorem 6. *For any $\delta>0$ there exists $e_0^*>0$ and $C>0$ such that for any $0<e_0<e_0^*$ the map $\mathcal{P}_{e_0}$ in (42) has a collection of invariant 1-dimensional tori $\{\mathbb{T}_i\}_{i=1}^N\subset\tilde{\Lambda}^3_{e_0}$ such that*

- $\mathbb{T}_1 \cap \{I = I_- + \delta\} \neq \emptyset$ *and* $\mathbb{T}_N \cap \{I = I_+ - \delta\} \neq \emptyset$.
- *Hausdorff* $\operatorname{dist}(\mathbb{T}_i, \mathbb{T}_{i+1}) < Ce_0^{3/2}$.
- *These tori form a transition chain. Namely,* $W^u_{\mathbb{T}_i} \pitchfork W^s_{\mathbb{T}_{i+1}} \neq \emptyset$ *for each* $i = 1, \dots, N-1$.

Proof. Once we have computed the first orders in e_0 of both the outer and inner maps, we want to understand their properties and compare their dynamics. To make this comparison we will perform two steps of averaging [AKN88, LM88]. This change of coordinates will straighten the I-component of the inner map at order $\mathcal{O}(e_0^3)$ in such a way that with the new system of coordinates will be easier to compare the dynamics of both maps. Nevertheless, before performing averaging, we have to perform a preliminary change of coordinates to straighten the symplectic form $\Omega^3_{e_0}$ to deal with the canonical form $dI \wedge dt$.

Lemma 5.1. *There exists a* e_0*-close to the identity change of variables*

$$(I, t) = \left(I', t'\right) + e_0 \varphi_1 \left(I', t'\right), \tag{78}$$

defined on $\widetilde{\Lambda}^3_{e_0}$*, which transforms the symplectic form* $\Omega^3_{e_0}$ *defined in* (45) *into the canonical form*

$$\Omega_0 = dI' \wedge dt'.$$

In the new coordinates,

- *The inner map* $\mathcal{F}^{\text{in}}_{e_0}$ *in* (46) *reads*

$$\mathcal{F}^{\text{in}'}_{e_0} : \begin{pmatrix} I' \\ t' \end{pmatrix} \mapsto \begin{pmatrix} I' + e_0 A_1 \left(I', t'\right) + e_0^2 A_2' \left(I', t'\right) + \mathcal{O}\left(\mu e_0^3\right) \\ t' + \mu \mathcal{T}_0 \left(I'\right) + e_0 \mathcal{T}_1' \left(I', t'\right) + e_0^2 \mathcal{T}_2' \left(I', t'\right) + \mathcal{O}\left(\mu e_0^3\right) \end{pmatrix} \tag{79}$$

  where A_1 *is the function given in Lemma 4.7 and* A_2', $\mathcal{T}_1'$ *and* $\mathcal{T}_2'$ *satisfy*

$$\mathcal{N}\left(A_2'\right) = \{0, \pm 1, \pm 2\}, \ \mathcal{N}\left(\mathcal{T}_1'\right) = \{\pm 1\} \ \text{ and } \ \mathcal{N}\left(\mathcal{T}_2'\right) = \{0, \pm 1, \pm 2\}.$$

- *The outer maps* $\mathcal{F}^{\text{out,f}}_{e_0}$ *and* $\mathcal{F}^{\text{out,b}}_{e_0}$ *in* (49) *read*

$$\mathcal{F}^{\text{out},*'}_{e_0} : \begin{pmatrix} I' \\ t' \end{pmatrix} \mapsto \begin{pmatrix} I' + e_0 B^* \left(I', t'\right) + \mathcal{O}\left(\mu e_0^2\right) \\ t' + \mu \omega^*(I') + \mathcal{O}(\mu e_0) \end{pmatrix}, \ * = \text{f}, \text{b}, \tag{80}$$

  where B^* *are the functions given in Lemma 4.9.*

Proof. We will see that there exists a change of coordinates of the form

$$\begin{cases} I = I' + e_0^2 f_2 \left(I', t'\right) + \mathcal{O}\left(e_0^3\right) \\ t = t' + e_0 g_1 \left(I', t'\right) + e_0^2 g_2 \left(I', t'\right) + \mathcal{O}\left(e_0^3\right) \end{cases} \tag{81}$$

with

$$\mathcal{N}(g_1) = \{\pm 1\}, \ \mathcal{N}(g_2) = \{0, \pm 1, \pm 2\} \ \text{ and } \ \mathcal{N}(f_2) = \{0, \pm 1, \pm 2\}, \tag{82}$$

which straightens the symplectic form $\Omega^3_{e_0}$. In fact, we look for the inverse change. Namely, we look for a change of variables of the form

$$\begin{cases} I' = I + e_0^2 \widetilde{f}_2 \left(I, t\right) + e_0^3 \widetilde{f}_{\geq}(I, t) \\ t' = t + e_0 \widetilde{g}_1 \left(I, t\right) \end{cases} \tag{83}$$

such that the pullback of $\Omega_0 = dI' \wedge dt'$ with respect to this change is the symplectic form $\Omega^3_{e_0}$. Even if we do not write it explicitly, $\widetilde{f}_{\geq}$ depends on e_0. To obtain this change, it is enough to solve the equations

$$\begin{aligned}\partial_t \widetilde{g}_1 &= a_1^3\\ \partial_I \widetilde{f}_2 &= a_2^3\\ \partial_I \widetilde{f}_{\geq} &= b\end{aligned}$$

where

$$b = a^3_{\geq} - \partial_t \widetilde{g}_1 \partial_I \widetilde{f}_2 - e_0 \partial_t \widetilde{g}_1 \partial_I \widetilde{f}_{\geq} + \partial_I \widetilde{g}_1 \partial_t \widetilde{f}_2 + e_0 \partial_I \widetilde{g}_I \partial_t \widetilde{f}_{\geq}$$

and a_1^3, a_2^3 and $a^3_{\geq}$ are the functions considered in (45). These equations can be solved iteratively.

Recall that by Corollary 4.8 we have that $\mathcal{N}(a_1^3) = \{\pm 1\}$. Then, one can take $\widetilde{g}_1$ as the primitive of a_1^3 with zero average, which satisfies

$$\mathcal{N}\left(\widetilde{g}_1\right) = \{\pm 1\}. \tag{84}$$

The other equations can be solved taking

$$\begin{aligned}\widetilde{f}_2(I,t) &= \int_0^I a_2^3(J,t)dJ\\ \widetilde{f}_{\geq}(I,t) &= \int_0^I b(J,t)dJ.\end{aligned}$$

Note that b depends on $\widetilde{g}_1$ and $\widetilde{f}_2$, which have been already obtained. Since by Corollary 4.8 we have that $\mathcal{N}(a_2^3) = \{0, \pm 1, \pm 2\}$, one can deduce that

$$\mathcal{N}\left(\widetilde{f}_2\right) = \{0, \pm 1, \pm 2\}. \tag{85}$$

To obtain the change (81) it is enough to invert the change (83). Then, formulas (84) and (85) imply (82).

To finish the proof it only remains to check the properties of the inner and outer maps in the new coordinates. To this end one only needs to take into account (82). □

Once we have straightened the symplectic form, we can perform two steps of averaging to the inner map.

Lemma 5.2. *There exists a e_0-close to the identity symplectic change of variables*

$$\left(I', t'\right) = (\mathcal{I}, \tau) + e_0 \varphi_2(\mathcal{I}, \tau) \tag{86}$$

defined on $\widetilde{\Lambda}^3_{e_0}$, which:

- *Transforms the inner map $\mathcal{F}^{\mathrm{in}'}_{e_0}$ in (79) into*

$$\widetilde{\mathcal{F}}^{\mathrm{in}}_{e_0} : \begin{pmatrix} \mathcal{I} \\ \tau \end{pmatrix} \mapsto \begin{pmatrix} \mathcal{I} + \mathcal{O}\left(\mu e_0^3\right) \\ \tau + \mu \mathcal{T}_0\left(\mathcal{I}\right) + e_0^2 \widetilde{\mathcal{T}}_2\left(\mathcal{I}\right) + \mathcal{O}\left(\mu e_0^3\right) \end{pmatrix} \tag{87}$$

- *Transforms the outer maps* $\mathcal{F}_{e_0}^{\mathrm{out,f}'}$ *and* $\mathcal{F}_{e_0}^{\mathrm{out,b}'}$ *in* (80) *into*

$$\widetilde{\mathcal{F}}_{e_0}^{\mathrm{out},*} : \begin{pmatrix} \mathcal{I} \\ \tau \end{pmatrix} \mapsto \begin{pmatrix} \mathcal{I} + e_0 \widetilde{B}^*(\mathcal{I},\tau) + \mathcal{O}\left(\mu e_0^2\right) \\ \tau + \mu\omega^*(\mathcal{I}) + \mathcal{O}(\mu e_0) \end{pmatrix}, \quad * = \mathrm{f}, \mathrm{b}, \tag{88}$$

where

$$\widetilde{B}^*\left(\mathcal{I},\tau\right) = \widetilde{B}^{*,+}\left(\mathcal{I}\right) e^{i\tau} + \widetilde{B}^{*,-}\left(\mathcal{I}\right) e^{-i\tau}$$

with

$$\widetilde{B}^{*,\pm}\left(\mathcal{I}\right) = B^{*,\pm}\left(\mathcal{I}\right) - \frac{e^{\pm i\mu\omega^*(\mathcal{I})} - 1}{e^{\pm i\mu\mathcal{T}_0(\mathcal{I})} - 1} A_1^{\pm}\left(\mathcal{I}\right).$$

Moreover, these functions satisfy

$$\widetilde{B}^{*,\pm}\left(\mathcal{I}\right) \neq 0 \qquad \text{for } \mathcal{I} \in \mathcal{D}^*, \tag{89}$$

where $\mathcal{D}^*$ *are the domains considered in Corollary 3.2.*

Note that we can do two steps of averaging globally in the whole cylinder $\widetilde{\Lambda}_{e_0}$ due to the absence of resonances in the first orders in e_0. Namely, there are no *big gaps*. This is quite in contrast with the typical situation in Arnold diffusion (see e.g. [DdlLS06]).

Proof. We perform two steps of (symplectic) averaging. To this end we consider a generating function of the form

$$\mathcal{S}(\mathcal{I}, t') = \mathcal{I}t' + e_0\mathcal{S}_1(\mathcal{I}, t') + e_0^2\mathcal{S}_2(\mathcal{I}, t'),$$

which defines the change (86) implicitly as

$$\begin{aligned} I &= \mathcal{I} + e_0\partial_{t'}\mathcal{S}_1(\mathcal{I}, t') + e_0^2\partial_{t'}\mathcal{S}_2(\mathcal{I}, t') \\ \tau &= t' + e_0\partial_{\mathcal{I}}\mathcal{S}_1(\mathcal{I}, t') + e_0^2\partial_{\mathcal{I}}\mathcal{S}_2(\mathcal{I}, t'). \end{aligned}$$

By Theorem 3.3 we have (27) and by Theorem 5 we know which t'-harmonics have the functions A_i and $\mathcal{T}_i$. Then, it is easy to see that the functions $\mathcal{S}_i$ that correspond to two steps of averaging are globally defined in $\widetilde{\Lambda}_{e_0}^3$. Moreover, in these new variables, taking into account that the inner map is exact symplectic, one can see that the inner map is of the form (87).

To obtain a perturbative expression for the outer maps $\widetilde{\mathcal{F}}_{e_0}^{\mathrm{out},*}$, we need to know $\mathcal{S}_1$ explicitly. It is given by

$$\mathcal{S}_1(\mathcal{I}, t) = -\frac{iA_1^+(\mathcal{I})}{e^{i\mu\mathcal{T}_0(\mathcal{I})} - 1} e^{it} + \frac{iA_1^-(\mathcal{I})}{e^{-i\mu\mathcal{T}_0(\mathcal{I})} - 1} e^{-it}.$$

If we apply this change to the outer maps $\mathcal{F}_{e_0}^{\mathrm{out},*}$ in (73), we obtain (88).

The statement (89) is based on convincing numerical data (see Appendix C.3). □

In the new coordinates $(\mathcal{I}, \tau)$ the inner map $\widetilde{\mathcal{F}}_{e_0}^{\mathrm{in}}$ in (87) is a e_0^3-close to integrable map. Moreover, thanks to Theorem 3.3 is twist and therefore we can apply KAM theory to proof the existence of invariant curves in $\widetilde{\Lambda}_{e_0}^3$. We use a version of the KAM Theorem from [DdlLS00] (see also [Her83]).

KAM theorem. *Let* $f : [0,1] \times \mathbb{T} \to [0,1] \times \mathbb{T}$ *be an exact symplectic* $\mathcal{C}^l$ *map with* $l > 4$. *Assume that* $f = f_0 + \delta f_1$, *where* $f_0(I, \psi) = (I, \psi + A(I))$, A *is* $\mathcal{C}^l$, $|\partial_I A| > M$ *and* $\|f_1\|_{\mathcal{C}^l} \leq 1$. *Then, if* $\delta^{1/2}M^{-1} = \rho$ *is sufficiently small, for a set of* ω *of Diophantine numbers of exponent* $\theta = 5/4$, *we can find invariant tori which are the graph of* $\mathcal{C}^{l-3}$ *functions* u_ω, *the motion on them is* $\mathcal{C}^{l-3}$

conjugate to the rotation by ω*, and* $\|u_\omega\|_{\mathcal{C}^{l-3}} \leq C\delta^{1/2}$.

Applying this theorem to the map $\widetilde{\mathcal{F}}_{e_0}^{\text{in}}$ we obtain the KAM tori (see Remark 4.1 for the matter of regularity). Moreover, this theorem ensures that the distance between these tori is no bigger than $e_0^{3/2}$. Then, the results of Lemma 5.2 and KAM theorem lead to the existence of a transition chain of invariant tori.

The transition chain is obtained comparing the outer and inner dynamics. We do this comparison in the coordinates $(\mathcal{I}, \tau)$ given by Lemma 5.2 and therefore we deal with the maps $\widetilde{\mathcal{F}}_{e_0}^{\text{in}}$ and $\widetilde{\mathcal{F}}_{e_0}^{\text{out},*}$ in (87) and (88) respectively.

KAM theorem ensures that there exists a torus $\mathbb{T}_1$ such that $\mathbb{T}_1 \cap \{I = I_- - \delta\} \neq \emptyset$. Then, either $\widetilde{\mathcal{F}}_{e_0}^{\text{out,f}}$ or $\widetilde{\mathcal{F}}_{e_0}^{\text{out,b}}$ are defined for points in $\mathbb{T}_1$. Assume, without loss of generality that $\widetilde{\mathcal{F}}_{e_0}^{\text{out,f}}$ is defined for points in $\mathbb{T}_1$. Then, thanks to (89), $\mathcal{F}_{e_0}^{\text{out,f}}(\mathbb{T}_1)$ satisfies

$$\text{dist}\left(\mathbb{T}_1, \mathcal{F}_{e_0}^{\text{out,f}}(\mathbb{T}_1)\right) \geq Ce_0$$

for a constant $C > 0$ independent of e_0. Then, KAM theorem ensures that there exists a torus $\mathbb{T}_2$ such that $\mathbb{T}_2 \cap \mathcal{F}_{e_0}^{\text{out,f}}(\mathbb{T}_1) \neq 0$. Iterating this procedure, choosing at each step either $\widetilde{\mathcal{F}}_{e_0}^{\text{out,f}}$ or $\widetilde{\mathcal{F}}_{e_0}^{\text{out,b}}$, one obtains the transition chain. □

To finish the proof of Theorem 2 it only remains to prove the existence of a diffusing orbit using a shadowing method. We use a result stated in [FM00].

Lemma 5.3. *Let* f *be a* $\mathcal{C}^1$ *sympletic map in a* $2(d+1)$ *symplectic manifold. Assume that the map leaves invariant a* $\mathcal{C}^1$ d*-dimensional torus* τ *and the motion on the torus is an irrational rotation. Let* Γ *be a* $d+1$ *manifold intersecting* W_τ^u *transversally. Then,*

$$W_\tau^s \subset \overline{\bigcup_{i>0} f^{-i}(\Gamma)}.$$

An immediate consequence of this lemma is that any finite transtion chain can be shadowed by a true orbit, which finishes the proof of Theorem 2.

In terms of the elliptical elements of the asteroid, such a diffusing orbit can now be described as follows. The orbit starts near the resonant cylinder Λ. The eccentricity of the primaries is small: this is an essential feature of both the proof above and the qualitative behavior of the orbit. So, over a time interval of length $\ll 1/e_0$, the orbit closely follows a hyperbolic periodic orbit of the circular problem. The semi major axis is roughly constant equal to $7^{2/3}$ and the Jacobi constant to -1.81. The asteroid turns around the primaries, making one full turn over a time interval of length 7. In the frame rotating approximately with the primaries, the Keplerian ellipse itself of the asteroid rotates counterclockwise with fast frequency ~ -1; in the inertial frame of reference, it rotates only μ-slowly (see e.g. [AKN88, Féj02]), while the eccentricity e slowly oscillates around $e = 0.48$.

At some point (as soon as we can if we want to save time), the orbit undergoes a heteroclinic excursion, during which a heteroclinic orbit is shadowed over a time interval of size $\mathcal{O}(-\ln(\mu e_0)/\sqrt{\mu})$. During this excursion, the semi major axis itself undergoes an oscillation of magnitude $\mathcal{O}(\sqrt{\mu})$, eventually coming back to its initial approximate value $7^{2/3}$. On the other hand, the Jacobi constant and the eccentricity have increased by $\mathcal{O}(\mu e_0)$. Excursions may then repeat, piling up changes in the eccentricity to reach the value $e = 0.66$ in finite time.

A Numerical study of the hyperbolic cylinder of the circular problem.

We devote this appendix to the numerical study of the hyperbolic invariant manifold of the circular problem given in Corollary 3.1 and its invariant manifolds. In other words, we show numerical results which justify the properties of the circular problem stated in Theorem 3.

Numerical analysis has several sources of error: mainly round-off errors in computer arithmetics, and approximations of ideal mathematical objects (e.g. linear approximation of local stable/unstable manifolds). In our analysis, we have tried to evaluate such errors, and check that they are appropriately small. We do *not* claim to give a fully rigorous proof of Theorem 3, which would require Computer-Assisted techniques as in [WZ03]. Indeed, we have focused our efforts to keep the numerics relatively simple and, hopefully, convincing. One could think of several possible numerical computations to prove our result. The most numerically demanding one would be to check directly that some given orbit has an adequate drift of eccentricity. This computation would not bring much light to the mechanism of instability, and moreover it would involve formidable numerical analysis problems, due to the necessarily very long time of integration. On the contrary, our line of proof allows us to use numerical verifications involving only orbits of the circular problem –a dramatic simplification, as we will see below.

Let us make a few more specific comments on the strategy of our numerical analysis. As mentioned in Section 3, the circular problem has a conserved quantity, the Jacobi constant which we denote by J (see (5)), which corresponds to energy when the system is expressed in rotating coordinates. Thus it is natural to fix the Jacobi constant $J = J_0$ and perform our analysis for a given J_0. This allows us to reduce the dimension of the computations by one. Finally, we let J vary and repeat the computations for all J in the range of interest $J \in [J_-, J_+]$.

Another important comment is on the choice of coordinates. For numerics we prefer Cartesian coordinates, since the equations of motion are explicit in these coordinates. Thus we carry out our computations of the hyperbolic structure of the circular problem in Cartesian (Appendix A).

On the other hand, for perturbative analysis we have used Delaunay coordinates throughout this paper. Thus, in Appendix B we explain how to change coordinates from Cartesian to Delaunay, and we carry out our computations of the inner and outer maps of the circular and elliptic problems in Delaunay (Appendix C).

Regarding the integration method, we use a variable-order Taylor method specially generated to integrate the equations of motion and variational equations of the circular problem. The Taylor method has been generated using the "taylor" package of À. Jorba and M. Zou (see `http://www.maia.ub.es/~angel/taylor/`). The main advantage of using a Taylor method is that it is very fast for long-time integrations (without sacrificing accuracy).

A.1 Computation of the periodic orbits

Consider the circular problem in rotating Cartesian coordinates

$$J(x, y, p_x, p_y) = \frac{1}{2}(p_x^2 + p_y^2) + yp_x - xp_y - \frac{1-\mu}{r_1} - \frac{\mu}{r_2}, \tag{90}$$

where

$$r_1^2 = (x - \mu_2)^2 + y^2,$$
$$r_2^2 = (x + \mu_1)^2 + y^2.$$

Recall that the energy of the circular problem in rotating coordinates coincides with the Jacobi constant J in (5). From now on in this appendix we will refer to J as the energy of the system.

We follow the convention to place the large mass (Sun) to the left of the origin, and the small mass (Jupiter) to the right. (This is opposite to the astrodynamics convention). Thus we choose $\mu_1 = \mu$ as the small mass, and $\mu_2 = 1 - \mu$ as the large mass. Notice that equation (90) is reversible with respect to the involution

$$R(x, p_x, y, p_y) = (x, -p_x, -y, p_y). \tag{91}$$

Thus, a solution of the system is symmetric if and only if it intersects the symmetry axis $\mathrm{Fix}(R) = \{y = 0,\ p_x = 0\}$. This symmetry will facilitate our numerical computations. Note that the involution R is just the involution (20) expressed in rotating Cartesian coordinates.

Let the energy be fixed to $J = J_0$. We look for a resonant periodic orbit λ_{J_0} of (90) in the level of energy J_0. As a first approximation to λ_{J_0}, we look for a resonant periodic orbit of the two-body problem, i.e. of the Hamiltonian (19) with $\mu = 0$. Let us denote the approximate periodic orbit by $\tilde{\lambda}_{J_0} = (L, \ell, G, g)$. The actions L and G are determined by the resonant condition $L^3 = 7$ and energy condition $-\frac{1}{2L^2} - G = J_0$. To determine $\tilde{\lambda}_{J_0}$ completely, we choose that the asteroid is initially at the perihelion, i.e. we impose an initial condition $\tilde{\lambda}_{J_0}(0) = (L^0, \ell^0, G^0, g^0)$ with $\ell^0 = 0$ and $g^0 = 0$. Switching to Cartesian coordinates, we obtain an initial condition (x^0, p_x^0, y^0, p_y^0) with $p_x^0 = 0$ and $y^0 = 0$.

Next we refine the trajectory $\tilde{\lambda}_{J_0}$ into a true periodic orbit λ_{J_0} for the system (90) with $\mu = 10^{-3}$. Consider the Poincaré section

$$\Sigma^+ = \{y = 0,\ p_y > 0\}$$

in the circular problem (90), and let $P\colon\ \Sigma^+ \to \Sigma^+$ be the associated Poincaré map. Since we are in rotating coordinates, this section corresponds to collinear configurations of the three bodies.

Remark A.1. In numerical integrations, we use a variable-order Taylor method with local error tolerance 10^{-16}. Moreover, a point is considered to be on the Poincaré section whenever $|y| < 10^{-16}$ and $p_y > 0$.

Furthermore, the momentum variable p_y can be eliminated. Indeed, since $\partial_{p_y} J \neq 0$, p_y in the region of the phase space we deal with, it can be recovered from the other variables using the energy condition $J(x, p_x, y, p_y) = J_0$. Hence, the Poincaré map is a two-dimensional symplectic map at each energy level, acting only on (x, p_x).

Notice that, in the rotating frame, a 7:1 resonant periodic orbit makes 6 turns around the origin. See Figure 5. In principle, we could look for the periodic orbit as a periodic point $p = (x, p_x)$ of the Poincaré map: $p = P^6(p)$. This would imply solving a system of two equations. Thanks to the reversibility (91), in fact it is only necessary to solve one equation. Notice that our initial condition (x, p_x) is at the symmetry section $\{y = 0,\ p_x = 0\}$, so the periodic orbit must be symmetric. Thus it is enough to impose the condition that the trajectory $\lambda_{J_0}(t)$ after *half* the period is again at the symmetry section. Hence we set up the problem as simple one-dimensional root finding: we look for a point $p = (x, 0)$, such that its third iterate $P^3(p)$ has momentum $p_x = 0$:

$$\pi_{p_x}(P^3(p)) = 0.$$

(Here, $\pi_{p_x}\colon \mathbb{R}^2 \to \mathbb{R}$ is the projection onto the p_x component).

In order to solve this problem, we use a a Newton-like method. Specifically, we use a modified version of Powell's Hybrid method (see the GSL manual [G$^+$] for details) without scaling. In our

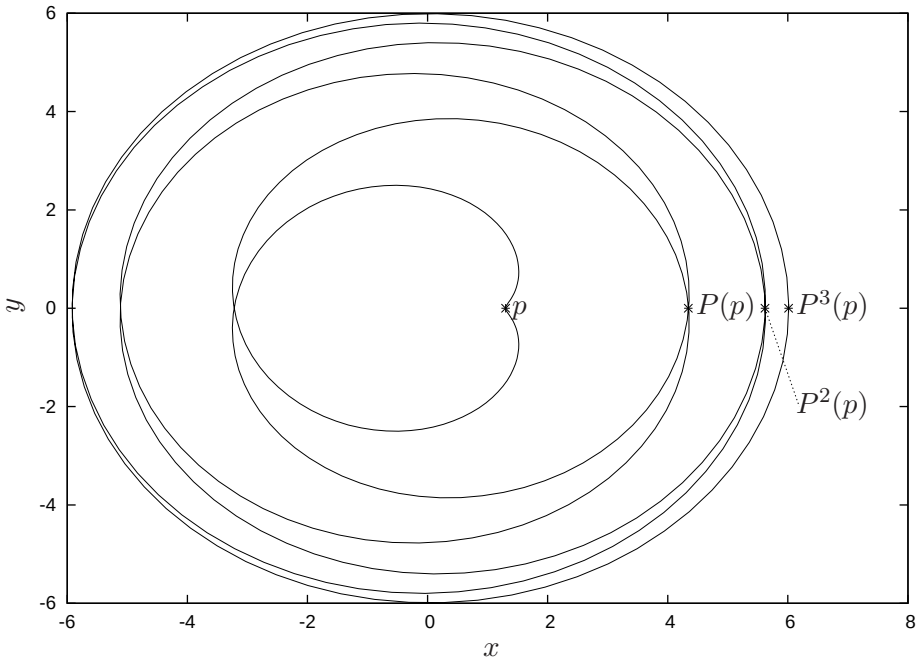

Figure 5: Resonant periodic orbit $\lambda_{-1.6}$ of the circular problem in rotating Cartesian coordinates.

computations, the Newton method converges in less than 5 iterations. As a test of the software, we have checked that the rate of convergence of the Newton method is quadratic.

Remark A.2. We ask for an accuracy of 10^{-14} in the Newton method, i.e. a point $p = (x, 0)$ is accepted as a root if and only if its third iterate $P^3(p)$ has momentum $|p_x| < 10^{-14}$.

For the Newton method, we need to compute the derivative of the Poincaré map. For each $\xi \in \mathbb{R}^4$, let $u(t, \xi)$ be the solution of the system with initial condition $u(0, \xi) = \xi$. Let $T : \Sigma^+ \to \mathbb{R}$ be the Poincaré return time. The derivative of the Poincaré map at a point $p \in \mathbb{R}^4$ is given by the partial derivative $DP(p) = u_\xi(T(p), p)$. It is well-known that $u_\xi(t, p)$ is the matrix solution of the variational equation

$$\dot{W} = Df(u(t, p))W,$$

where f is the vector field of the circular problem. We compute $DP(p)$ by numerically integrating the variational equation using the Taylor method mentioned above.

For illustration, let us show some numerical results corresponding to the energy value $J = -1.6$. The first approximation $\tilde{\lambda}_{-1.6}$ from the two-body problem has initial condition $p^0 = (x^0, p_x^0) = (1.30253\cdots, 0)$. After refining this initial condition via the Newton method, we obtain a resonant periodic orbit $\lambda_{-1.6}$ of the circular problem passing through the point $p = (x, p_x) = (1.29858\cdots, 0)$, with period $T_{-1.6} = 44.01796\cdots \sim 14\pi$. See Figure 5. The periodic orbit $\lambda_{-1.6}$ is symmetric, with the points p and $P^3(p)$ located at the symmetry section (they have $y = 0$ and $p_x = 0$). Notice that, in rotating coordinates, the trajectory of the asteroid makes 6 turns around the origin before closing up at the point p.

Finally, we let J change and, using this procedure, we are able to obtain the resonant periodic orbit for energy levels

$$J \in [\bar{J}_-, \bar{J}_+] = [-2.04, -1.56]. \tag{92}$$

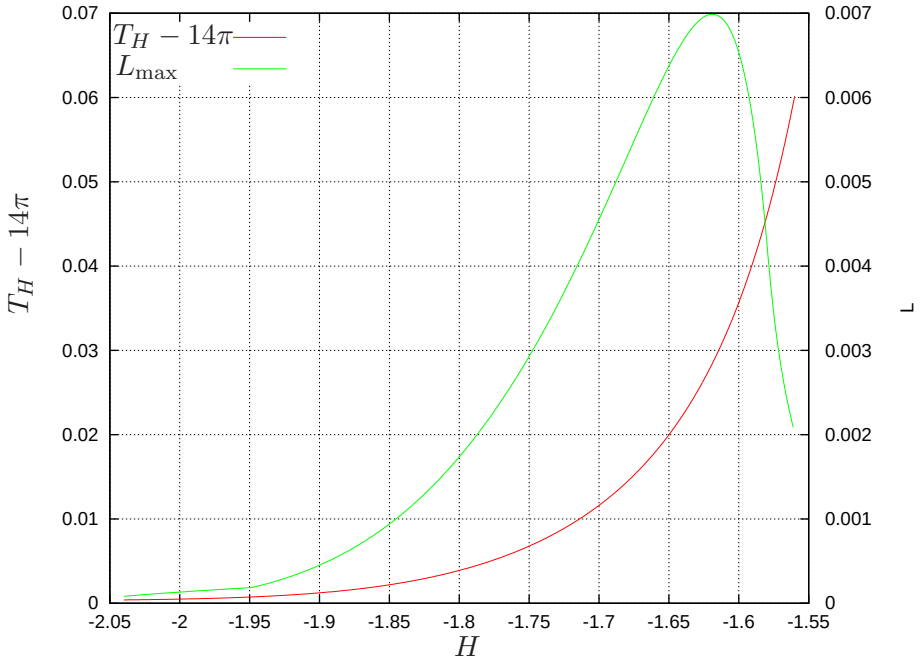

Figure 6: Resonant family of periodic orbits. We show normalized period $T_H - 14\pi$, and maximum deviation of L component with respect to the resonant value $7^{1/3}$ (see equation (93)).

See Figure 6. This family of resonant periodic orbits constitutes the normally hyperbolic invariant manifold Λ_0 given in Corollary 3.1. Notice that the period T_J stays close to the resonant period 14π of the unperturbed system. From Figure 6, we obtain the bound

$$|T_J - 14\pi| < 60\mu,$$

which is the first bound given in Theorem 3.

To determine the stability of the periodic orbit λ_{J_0}, we compute the eigenvalues λ and λ^{-1} of the matrix $DP^6(p)$, where $DP^6(p)$ is the linearization of the iterated Poincaré map P^6 about the fixed point p.

Figure 7 shows the characteristic exponents $\ln(\lambda)$, $\ln(\lambda^{-1})$ as a function of energy. The family of periodic orbits is strongly hyperbolic as $J \to \bar{J}_+$, and weakly hyperbolic as $J \to \bar{J}_-$. Note that one would expect that we are in a nearly integrable regime since μ is small. Then one would expect the eigenvalues to be close to 1. Nevertheless, in this problem the non-integrability is very noticeable when one increases μ to $\mu = 10^{-3}$. This is due to the effect of the perturbing body (Jupiter) on the asteroid, as the asteroid passes close to it.

Furthermore, we verify that (the square of) the semi-major axis L stays close to the resonant value $7^{1/3}$. Integrating the periodic orbit in Delaunay coordinates $\lambda_J(t) = (L_J(t), \ell_J(t), G_J(t), g_J(t))$ over one period T_J, we compute the quantity

$$L_{\max}(J) = \max_{t\in[0,T_J)} |L_J(t) - 7^{1/3}|. \tag{93}$$

The function $L_{\max}(J)$ is plotted in Figure 6. Notice that we obtain the bound

$$|L_J(t) - 7^{1/3}| < 7\mu$$

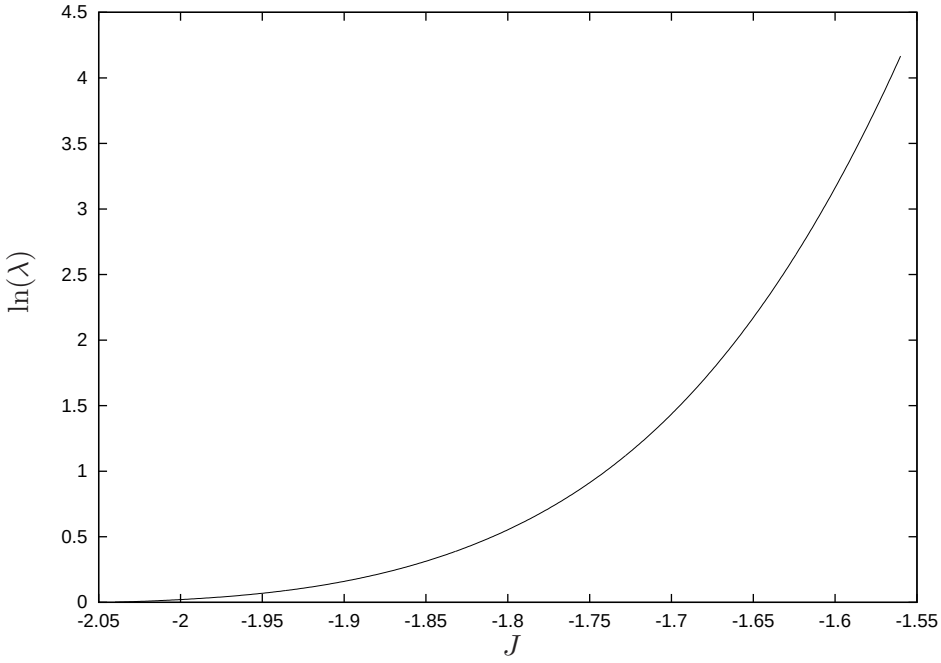

Figure 7: Characteristic exponent $\ln(\lambda)$ as a function of energy level J (the other exponent is $-\ln(\lambda)$).

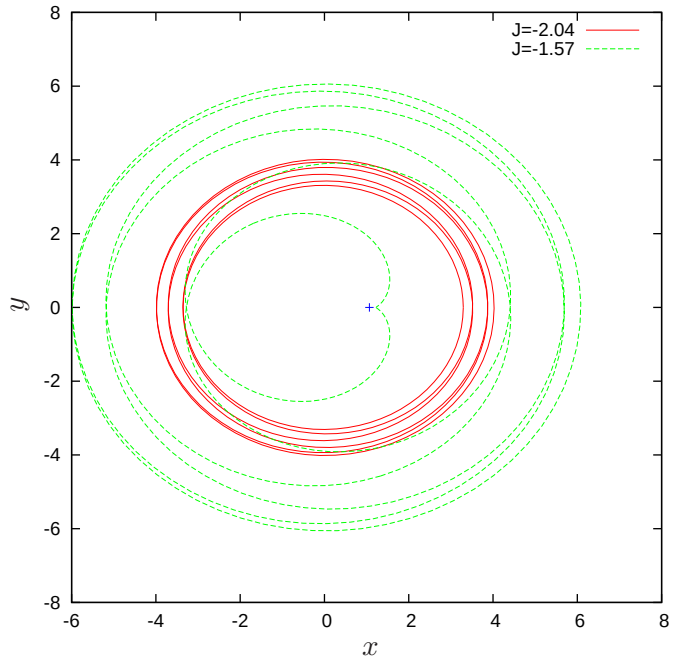

Figure 8: Extremal periodic orbits of the family: circular periodic orbit with $J = \bar{J}_-$ (in red), elliptical periodic orbit with $J = \bar{J}_+$ (in green). The Lagrange equilibrium point L_2 is marked with a '+' symbol.

for all $t \in \mathbb{R}$ and $J \in [\bar{J}_-, \bar{J}_+]$, which is the second bound given in Theorem 3.

Let us briefly describe the family of periodic orbits λ_J. For illustration, see Figure 8. At one endpoint of the family, as $J \to \bar{J}_-$, the periodic orbit λ_J tends to a circular orbit of period 14π centered at the origin and passing far away from the primaries (Sun and Jupiter). Moreover, λ_J looses hyperbolicity when $J \to \bar{J}_-$. For instance, the periodic orbit $\tilde{\lambda}_{\bar{J}_-}$ of the two-body problem approximation has eccentricity $e(\bar{J}_-) = 0.09989\cdots$.

At the other endpoint of the family, as $J \to \bar{J}_+$, the periodic orbit λ_J tends to a homoclinic loop of the Lagrangian equilibrium point L_2 that makes 6 turns around the Sun-Jupiter system. (In rotating Cartesian coordinates, L_2 is located on the x axis at the point $x_2 \simeq 1.068$). This explains the fact that the period T_J "explodes" as $J \to \bar{J}_+$. Since we are interested in working close to the resonance, we avoid energies $J > \bar{J}_+$ where the period explodes.

A.2 Computation of invariant manifolds

In this appendix, we compute the stable and unstable invariant manifolds associated to the periodic orbits found in the previous section.

Consider first a fixed energy level $J = J_0$. Let λ_{J_0} be the resonant periodic orbit of the circular problem found in the previous section. To compute the invariant manifolds of the periodic orbit, we continue using the iterated Poincaré map. Thus we look for (one dimensional) invariant manifolds of a hyperbolic fixed point at each energy level. Let $p \in \lambda_{J_0}$ be a hyperbolic fixed point of the iterated Poincaré map $\widetilde{P} = P^6$. Let $\lambda,\ \lambda^{-1}$ be the eigenvalues of $D\widetilde{P}(z)$ with $\lambda > 1$, and v_u, v_s be the associated eigenvectors.

Assume that we want to compute the unstable manifold $W^u(p)$. Let η be a small displacement in the unstable direction v_u. We approximate a piece of the local manifold by the linear segment between the points $p+\eta v_u$ and $\widetilde{P}(p+\eta v_u)$. We call this segment a *fundamental domain*. We discretize the fundamental domain into an array of points, and iterate them by $\widetilde{P}$ to globalize the manifold. (The stable manifold is computed analogously using the inverse map $\widetilde{P}^{-1}$.)

The error commited in the local approximation $\widetilde{P}(p+\eta v_u) = p+\lambda\eta v_u+\mathcal{O}(\eta^2)$ of the manifold is given by

$$\mathrm{err}(\eta) = \left\| \widetilde{P}(p+\eta v_u) - p - \lambda\eta v_u \right\| \in \mathcal{O}\left(\eta^2\right).$$

Remark A.3. For each energy level J, we choose a displacement $\eta = \eta(J)$ such that the local error is $\mathrm{err}(\eta) < 10^{-12}$.

One can think of p as a fixed point of the iterated Poincaré map $\widetilde{P} = P^6$, or as a 6-periodic point of the Poincaré map P. If $p_i = P^i(p)$ are the iterates of p for $i = 0, \ldots, 5$, then p_i are also fixed points of $\widetilde{P}$. They have associated unstable and stable manifolds, which can be obtained from $W^{u,s}(p)$ by iteration.

For illustration, let us show some numerical results corresponding to the energy value $J = -1.6$. Figure 9 shows the manifolds of all iterates $\{p_i\}_{i=0,\ldots,5}$. Notice that the dynamics in Figure 9 is reversible with respect to the symmetry section $\{y = 0,\ p_x = 0\}$, as discussed in the previous section (see (91)). Figure 9 shows that the manifolds do intersect transversally at different homoclinic points. We are interested in measuring the splitting angle between the manifolds. Unfortunately, the homoclinic points do not lie on the symmetry axis, which would be very useful in order to compute them.

In order to have the homoclinic points lie on the symmetry axis, we recompute the manifolds on the new Poincaré section

$$\Sigma^- = \{y = 0,\ p_y < 0\}.$$

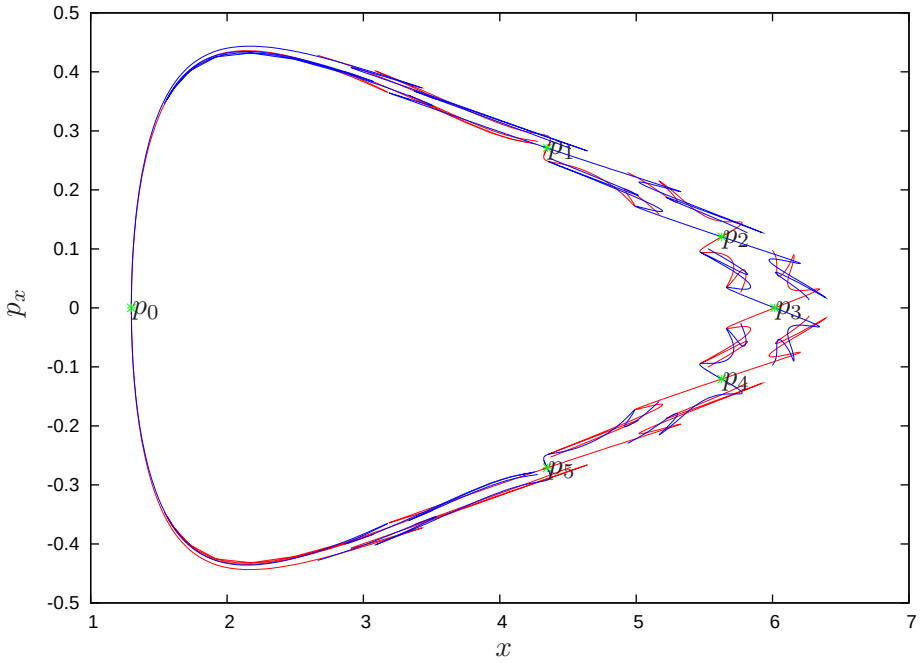

Figure 9: Invariant manifolds of the fixed points $p_0, p_1, \ldots, p_5$ on the section Σ^+. Unstable manifolds are plotted in red, stable in blue. The fixed points are marked in green.

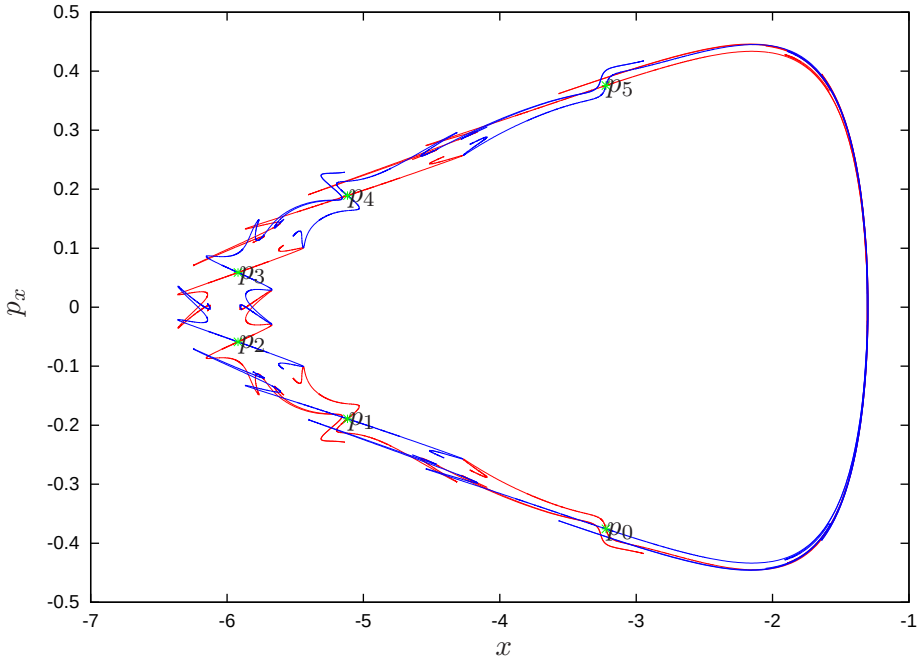

Figure 10: Invariant manifolds on the section Σ^-.

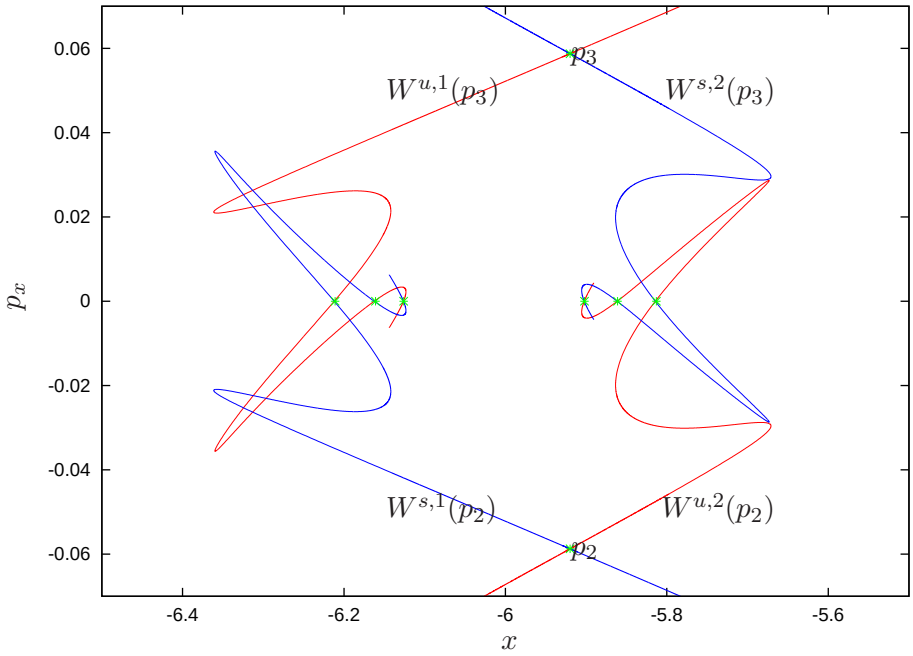

Figure 11: Invariant manifolds of the points p_2 and p_3 on the section Σ^-. Due to the symmetry, points that lie on the line $p_x = 0$ (marked in green) are intersection points.

Numerically, we just transport points on the unstable manifold from section Σ^+ to section Σ^- by the forward flow, and points in the stable manifold by the backward flow. See Figures 10 and 11. Now the points that lie on the symmetry line $p_x = 0$ are homoclinic points.

A.3 Computation of transversal homoclinic points and splitting angle

In this appendix, we compute the angle between the invariant manifolds at one of the transversal intersections. We will restrict the range of energy values to

$$J \in [J_-, J_+] = [-1.81, -1.56], \tag{94}$$

or equivalently the range of eccentricities to $e \in [e_-, e_+] = [0.48, 0.67]$. This is the range where we can validate the accuracy of our computations (see Appendix A.4). Below $e_- = 0.48$, the splitting size becomes comparable to the numerical error that we commit in double precision arithmetic.

Remark A.4. In this paper we concentrate on proving the existence of global instabilities in the Restricted three-body problem; we are not so much concerned with finding the *maximal* range of eccentricities along which the asteroid drifts. Thus we do not investigate the transversality of the splitting below e_-. However, we are convinced that the maximal range of eccentricities is larger than $[e_-, e_+]$, in particular that the lower bound can be pushed well below e_-. We think that our mechanism of instability applies to this larger range of eccentricities. In fact, it is possible to study such exponentially small splitting using more sophisticated numerical methods, such as multiple-precision arithmetic, and high-order approximation of local invariant manifolds, see for instance [FS90, DRR99, GS08].

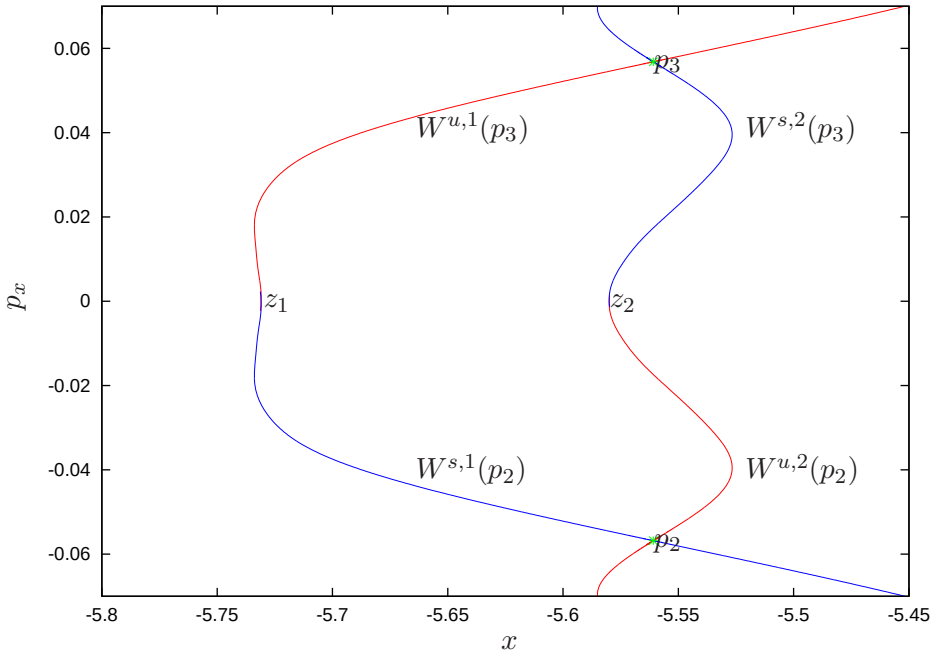

Figure 12: Invariant manifolds of the points p_2 and p_3 for the energy level $J = -1.74$.

Consider first a fixed energy level $J = J_0$ that is close to the unperturbed situation, e.g. $J = -1.74$. The corresponding manifolds are given in Figure 12. In general, there are uncountably many intersection points. For instance, in Figure 11 we show six intersections on the symmetry line. However, when the perturbation is small, there is one distinguished intersection point located "in the middle" of the homoclinic. We call it the *primary* intersection point.

Let us compute the primary intersection point z_1 corresponding to the "outer" splitting of the manifolds $W^{u,1}(p_3)$ and $W^{s,1}(p_2)$. For $J = -1.74$, the *primary* intersection z_1 corresponds to the *first* intersection of the manifolds with the $p_x = 0$ line, as we grow the manifolds from the fix points. Thanks to the symmetry, it is enough to look for the intersection of $W^{u,1}(p_3)$ with the $p_x = 0$ axis, because $W^{s,1}(p_2)$ must also intersect the axis at the same point.

To compute the intersection point z_1, we continue using a linear approximation of the local manifold, and propagate a fundamental domain in the local manifold by iteration. Let v_u be the unstable eigenvector associated to the point p_3. Consider the fundamental segment l_u between the points $p_3 + \eta v_u$ and $\widetilde{P}(p_3 + \eta v_u)$, as in the previous section. First we look for the *smallest* natural n such that $\widetilde{P}^n(l_u)$ intersects the $p_x = 0$ axis. Then we use a standard numerical method (bisection-like one-dimensional root finding) to find a point z_u in the fundamental segment l_u such that

$$\pi_{p_x}(\widetilde{P}^n(z_u)) = 0.$$

Thus we obtain the homoclinic point $z_1 = \widetilde{P}^n(z_u)$ in Figure 12. Numerically, we verify that z_1 is in the the $p_x = 0$ axis within 10^{-10} tolerance.

Finally, we vary energy J and use a continuation method to obtain the family of primary intersections $\{z_1\}_J$, using as seed the primary intersection $z_1|_{J=-1.74}$ found above. See Figure 13.

Remark A.5. For low energy levels (such as $J = -1.74$), corresponding to weak hyperbolicity, the invariant manifolds behave as if they were close to integrable, and the primary intersection

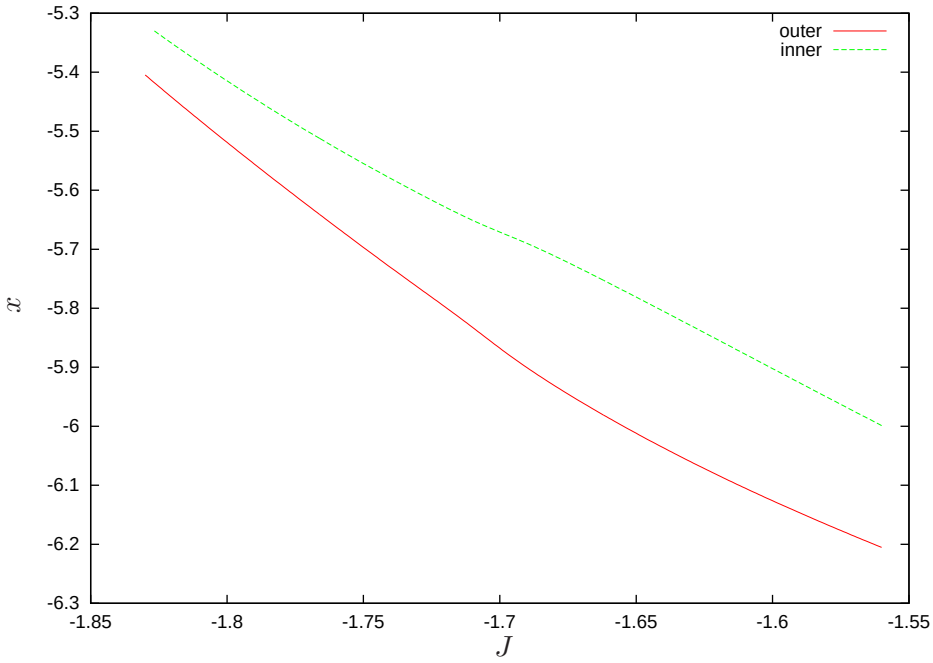

Figure 13: Family of primary intersection points corresponding to outer and inner splitting. For every energy level J, we plot the x coordinate of the intersection point z_1 and z_2 (the p_x coordinate is equal to zero). Notice that both families are continuous.

corresponds to the *first* intersection of the manifolds with the $p_x = 0$ axis. For high energy levels (such as $J = -1.6$), corresponding to strong hyperbolicity, the manifolds develop some folds, and thus the primary intersection may not correspond to the *first* intersection of the manifolds with the $p_x = 0$ axis. See Figure 11.

In practice, we first identify the primary intersection at low energy levels, and then use a continuation method to obtain the primary family of intersections up to high energy levels.

Analogously, we compute the family of primary intersections $\{z_2\}_J$ corresponding to the inner splitting. See Figure 13.

Let us now compute the splitting angle between the manifolds $W^{u,1}(p_3)$ and $W^{s,1}(p_2)$ at the point z_1. For illustration, we show some numerical results corresponding to the energy value $J = -1.74$. First we need the tangent vectors w_u and w_s to the manifolds at z_1. See Figure 14. As found above, let z_u be the point in the unstable fundamental segment that maps to z_1, i.e. $\widetilde{P}^n(z_u) = z_1$. Consider the tangent vector v_u to the manifold $W^{u,1}(p_3)$ at the point z_u. (Recall that at this point the linear approximation is good enough, so we can use as v_u the unstable eigenvector.) Multiply v_u by the Jacobian of $\widetilde{P}$ at the successive iterates $\widetilde{P}^i(p_u)$, for $i = 0, ..., n-1$. This way, we obtain the tangent vector to the unstable manifold at z_1. Let us denote this vector $w_u = (w_1, w_2)$. We normalize it to $\|w_u\| = 1$.

Due to reversibility, the vector w_s tangent to the stable manifold at z_1 is $w_s = (w_1, -w_2)$. See Figure 14. Notice that we choose the tangent vectors with the appropriate orientation, i.e. with the same orientation as the trajectories on the manifolds.

Thus the oriented splitting angle between w_u and w_s is

$$\sigma = 2 \arctan_2(-w_1, -w_2),$$

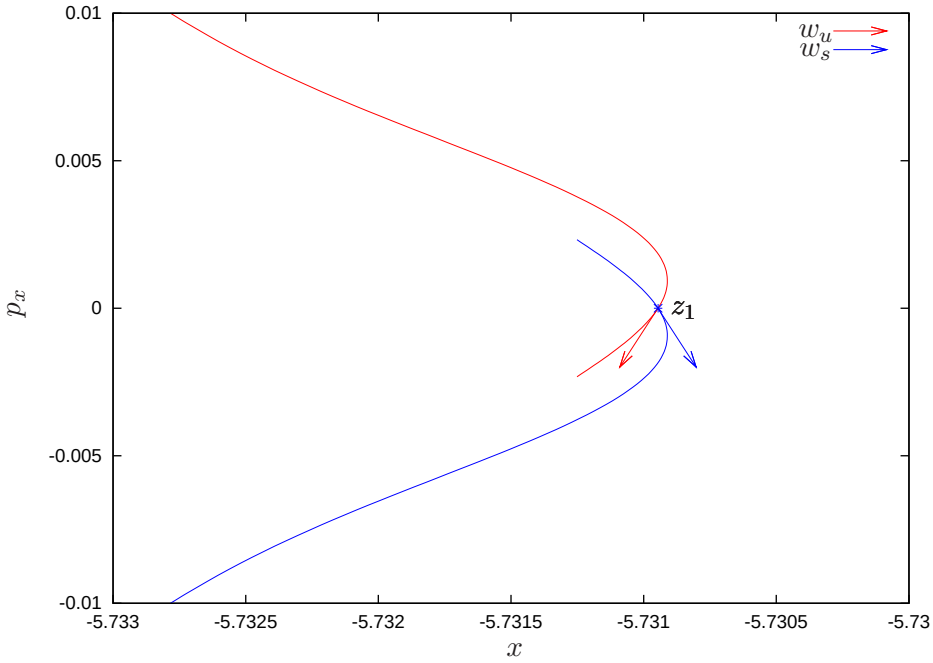

Figure 14: Outer splitting of the manifolds for energy level $J = -1.74$. This is a magnification of Figure 12 at the intersection point z_1. We show the vectors w_u, w_s tangent to the unstable and stable manifolds at z_1. The splitting angle σ is the angle between w_u and w_s.

inner	outer
$(-1.695, -1.694)$	$(-1.701, -1.700)$
$(-1.726, -1.725)$	$(-1.731, -1.730)$
$(-1.756, -1.755)$	$(-1.760, -1.759)$
$(-1.781, -1.780)$	$(-1.784, -1.783)$
$(-1.802, -1.801)$	$(-1.805, -1.804)$

Table 1: Subintervals of $J \in [J_-, J_+]$ containing the zeros of inner splitting (left column) and outer splitting (right column).

where $\arctan_2$ is the arctangent function of two variables, which uses the signs of the two arguments to determine the sign of the result.

Finally, we let J change and, using this procedure, we are able to obtain the splitting angle for energy levels $J \in [J_-, J_+]$. See Figure 15. The splitting angle is nonzero for all energy values except for a discrete set of them. The splitting angle oscillates around zero with decreasing amplitude as $J \to J_-$. Numerically, we find that the zeros of the splitting angle are contained in the intervals listed in Table 1.

Notice that the inner and outer splittings behave similarly. However, they become zero at different values of J, as seen in Table 1. Thus, when one of the intersections becomes tangent, the other one is still transversal, and we can always use one of them for diffusion.

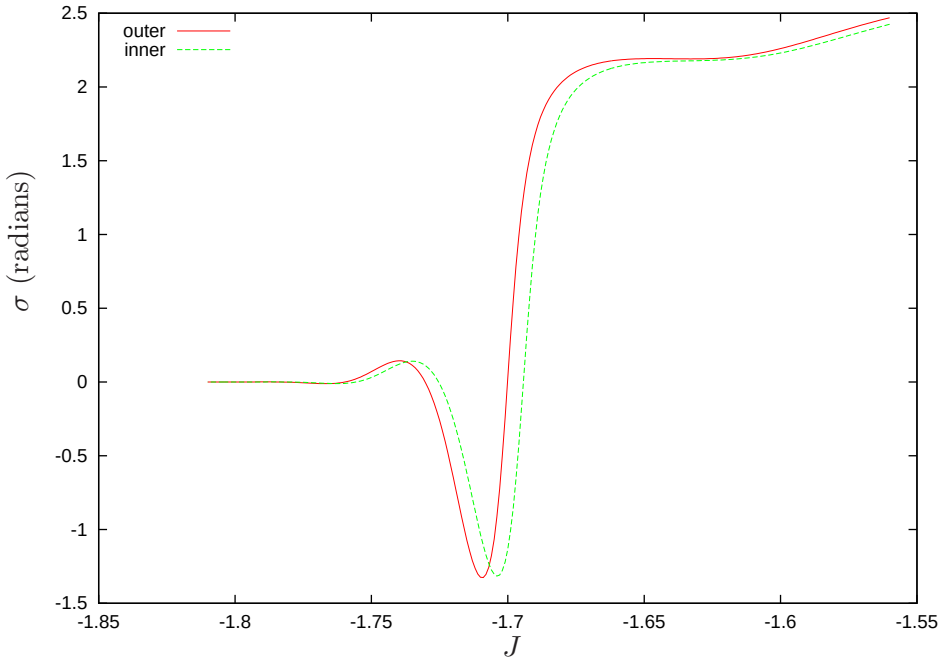

Figure 15: Splitting angle associated to inner and outer splitting.

p_x	x^u	x^s	$x^u - x^s$
-0.00002	-5.481541931871417	-5.481541932226887	0.000000000355470
-0.00001	-5.481541931790012	-5.481541931967703	0.000000000177691
0.00000	-5.481541931822124	-5.481541931822124	0.000000000000000
0.00001	-5.481541931967703	-5.481541931790012	-0.000000000177691
0.00002	-5.481541932226887	-5.481541931871417	-0.000000000355470

Table 2: Sampling of the manifolds $W^{u,1}(p_3)$ and $W^{s,1}(p_2)$ at different values of p_x, and their difference (last column).

A.4 Accuracy of computations

For small eccentricities, the splitting angle σ becomes very small. We need to check the validity of σ, making sure that the size of (accumulated) numerical errors in the computation is smaller than the size of σ.

The smallest splitting angle in Figure 15, corresponding to $J_- = -1.81$, is

$$\sigma(J_-) = -1.777970294158603 \times 10^{-5}.$$

We check the validity of $\sigma(J_-)$ by recomputing this angle using an alternative numerical method. First we compute the intersection of the manifolds $W^{u,1}(p_3)$ and $W^{s,1}(p_2)$ with the horizontal axis defined by

$$p_x = \frac{j}{10^5}$$

for $j \in (-2, -1, 1, 2)$.

In Table 2 we tabulate the x coordinate of $W^{u,1}(p_3)$ and $W^{s,1}(p_2)$ on these axes, and their difference $d = x^u - x^s$ gives the distance between the manifolds. We apply numerical differen-

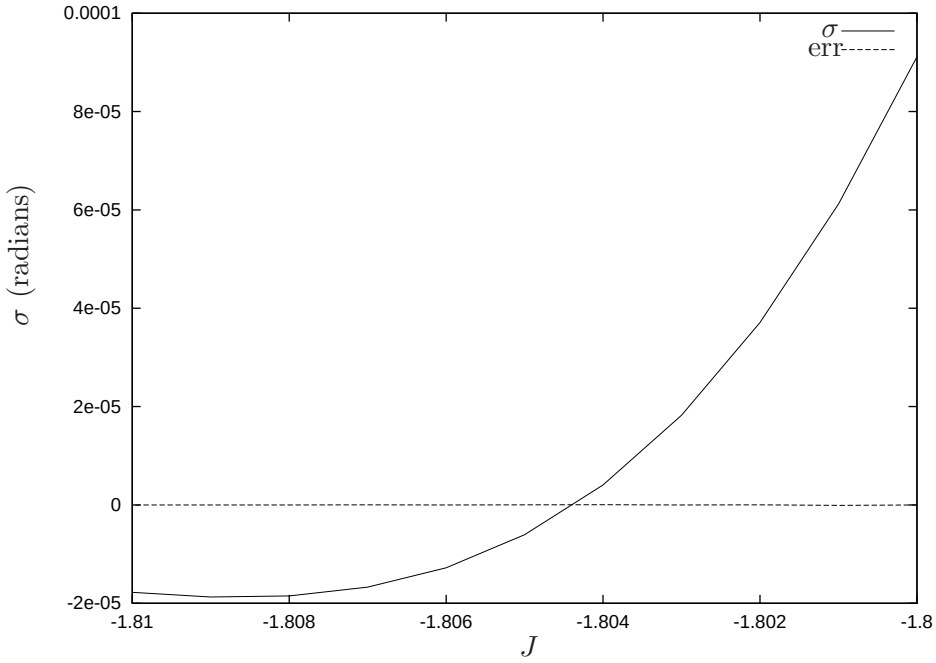

Figure 16: Splitting angle $\sigma(J)$ and estimate of the numerical error $\mathrm{err}(J)$ as a function of energy level J.

tiation to the last column of this table, using central differences centered at z_1 with step sizes 0.00002 and 0.00004, and obtain the values:

$$d_1 = \frac{d(0.00001) - d(-0.00001)}{0.00002} = -0.0000177691.$$

$$d_2 = \frac{d(0.00002) - d(-0.00002)}{0.00004} = -0.0000177735.$$

Finally, we use Richardson extrapolation and obtain:

$$d = \frac{4d_1 - d_2}{3} = -0.00001776763333333333.$$

Thus, using this alternative method, we obtain the splitting angle

$$\sigma(J_-) = \mathrm{atan}(-0.00001776763333333333) = -0.00001776763333146364.$$

Compare the splitting angle computed using the two methods. They differ by approximately 10^{-8}. This gives an estimate of the numerical error commited in our computation of the splitting angle.

We repeat this test for a range of energies $J \in [-1.81, -1.8]$. In Figure 16, we compare the splitting angle $\sigma(J)$ and the estimate of the numerical error $\mathrm{err}(J)$. This error stays below 10^{-7}, and it is several orders of magnitude smaller than the splitting angle. For higher energy values $J \in [-1.8, -1.56]$, the splitting angle is large, so the numerical error is certainly smaller. Therefore we are confident that the splitting angle has been accurately computed in the range of eccentricities considered, $[J_-, J_+]$.

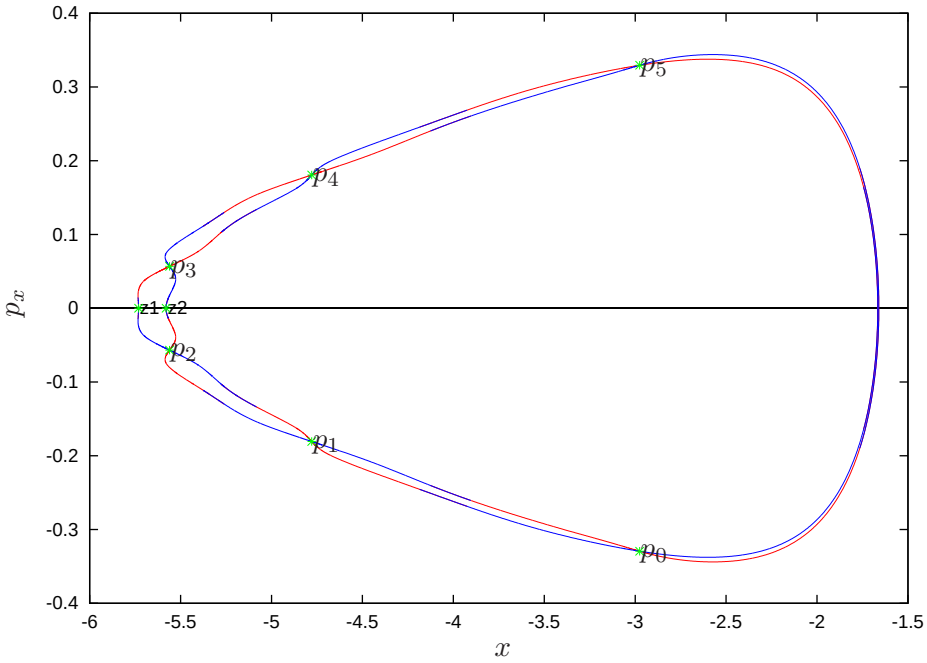

Figure 17: Energy $J = -1.74$. Resonance structure in Cartesian coordinates. The axis of symmetry is marked with a horizontal line.

B The resonance in Delaunay coordinates

In Appendix A we have studied the periodic orbits and the invariant manifolds in rotating Cartesian coordinates (x, y, p_x, p_y). Nevertheless, the study of the inner and outer maps are done in rotating Delaunay coordinates. Indeed since these coordinates are action-angle coordinates for the two body problem, it is much more convenient to use them to study the mean motion resonance.

The Poincaré section $\{y = 0\}$ is completely different from the section $\{g = 0\}$ which will be used from now on (see (22)). In particular, the periodic orbits $\{\lambda_J\}_{J\in[\bar{J}_-,\bar{J}_+]}$ obtained in Appendix A.1 intersect the section $\{y = 0\}$ six times whereas they intersect $\{g = 0\}$ seven times. However, we remark that the homoclinic points z_1 and z_2 lie on the symmetry axis both in Cartesian and in Delaunay variables. See Figures 17 and 18.

To obtain the intersection of these periodic orbits with $\{g = 0\}$ we just need to express the 6-periodic points of the Poincaré map P obtained in Appendix A.1 in Delaunay coordinates and then iterate them by the flow of the circular problem expressed in Delaunay coordinates until they hit the section $\{g = 0\}$. We do the same with the homoclinic points. In Appendix B.1 we explain how to compute the change of coordinates and the vector field in Delaunay coordinates.

B.1 From Cartesian to Delaunay and computation of $\partial_G \Delta H_{\text{circ}}$

We explain an easy way to obtain the rotating Delaunay coordinates from rotating Cartesian (or polar) coordinates in the circular problem. First recall that G can be computed as

$$G = r\left(-p_x \sin\phi + p_y \cos\phi\right).$$

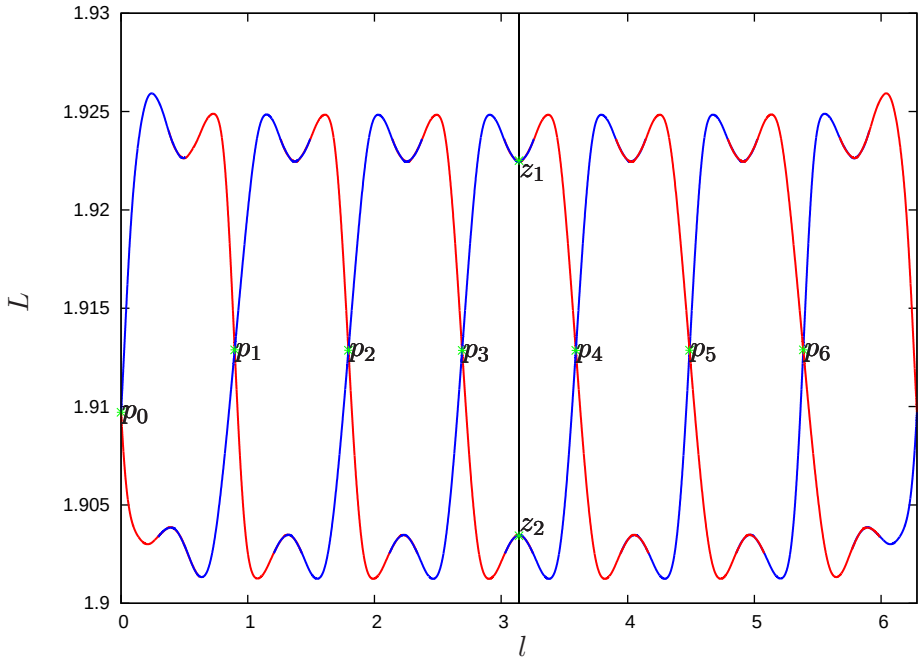

Figure 18: Energy $J = -1.74$. Resonance structure in Delaunay coordinates. The symmetry corresponds to $l = 0$ and $l = \pi$ and is marked with a vertical line.

The potential $\mu\Delta H_{\text{circ}}$ in Cartesian coordinates only depends on the position (x, y) of the asteroid, and can be easily computed. Then, one can use the equation

$$J = -\frac{1}{2L^2} - G + \mu\Delta H_{\text{circ}}$$

to obtain L. Knowing L and G we can obtain the eccentricity e by

$$e = \sqrt{1 - \frac{G^2}{L^2}}.$$

Using that $r = L^2(1 - e\cos u)$, one can obtain u and from here ℓ using Kepler's equation $u - e\sin u = \ell$. On the other hand, from u we can obtain v using

$$\tan\frac{v}{2} = \sqrt{\frac{1+e}{1-e}}\tan\frac{u}{2}.$$

Finally, we can deduce g using that $\phi = v + g$.

We devote the rest of this appendix to compute $\partial_G \Delta H_{\text{circ}}$. The other derivatives of ΔH_{circ} can be computed analogously. Let us define

$$D[r_0] = D[r_0](r, v, g) = \left(r^2 + r_0^2 - 2rr_0\cos(v+g)\right)^{-1/2}.$$

Then

$$\Delta H_{circ}(L, \ell, G, g) = -(1-\mu)D[-\mu] - \mu D[1-\mu] - D[0].$$

Thus by the chain rule there only remains to compute $\partial_G r$ and $\partial_G v$. First, let us point out that

$$\partial_G e = -\frac{G}{eL^2} = \frac{e^2-1}{eG}.$$

On the other hand, using that $\ell = u - e\sin u$, one has that

$$\partial_e u = \frac{\sin u}{1 - e\cos u}.$$

Then, since $r(L,e,\ell) = L^2(1 - e\cos u(e,\ell))$, using that

$$\cos v = \frac{\cos u - e}{1 - e\cos u}, \tag{95}$$

we have that

$$\partial_e r(L,e,\ell) = L^2\cos v$$

and therefore,

$$\partial_G r(L,\ell,G) = -\frac{G\cos v}{e}.$$

To compute $\partial_G v$, let us point out that $\partial_G v = \partial_e v \partial_G e$. Therefore it only remains to compute $\partial_e v$, we obtain it using formula (95) and

$$\sin v = \frac{\sqrt{1-e^2}\sin u}{1 - e\cos u}.$$

Then,

$$\partial_e v = \frac{\sin v}{1-e^2}\left(2 + e\cos v\right).$$

and therefore,

$$\partial_G v = -\frac{\sin v}{eG}\left(2 + e\cos v\right).$$

C Numerical study of the inner and outer dynamics

C.1 Inner and outer dynamics of the circular problem

In this appendix, we numerically compute the inner map $\mathcal{F}_0^{\text{in}}$ and the outer maps $\mathcal{F}_0^{\text{out},*}$ of the circular problem, given in Section 3. Recall that to compute these maps we deal with the extended system given by the Hamiltonian H in (17) with $e_0 = 0$ restricted to the energy level $H = 0$ and thus, we have that $I = -J$. Then, we consider $I \in [I_-, I_+] = [-J_+, -J_-]$, where the range $[-J_+, -J_-]$ is given in (94).

As seen in Section 3.2, the inner map has the form

$$\mathcal{F}_0^{\text{in}} : \begin{pmatrix} I \\ t \end{pmatrix} \mapsto \begin{pmatrix} I \\ t + \mu\mathcal{T}_0(I) \end{pmatrix}, \tag{96}$$

where $T_J = 14\pi + \mu\mathcal{T}_0(I)$ is the period of the periodic orbit obtained in Theorem 3 on the corresponding level of energy J, which now corresponds to an invariant hyperplane $I =$ constant.

Recall that we computed the periodic orbit λ_J as well as its period T_J in Appendix A.1. In particular, Figure 6 shows a plot of the function $T_J - 14\pi = \mu\mathcal{T}_0(I)$. Notice that the derivative

of the function $\mathcal{T}_0(I)$ is nonzero for the whole range $[I_-, I_+]$. This shows that the inner map is twist. Moreover, Figure 6 shows that

$$0 < \mu\mathcal{T}_0(I) < 60\mu < \pi.$$

Therefore, the function $\mathcal{T}_0(I)$ satisfies the properties stated in Lemma 3.3.

As a test, we have computed the same function $\mathcal{T}_0(I)$ using two different methods. First by computing the period of the periodic orbit, as above. Then by computing the integral expression (39) using numerical integration. The difference in $\mathcal{T}_0(I)$ using both methods is of the order 10^{-12}.

As seen in Section 3.3, the outer maps have the form

$$\mathcal{F}_0^{\mathrm{out},*} : \begin{pmatrix} I \\ t \end{pmatrix} \mapsto \begin{pmatrix} I \\ t + \mu\omega^*(I) \end{pmatrix}, \quad * = \mathrm{f}, \mathrm{b}. \tag{97}$$

For simplicity, let us only discuss the computation of $\omega^{\mathrm{f}}(I)$ ($\omega^{\mathrm{b}}(I)$ is computed analogously). Recall from Lemma 3.7 that the function $\omega^{\mathrm{f}}(I)$ is defined as

$$\omega^{\mathrm{f}}(I) = \omega^{\mathrm{f}}_{\mathrm{out}}(I) + \omega^{\mathrm{f}}_{\mathrm{in}}(I),$$

where, taking into account that the homoclinic orbit is symmetric with respect to the involution (20),

$$\omega^{\mathrm{f}}_{\mathrm{out}}(I) = \omega^{\mathrm{f}}_{+}(I) - \omega^{\mathrm{f}}_{-}(I) = 2\omega^{\mathrm{f}}_{+}(I) \tag{98}$$

with

$$\omega^{\mathrm{f}}_{+}(I) = \lim_{N\to+\infty} \left(\int_0^{14N\pi} \frac{(\partial_G \Delta H_{\mathrm{circ}}) \circ \gamma^{\mathrm{f}}_I(\sigma)}{-1 + \mu(\partial_G \Delta H_{\mathrm{circ}}) \circ \gamma^{\mathrm{f}}_I(\sigma)}\, d\sigma + N\mathcal{T}_0(I) \right), \tag{99}$$

$$\omega^{\mathrm{f}}_{\mathrm{in}}(I) = \int_0^{-12\pi} \frac{(\partial_G \Delta H_{\mathrm{circ}}) \circ \lambda^4_I(\sigma)}{-1 + \mu(\partial_G \Delta H_{\mathrm{circ}}) \circ \lambda^4_I(\sigma)}\, d\sigma. \tag{100}$$

To obtain $\omega^{\mathrm{f}}(I)$, we compute the integrals (99) and (100) numerically, using a standard algorithm from the GSL library [G$^+$]. The integrals are computed within a relative error limit 10^{-9}.

The function $\partial_G \Delta H_{\mathrm{circ}}$ involved in both integrals is given explicitly in Appendix B.1. The integral $\omega^{\mathrm{f}}_{\mathrm{in}}(I)$ is evaluated on a periodic trajectory $\lambda^4_I(\sigma)$ of the reduced circular problem (namely, with reparameterized time, see (31)) with initial condition p_4, a fixed point of the Poincaré map $\mathcal{P}_0^7$ found in Appendix B. The integral $\omega^{\mathrm{f}}_{+}(I)$ is evaluated on a homoclinic trajectory $\gamma^{\mathrm{f}}_I(\sigma)$ of the reduced circular problem with initial condition z_2, the primary homoclinic point corresponding to the inner splitting found in Appendix A.3.

Next we make a couple of important remarks about the numerical computation of the integral $\omega^{\mathrm{f}}_{+}(I)$. The key point is that the homoclinic orbit γ^{f}_I was already computed in Appendix A.3 with high accuracy, and we can exploit this information here. Recall that the primary homoclinic point z_2 was obtained as the n-th iterate of a point z_u in the local fundamental segment l_u under the Poincaré map:

$$z_2 = \{\mathcal{P}_0^7\}^n(z_u). \tag{101}$$

Moreover, recall that the point z_u was chosen to be suitably close to the fixed point p_3 for each energy level J. See Remark A.3.

Notice that the integral $\omega^{\mathrm{f}}_{+}(I)$ is defined by a limit as $N \to \infty$, i.e. as the homoclinic orbit $\gamma^{\mathrm{f}}_I(\sigma)$ asymptotically approaches the periodic orbit $\lambda^3_I(\sigma)$ in forward time (see equation (40)).

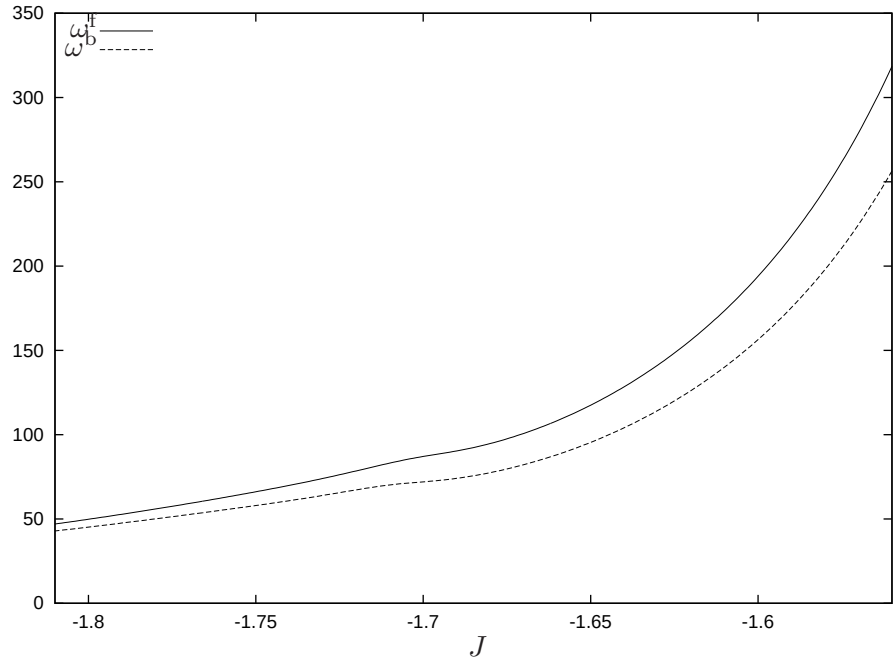

Figure 19: Functions $\omega^{\mathrm{f}}(I)$ and $\omega^{\mathrm{b}}(I)$ involved in the definition of the outer map (97) of the circular problem as a function of the Jacobi constant J (recall that in the circular problem $I = -J$).

Numerically, of course, we should stop integrating at an upper endpoint N large enough such that the integral converges. In practice, we choose the upper endpoint $N = N(I)$ to be the number of iterates $n = n(I)$ in (101). This means that we evaluate the integral along the homoclinic trajectory $\gamma_I^{\mathrm{f}}(\sigma)$ until it reaches the point z_u, which is suitably close to the periodic orbit.

Notice also that integrating the homoclinic trajectory $\gamma_I^{\mathrm{f}}(\sigma)$ forwards in the reduced system means integrating it backwards along the unstable manifold in the original system. This is numerically unstable, since numerical errors grow exponentially. In practice, we rewrite the integral (99) using the change of variables $\hat{\sigma} = \sigma - 14N\pi$ so that the homoclinic trajectory is integrated forwards along the unstable manifold, starting from the point z_u.

The computed values of the functions $\omega^{\mathrm{f}}(I)$ and $\omega^{\mathrm{b}}(I)$ are shown in Figure 19. Note that they are plotted as a function of the Jacobi constant J instead of as a function of I, so that they can be compared with Figure 6, where we have plotted $\mu\mathcal{T}_0(I) = T_J - 14\pi$ as a function of J.

To test the computation of the function ω_+^{f}, we directly verify the definition of the outer map in 3.4. Let $z_2 = (L_h, \ell_h, G_h, 0)$ be the primary homoclinic point, and let $p_3 = (L_p, \ell_p, G_p, 0)$ be the periodic point. Given a point $(L_h, \ell_h, G_h, 0, I, t)$ in the extended circular problem, we check that it is forward asymptotic (in the reparametrized time) to the point $(L_p, \ell_p, G_p, 0, I, t+\omega_+^{\mathrm{f}}(I))$, where $t \in \mathbb{T}$ is arbitrary. Thus we check that the distance

$$\mathrm{dist}^+(s) = |\Phi_0\{s, (L_h, \ell_h, G_h, 0, I, t)\} - \Phi_0\{s, (L_p, \ell_p, G_p, 0, I, t + \omega_+^{\mathrm{f}}(I))\}| \xrightarrow{s\to\infty} 0$$

with exponential decay.

The result of the test is shown in Figure 20 for values of the energy $J \in [J_-, J_+]$ (recall that $J = -I$). Notice that the vertical axis is in logarithmic scale. Let $s = 14N\pi$. We plot the

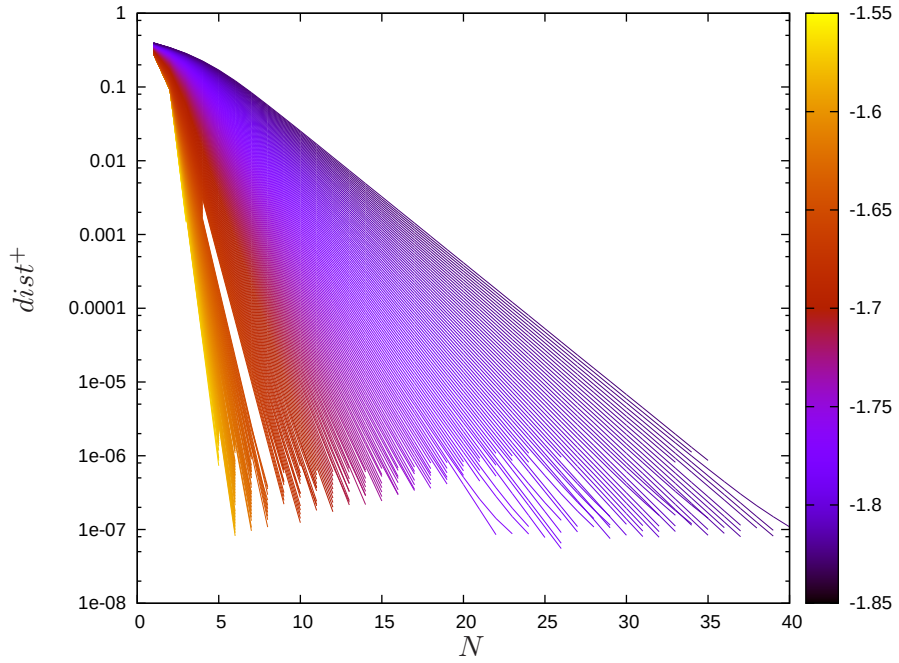

Figure 20: Exponential decay of the function dist^+ as a function of N (multiples of the period) for different energy levels. The energy levels $J \in [J_-, J_+]$ are color-coded.

distance dist^+ as a function of N (multiples of the period). The test shows exponential decay of the distance function for all energy values, i.e. straight lines in the plot.

Recall that the periodic orbits $\lambda_I^{3,4}(s)$ become more hyperbolic as the energy I decreases. Thus, the rate of exponential convergence between the homoclinic and the periodic trajectory also increases, i.e. the straight lines have increasing slope in the plot. As explained above, the length of integration $N = N(I)$ along the homoclinic orbit is suitably chosen for each energy level. For $I \to I_-$, there is exponential decay up to time $s = 40 \cdot (14\pi) \approx 1760$.

C.2 Inner and outer dynamics of the elliptic problem

In this appendix, we numerically compute the first orders in e_0 of the inner map $\mathcal{F}_{e_0}^{\text{in}}$ and the outer maps $\mathcal{F}_{e_0}^{\text{out},*}$ of the elliptic problem, given in Section 4. In order to compare the inner and outer dynamics of the elliptic problem through Lemma 5.2, only some specific terms in the expansions of the inner and outer maps are necessary. Namely, we only need to compute the term A_1 in the expansion of the inner map (62), and the terms B^* in the expansion of the outer maps (73).

Recall from Section 4.4 that A_1 can be split as

$$A_1(I,t) = A_1^+(I)e^{it} + A_1^-(I)e^{-it}.$$

Since A_1^+ and A_1^- are complex conjugate, it is only necessary to compute one of them. Let us compute the positive harmonic,

$$A_1^+(I) = -i\mu \int_0^{-14\pi} \frac{\Delta H_{\text{ell}}^{1,+} \circ \lambda_I^3(\sigma)}{-1 + \mu \partial_G \Delta H_{\text{circ}} \gamma_I^3(\sigma)} e^{i\widetilde{\lambda}_I^3(\sigma)} d\sigma. \tag{102}$$

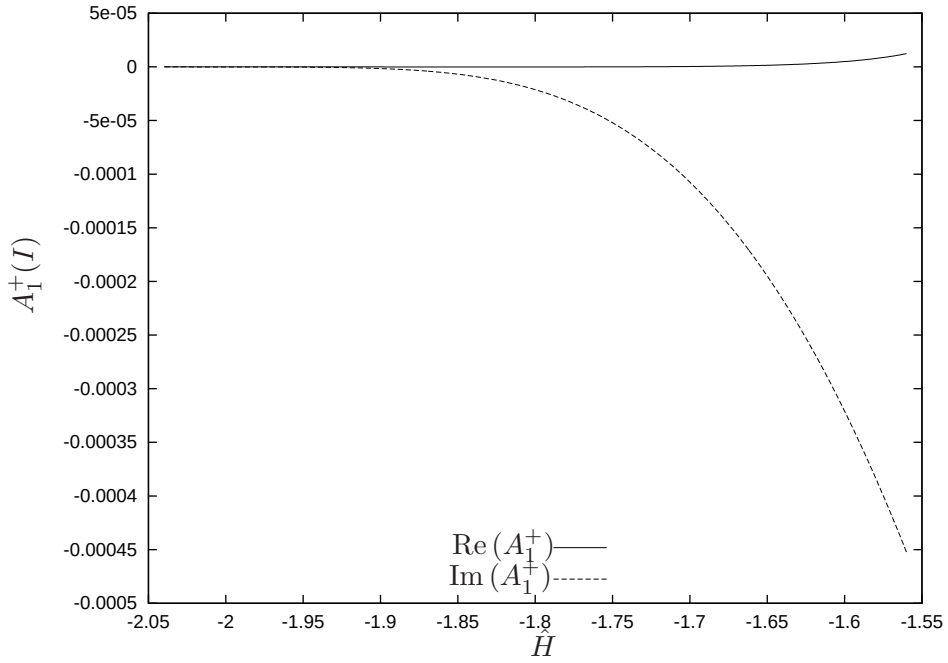

Figure 21: Function $A_1^+(I)$ (real and imaginary parts) involved in the definition of the inner map (62) of the elliptic problem as a function of the energy of the system in rotating coordinates $\hat{H}$. Recall that $\hat{H} = -I$.

Notice that the denominator is the same one used in the previous section for the inner and outer dynamics of the circular problem. Next we give the numerator $i\Delta H_{\mathrm{ell}}^{1,+}$ explicitly. Let

$$\begin{aligned}\Delta H_{\mathrm{ell}}^{1}(L,\ell,G,g,t) = &-\frac{1-\mu}{\mu}\mathcal{B}_1\left(-\frac{r(L,\ell,G)}{\mu}, v(L,\ell,G), g, t\right)\\ &-\frac{\mu}{1-\mu}\mathcal{B}_1\left(\frac{r(L,\ell,G)}{1-\mu}, v(L,\ell,G), g, t\right),\end{aligned}$$

where $\mathcal{B}_1$ is the function defined in Lemma 4.4. Then it is straightforward to see that

$$\begin{aligned}\Delta H_{\mathrm{ell}}^{1,+}(l,L,g,G) = &-\frac{1-\mu}{\mu}\mathcal{B}_1^+\left(-\frac{r(L,\ell,G)}{\mu}, v(L,\ell,G), g\right)\\ &-\frac{\mu}{1-\mu}\mathcal{B}_1^+\left(\frac{r(L,\ell,G)}{1-\mu}, v(L,\ell,G), g\right),\end{aligned} \tag{103}$$

where

$$\mathcal{B}_1^+(r,v,g) = -\frac{1-r\cos(v+g)-i2r\sin(v+g)}{2\Delta^3(r,v+g)}.$$

The computed value of the function A_1^+ is shown in Figure 21. We plot it as a function of the energy of the elliptic problem in rotating coordinates $\hat{H}$ in (16). Recall that since we are working in the energy level $H = 0$ of the extended Hamiltonian H in (17), we have that $I = -\hat{H}$.

For the outer map, we compute the functions $B^*(I)$. Similarly to A_1, it is only necessary to compute the positive harmonics $B^{*,+}$. Recall from Lemma 4.9 that the positive harmonics

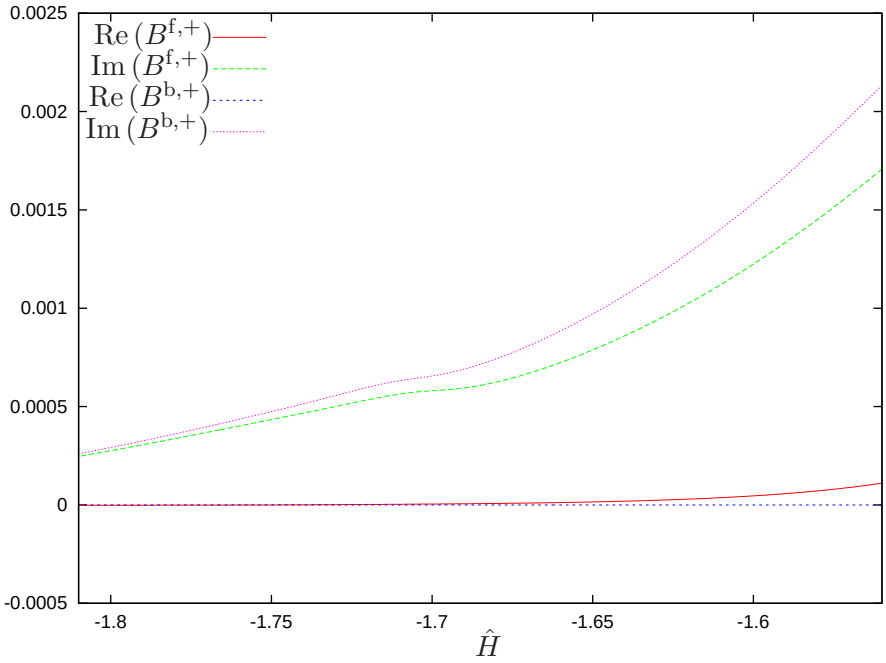

Figure 22: Functions $B^{\mathrm{f},+}$ and $B^{\mathrm{b},+}$ (real and imaginary parts) involved in the definition of the outer map (73) of the elliptic problem.

$B^{\mathrm{f},+}(I)$ and $B^{\mathrm{b},+}(I)$ are defined as

$$\begin{aligned} B^{\mathrm{f},+}(I) &= B^{\mathrm{f},+}_{\mathrm{out}}(I) + B^{\mathrm{f},+}_{\mathrm{in}}(I) e^{i\mu\omega^{\mathrm{f}}_{\mathrm{out}}(I)} \\ B^{\mathrm{b},+}(I) &= B^{\mathrm{b},+}_{\mathrm{in}}(I) + B^{\mathrm{b},+}_{\mathrm{out}}(I) e^{i\mu\omega^{\mathrm{b}}_{\mathrm{in}}(I)}, \end{aligned} \tag{104}$$

where $\omega^{\mathrm{f}}_{\mathrm{out}}$ and $\omega^{\mathrm{b}}_{\mathrm{in}}$ were obtained in Appendix C.1. To obtain $B^{*,+}_{\mathrm{out}}$ and $B^{*,+}_{\mathrm{in}}$, we compute the integrals (75)–(77) numerically, using the same techniques as in the previous Appendix C.1. In particular, the integrands of the Melnikov integrals (75) and (76), by construction, decay exponentially as $T \to \pm\infty$ and we take the same approximate limits of integration $\pm 14\pi N$ where $N = N(I)$ is the constant considered in Appendix C.1.

The computed values of the functions $B^{\mathrm{f},+}(I)$ and $B^{\mathrm{b},+}(I)$ are shown in Figure 22.

C.3 Comparison of the inner and outer dynamics of the elliptic problem

Finally, we verify the non-degeneracy condition

$$\widetilde{B}^{*,\pm}(\mathcal{I}) \neq 0 \qquad \text{for } \mathcal{I} \in \mathcal{D}^* \tag{105}$$

stated in Lemma 5.2, which implies the existence of a transition chain of tori. Since $B^{*,+}$ and $B^{*,-}$ are complex-conjugate, it is only necessary to compute one of them. Let us compute the positive harmonic,

$$\widetilde{B}^{*,+}(\mathcal{I}) = B^{*,+}(\mathcal{I}) - \frac{e^{i\mu\omega^*(\mathcal{I})} - 1}{e^{i\mu\mathcal{T}_0(\mathcal{I})} - 1} A^+_1(\mathcal{I}).$$

All the functions involved in the expression above are known: $\mathcal{T}_0$ and ω^* are obtained in Appendix C.1 and A^+_1 and $B^{*,+}$ are obtained in Appendix C.2.

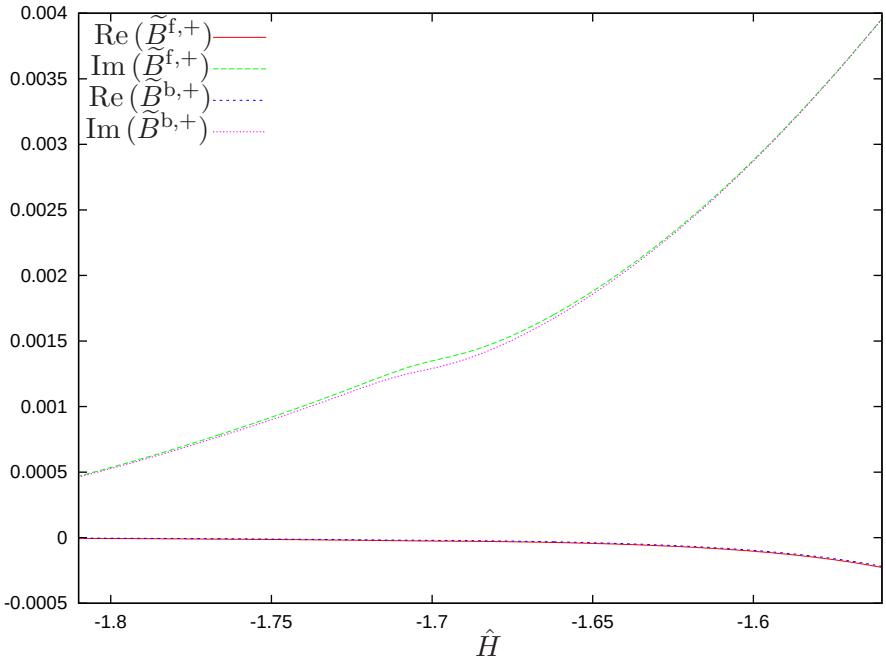

Figure 23: Functions $\widetilde{B}^{\mathrm{f},+}$ and $\widetilde{B}^{\mathrm{b},+}$ (real and imaginary parts).

The computed values of the functions $\widetilde{B}^{\mathrm{f},+}$ and $\widetilde{B}^{\mathrm{b},+}$ are shown in Figure 23. Therefore, we see that the functions $\widetilde{B}^{*,+}$ are not identically zero. This justifies the statement (89) in Lemma 5.2.

Remark C.1. Figure 23 also shows that $\widetilde{B}^{\mathrm{f},+}$ and $\widetilde{B}^{\mathrm{b},+}$ are almost identical, which is surprising for the authors. However, this fact is not relevant for the argument in Lemma 5.2; we only need that these functions do not vanish identically.

D Conjectures on the speed of diffusion

D.1 Speed of diffusion for a priori unstable systems and Positive measure

Consider the following nearly integrable Hamiltonian system proposed by Arnold [Arn64]:

$$H_\varepsilon(p,q,I,\phi,t) = \frac{1}{2}p^2 + \cos q - 1 + \frac{1}{2}I^2 + \varepsilon H_1(p,q,I,\phi,t), \qquad \text{where } p, I \in \mathbb{R},\ \phi, q, t \in \mathbb{T} \quad (106)$$

for an analytic perturbation εH_1. This system is called *a priori unstable*. Proving *Arnold diffusion* for this system consists in showing that, for all small $\varepsilon > 0$ and a generic εH_1, there exists orbits with

$$|I(t) - I(0)| > \mathcal{O}(1),$$

where $\mathcal{O}(1)$ is independent of ε.

There has been fascinating progress in this problem achieved by several groups (see [Ber08, CY04, DdlLS06, DH09, Tre04]). Treschev [Tre04] not only proved existence of Arnold diffusion, but also gave an optimal estimate on speed, namely, he constructed orbits

$$|I(t) - I(0)| > c\frac{\varepsilon}{|\ln \varepsilon|}\ t$$

for some $c > 0$. One can see that this estimate is optimal, i.e. $|I(t) - I(0)| < C\frac{\varepsilon}{|\ln \varepsilon|}\, t$ for some $C > c$.

Heuristically the mechanism of diffusion is the following. For small $\varepsilon > 0$ the Hamiltonian H_ε has a 3-dimensional normally hyperbolic invariant cylinder Λ_ε close to $\Lambda_0 = \{p = q = 0\}$. A hypothetical diffusing orbit starts close to Λ_ε and makes a homoclinic excursion. Each homoclinic excursion takes approximately $\mathcal{O}(|\ln \varepsilon|)$-time. Increment of $I(t)$ after such an excursion is $\mathcal{O}(\varepsilon)$.[5] If one can arrange that all excursions lead to increments of $I(t)$ of the same sign, the result follows.

It seems natural that orbits will be trapped inside the resonance $p = 0$ for polynomially long time. Using this heuristic description one can conjecture that increments $I(t)$ can behave as a random walk for positive conditional measure for polynomially large time.

Positive measure conjecture [6] *Consider the Hamiltonian H_ε with a generic perturbation εH_1. Pick an ε-ball B_ε of initial conditions, whose center projects into $(p, q) = 0$, and denote the Lebesgue probability measure supported on it by Leb_ε. Then, for some constants $c, C > 0$ independent of ε, the set of initial conditions satisfying*

$$|I(T) - I(0)| > 1 \qquad \textit{for some} \qquad 0 < T < C\frac{|\ln \varepsilon|}{\varepsilon^2}$$

is denoted Diff and has measure $Leb_{\sqrt{\varepsilon}}(\,Diff) > c$.

Since a typical excursion takes $\mathcal{O}(|\ln \varepsilon|)$-time and each increment is $\mathcal{O}(\varepsilon)$, we essentially conjecture that after $\mathcal{O}(\varepsilon^{-2})$ excursions with uniformly positive probability there will be drift of order $\mathcal{O}(\varepsilon)\mathcal{O}(\varepsilon^{-1}) = \mathcal{O}(1)$.

D.2 Structure of the restricted planar elliptic three-body problem

In this appendix we relate a priori unstable systems and the elliptic restricted planar three-body problem. Recall that we managed to write the Hamiltonian of the latter problem in the form

$$\begin{aligned} H_{\text{ell}}(L, \ell, G, g, t) =& H_{\text{circ}}(L, \ell, G, g, \mu) + \mu e_0 \Delta H_{\text{ell}}(L, \ell, G, g, t, \mu, e_0) \\ =& H_0^*(L, G) + \mu \Delta H_{\text{circ}}(L, \ell, G, g, \mu) + \mu e_0 \Delta H_{\text{ell}}(L, \ell, G, g, t, \mu, e_0) \\ =& -\tfrac{1}{2L^2} - G + \mu \Delta H_{\text{circ}}(L, \ell, G, g, \mu) + \mu e_0 \Delta H_{\text{ell}}(L, \ell, G, g, t, \mu, e_0). \end{aligned}$$

We have that

- H_0^* is an integrable Hamiltonian.
- H_{circ} is non-integrable and for H_{circ} in a certain interval $[J_-, J_+]$ there is a family of hyperbolic periodic orbits $\{p_J\}$ whose invariant manifolds intersect transversally along at least one homoclinic.
- H_{ell} is a $\mathcal{O}(\mu e_0)$-perturbation of H_{circ} such that a Melnikov integral evaluated along a transverse homoclinic being non-degenerate in two different ways: dependence on time is non-trivial and relation between inner and outer integrals is non-degenerate (see (9)).

[5] This is only an heuristic description as dynamics inside of the cylinder should come into play. Near so-called double resonance dynamics is different from the one near single resonances

[6] This conjecture is in a sense answers a question posed by Katok about measure of diffusing orbits

Having all these non-degeneracy conditions we prove the existence of diffusing orbits.

It is not difficult to prove, using averaging techniques, that for $\mu > 0$ small, there is a family of saddle periodic orbit $\{\gamma_J\}$ on some interval $[J_-, J_+]$. It seems, however, to be a non-trivial problem to establish the splitting of its separatrices. Due to reversibility (91) there are at least four homoclinic intersections (two for upper separatrices and two for lower ones). Having these two conditions it is natural to expect that at least one of the four associated Melnikov integrals is non-degenerate. Qualitative analysis shows that it should be possible to have a homoclinic excursion $\mathcal{O}(\mu e_0)$-close to the invariant cylinder. Such an excursion takes $\mathcal{O}(|\ln(\mu e_0)|)$-time. If the excursion is selected properly, then the result of the excursion is that the increment of the eccentricity is $\mathcal{O}(\mu e_0)$. This makes us believe that the instability time obeys $T \sim -\dfrac{\ln(\mu e_0)}{\mu^{3/2} e_0}$ stated in (6).

Let us point out that we believe that our diffusion mechanism survives even for non-infinitesimal e_0's, e.g. realistic $e_0 = 0.048$. To justify this, we review the above structure.

Notice that we use a 3-dimensional normally hyperbolic invariant cylinder and the intersection of its invariant manifolds to diffuse. The cylinder arises from the family of periodic orbits $\{\gamma_J\}_{J\in[J_-,J_+]}$ of the circular problem, which persist under the elliptic time-periodic perturbation $\mu e_0 \Delta H_{\text{ell}}(L, \ell, G, g, t, \mu, e_0)$ (see (16) and the derivation in the corresponding section). As the analysis carried out in Section 4.2 shows, in the neighborhood of this family $\{\gamma_J\}_{J\in[J_-,J_+]}$, the perturbation $\mu e_0 \Delta H_{\text{ell}}(L, \ell, G, \hat{g} - t, t, \mu, e_0)$ can be averaged out to $\mathcal{O}(\mu e_0^6)$. Thus, invariant cylinders could persist even for not very small e_0's. However, estimating remainders analytically after several steps of averaging is nearly impossible. Numerically though it might be feasible.

Once the existence of an invariant cylinder is established, we need to justify the existence of transverse intersections of its manifolds. As before, analytically it is an insurmountable task, but numerically it seems to be an achievable goal.

If these two steps are done, then one could try to compute numerically inner and outer maps and show that they do not have common invariant curves. This is again a difficult, but numerically realistic task (see [DMR08] for the computation of the outer map in another problem in Celestial Mechanics).

On the other hand, the above asymptotics probably does not hold in the neighborhood of circular motions of the massless body, which might be much more stable than more eccentric motions. Yet many other factors might influence the local stability or instability of various objects (see section 1.2.3).

D.3 The Mather accelerating problem and its speed of diffusion

The structure we use to build diffusion is similar to the Mather acceleration problem. Let us recall this problem and state an interesting result of Piftankin [Pif06] on speed of diffusion.

Consider a Hamiltonian system

$$H(q, p, t) = K(q, p) + V(q, t), \qquad q \in \mathbb{T}^2, \qquad p \in \mathbb{R}^2, \qquad t \in \mathbb{T},$$

where $K(q, p) = \frac{1}{2}\langle A^{-1}(q)p, p\rangle$ — kinetic energy corresponding to a riemannian metric $K(q, p) = \frac{1}{2}\langle A^{-1}(q)p, p\rangle$, $p = A(q)\,\dot{q}$, $\dot{q} \in T_q\mathbb{T}^2$ and $V(q, t)$ is a time-periodic potential energy. Since the system is not autonomous energy is not conserved.

H1 Suppose the geodesic flow associated to K has a hyperbolic periodic orbit Γ and transversal intersection of its invariant manifolds, which contains a homoclinic orbit $\gamma(t)$, $t \in \mathbb{R}$.

H2 The Melnikov integral is not constant. More exactly, define a function

$$\mathcal{L}(t) = \lim_{T\to+\infty} \int_{-T}^{T} V(\gamma(t),t)\,dt - \int_{-T+t^u}^{T+t^s} V(\gamma(t),t)\,dt.$$

The limit turns out to exist and is independent of a choice of $t^s,\ t^u$. This function is assumed to be non-constant.

Mather and his followers [Mat96, BT99, DdlLS00, GT08, Kal03, Pif06] proved existence of an orbit $(q_\tau(t), p_\tau(t)),\ t \in \mathbb{R}$ of unbounded energy. de la Llave [dlL04], Piftankin [Pif06], and Gelfreich-Turaev [GT08] proved that such an orbit can be chosen to have linear growth of energy

$$H(q_\tau(t), p_\tau(t)) \geq At + B \qquad \text{for all} \qquad t \geq 0$$

for some $A > 0$ and $B \in \mathbb{R}$.

Notice that for large energies $H \sim \varepsilon^{-2}$ the conformal change of coordinates

$$\hat{p} = \frac{p}{\varepsilon}, \qquad H = \varepsilon^{-2}\hat{H}, \qquad t = \varepsilon\hat{t}$$

leads to the new Hamiltonian

$$\hat{H}(q,p,t) = K(q,p) + \varepsilon^2 V(q, \varepsilon\hat{t}).$$

It was shown in [dlL04, Pif06, GT08] that there are orbits diffusing linearly in the size of the perturbation. In order to see these orbits, notice that $K(q,p)$ has a horseshoe. Then, $\hat{H}$ can be considered as a time-periodic perturbation over such a horseshoe. It is shown by different methods in [dlL04, Pif06, GT08] that for a generic time-periodic perturbation of a horseshoe there are linearly diffusing orbits.

D.4 Modified positive measure conjecture

For systems with the properties discussed above we can modify the positive measure conjecture as follows:

Positive measure conjecture for Mather type systems *Consider the Hamiltonian*

$$H_{\mu,\varepsilon}(L,\ell,G,g,t) = H_0^*(L,G) + \mu\Delta H_0(L,\ell,G,g,\mu) + \mu e_0 \Delta H_1(L,\ell,G,g,t,\mu,e_0)$$

such that

- *for some interval $[J_-, J_+]$ the Hamiltonian $H_0^* + \mu\Delta H_0$ has a family of saddle periodic orbits $\{p_J\}_{J\in[J_-,J_+]}$,*
- *for each $J \in [J_- J_+]$ there is at least one transverse intersection of its invariant manifolds,*
- *A Melnikov integral evaluated along a transverse homoclinic and inner dynamics are non-degenerate: the dependence of the Melnikov integral on time is non-trivial and the relation between inner and outer maps is non-degenerate (see (9)).*

Pick a μe_0-ball of initial conditions $B_{\mu e_0}$ whose action components are centered at a resonance between ℓ and g. Denote the Lebesgue probability measure supported on the ball $B_{\mu e_0}$ by Leb. Then for some constants $c, C > 0$ independent of μ and e_0, the set of initial conditions satisfying

$$|G(T) - G(0)| > 1 \qquad \textit{for some} \qquad 0 < T < C\frac{|\ln \mu e_0|}{\mu^{5/2} e_0^2}$$

is denoted Diff and has measure Leb (Diff) $> c$.

Here is an important difference between the system H_{μ,e_0} and an priori unstable one H_ε, given by (106): the Hamiltonian $H_0^* + \mu\Delta H_0$ already has "chaos" and a family of horseshoes on each energy surface with $J \in [J_- J_+]$, while $H_0 = H_\varepsilon - \varepsilon H_1$ is integrable. As we pointed out above, for a generic time-periodic perturbation over a horseshoe there are orbits diffusing linearly fast [dlL04, Pif06, GT08]. Yet we are interested in a set of conditional positive measure.

In order to see the time of diffusion on an heuristic level, notice that $H_0^* + \mu\Delta H_0$ has a family of saddle periodic orbits $\{p_J\}_{J\in[J_-,J_+]}$ whose exponents are $\sim \sqrt{\mu}$. Thus, one homoclinic excursion passing μe_0-close to separatrices takes $|\ln \mu e_0|/\sqrt{\mu}$-time. Each excursion might lead to increment of G of size $\sim \mu e_0$. Conjecturing that random walk approximation holds true to have $\mathcal{O}(1)$-changes in G, we need $\mathcal{O}(\mu^{-2} e_0^{-2})$ excursions.

Acknowledgements

The authors acknowledge useful discussions with Abed Bounemoura, Marc Chaperon, Alain Chenciner, Anatole Katok, Àngel Jorba, Mark Levi, John Mather, Gennadi Piftankin, Philippe Robutel and Ke Zhang. P. R. acknowledges the assistance of À. Jorba with the "taylor" package (see `http://www.maia.ub.es/~angel/taylor`).

The authors warmly thank the Observatoire de Paris, the University of Maryland at College Park, the Pennsylvania State University, the Universitat Politecnica de Catalunya and the Fields Institute for their hospitality, stimulating atmosphere, and support.

J. F. has been partially supported by the French ANR (Projet ANR-07-BLAN-0361 Hamilton-Jacobi et théorie KAM faible), M. G. and P. R by the Spanish MCyT/FEDER grant MTM2009-06973 and the Catalan SGR grant 2009SGR859, and V. K. by NSF.

References

[AKN88] V.I. Arnold, V.V. Kozlov, and A.I. Neishtadt. *Dynamical Systems III*, volume 3 of *Encyclopaedia Math. Sci.* Springer, Berlin, 1988.

[Arn63] V. I. Arnold. Small denominators and problems of stability of motion in classical and celestial mechanics. *Uspehi Mat. Nauk*, 18(6 (114)):91–192, 1963.

[Arn64] V.I. Arnold. Instability of dynamical systems with several degrees of freedom. *Sov. Math. Doklady*, 5:581–585, 1964.

[Ber08] P. Bernard. The dynamics of pseudographs in convex Hamiltonian systems. *J. Amer. Math. Soc.*, 21(3):615–669, 2008.

[BKZ11] P. Bernard, V. Kaloshin, and K. Zhang. Arnold diffusion along normally hyperbolic cylinders. Preprint, 2011.

[Bol06] S. Bolotin. Symbolic dynamics of almost collision orbits and skew products of symplectic maps. *Nonlinearity*, 19(9):2041–2063, 2006.

[BT99] S. Bolotin and D. Treschev. Unbounded growth of energy in nonautonomous Hamiltonian systems. *Nonlinearity*, 12(2):365–388, 1999.

[CC07] A. Celletti and L. Chierchia. KAM stability and celestial mechanics. *Mem. Amer. Math. Soc.*, 187(878):viii+134, 2007.

[Cha04] M. Chaperon. Stable manifolds and the Perron-Irwin method. *Ergodic Theory Dynam. Systems*, 24(5):1359–1394, 2004.

[CY04] C.Q. Cheng and J. Yan. Existence of diffusion orbits in a priori unstable Hamiltonian systems. *J. Differential Geom.*, 67(3):457–517, 2004.

[DdlLS00] A. Delshams, R. de la Llave, and T.M. Seara. A geometric approach to the existence of orbits with unbounded energy in generic periodic perturbations by a potential of generic geodesic flows of $\mathbb{T}^2$. *Comm. Math. Phys.*, 209(2):353–392, 2000.

[DdlLS06] A. Delshams, R. de la Llave, and T.M. Seara. A geometric mechanism for diffusion in hamiltonian systems overcoming the large gap problem: heuristics and rigorous verification on a model. *Mem. Amer. Math. Soc.*, 2006.

[DdlLS08] A. Delshams, R. de la Llave, and T. M. Seara. Geometric properties of the scattering map of a normally hyperbolic invariant manifold. *Adv. Math.*, 217(3):1096–1153, 2008.

[DGR11] A. Delshams, M. Gidea, and P Roldán. Arnold's mechanism of diffusion in the spatial circular restricted three-body problem: A semi-numerical argument. Preprint, 2011.

[DH09] A. Delshams and G. Huguet. Geography of resonances and Arnold diffusion in a priori unstable Hamiltonian systems. *Nonlinearity*, 22(8):1997–2077, 2009.

[dlL04] R. de la Llave. Orbits of unbounded energy in perturbations of geodesic flows by periodic potentials. A simple construction. Preprint, 2004.

[DMR08] A. Delshams, J. Masdemont, and P. Roldán. Computing the scattering map in the spatial Hill's problem. *Discrete Contin. Dyn. Syst. Ser. B*, 10(2-3):455–483, 2008.

[DRR99] A. Delshams and R. Ramírez-Ros. Singular separatrix splitting and the Melnikov method: an experimental study. *Experiment. Math.*, 8(1):29–48, 1999.

[Féj02] J. Féjoz. Global secular dynamics in the planar three-body problem. *Celestial Mech. Dynam. Astronom.*, 84(2):159–195, 2002.

[Féj04] J. Féjoz. Démonstration du 'théorème d'Arnold' sur la stabilité du système planétaire (d'après Herman). *Ergodic Theory Dynam. Systems*, 24(5):1521–1582, 2004.

[Féj10] J. Féjoz. Periodic and quasi-periodic motions in the n-body problem. Mémoire d'habilitation, Université P. et M. Curie, 2010.

[Fen72] N. Fenichel. Persistence and smoothness of invariant manifolds for flows. *Indiana Univ. Math. J.*, 21:193–226, 1971/1972.

[Fen77] N. Fenichel. Asymptotic stability with rate conditions. II. *Indiana Univ. Math. J.*, 26(1):81–93, 1977.

[Fen74] N. Fenichel. Asymptotic stability with rate conditions. *Indiana Univ. Math. J.*, 23:1109–1137, 1973/74.

[FM00] E. Fontich and P. Martín. Differentiable invariant manifolds for partially hyperbolic tori and a lambda lemma. *Nonlinearity*, 13(5):1561–1593, 2000.

[FS90] E. Fontich and C. Simó. The splitting of separatrices for analytic diffeomorphisms. *Ergodic Theory Dynam. Systems*, 10(2):295–318, 1990.

[G$^+$] M. Galassi et al. *GNU Scientific Library Reference Manual*.

[GDF$^+$89] A. Giorgilli, A. Delshams, E. Fontich, L. Galgani, and C. Simó. Effective stability for a Hamiltonian system near an elliptic equilibrium point, with an application to the restricted three-body problem. *J. Differential Equations*, 77(1):167–198, 1989.

[GG85] A. Giorgilli and L. Galgani. Rigorous estimates for the series expansions of Hamiltonian perturbation theory. *Celestial Mech.*, 37(2):95–112, 1985.

[GS08] V. Gelfreich and C. Simó. High-precision computations of divergent asymptotic series and homoclinic phenomena. *Discrete Contin. Dyn. Syst. Ser. B*, 10(2-3):511–536, 2008.

[GT08] V. Gelfreich and D. Turaev. Unbounded energy growth in Hamiltonian systems with a slowly varying parameter. *Comm. Math. Phys.*, 283(3):769–794, 2008.

[Her83] M.R. Herman. *Sur les courbes invariantes par les difféomorphismes de l'anneau. Vol. 1*, volume 103 of *Astérisque*. Société Mathématique de France, Paris, 1983.

[Her98] M. Herman. Some open problems in dynamical systems. In *Proceedings of the International Congress of Mathematicians (Berlin, 1998)*, volume Extra Vol. II, pages 797–808 (electronic), 1998.

[Kal03] V. Kaloshin. Geometric proofs of Mather's connecting and accelerating theorems. In *Topics in dynamics and ergodic theory*, volume 310 of *London Math. Soc. Lecture Note Ser.*, pages 81–106. Cambridge Univ. Press, Cambridge, 2003.

[Kol57] A. N. Kolmogorov. Théorie générale des systèmes dynamiques et mécanique classique. In *Proceedings of the International Congress of Mathematicians, Amsterdam, 1954, Vol. 1*, pages 315–333. Erven P. Noordhoff N.V., Groningen, 1957.

[Lap89] P.-S. Laplace. Variations séculaires des orbites des planètes. *Mém. Acad. royale des sciences de Paris, année 1787*, Œuvres complètes, Tome XI:295–301, 1789. `http://gallica.bnf.fr/ark:/12148/bpt6k77599c/f300`.

[Las94] J. Laskar. Large scale chaos in the solar system. *Astron. Astrophys.*, 287, 1994.

[Las06] J. Laskar. *Sfogliando La 'Méchanique analitique'*, chapter Lagrange et la stabilité du système solaire. Edizioni Universitarie di Lettere Economia Diritto, 2006.

[Las10] J. Laskar. Le système solaire est-il stable ? In *Le Chaos*, number XIV in Séminaire Poincaré, pages 221–246. Birkhäuser, 2010.

[LM88] P. Lochak and C. Meunier. *Multiphase Averaging for Classical Systems*, volume 72 of *Appl. Math. Sci.* Springer, New York, 1988.

[Mat96] J. N. Mather. Manuscript. Unpublished, 1996.

[Mey75] K. R. Meyer. The implicit function theorem and analytic differential equations. In *Dynamical systems—Warwick 1974 (Proc. Sympos. Appl. Topology and Dynamical Systems, Univ. Warwick, Coventry, 1973/1974; presented to E. C. Zeeman on his fiftieth birthday)*, pages 191–208. Lecture Notes in Math., Vol. 468. Springer, Berlin, 1975.

[Moe96] R. Moeckel. Transition tori in the five-body problem. *J. Differential Equations*, 129(2):290–314, 1996.

[Mor02] A. Morbidelli. *Modern celestial mechanics: aspects of solar system dynamics*. Taylor and Francis, 2002.

[Nie96] L. Niederman. Stability over exponentially long times in the planetary problem. *Nonlinearity*, 9(6):1703–1751, 1996.

[NS04] A. I. Neishtadt and V. V. Sidorenko. Wisdom system: dynamics in the adiabatic approximation. *Celestial Mech. Dynam. Astronom.*, 90(3-4):307–330, 2004.

[Pif06] G. N. Piftankin. Diffusion speed in the Mather problem. *Nonlinearity*, 19(11):2617–2644, 2006.

[PT07] G. N. Piftankin and D. V. Treshchëv. Separatrix maps in Hamiltonian systems. *Uspekhi Mat. Nauk*, 62(2(374)):3–108, 2007.

[Rob05] P. Robutel. Frequency analysis and global dynamics of a planetary system. In D. Benest, editor, *Hamiltonian systems and Fourier analysis: new prospects for gravitational dynamics*, Advances in astronomy and astrophysics, pages 179–198. Cambridge Scientific Publishers, 2005.

[SM95] C. L. Siegel and J. K. Moser. *Lectures on celestial mechanics*. Classics in Mathematics. Springer-Verlag, Berlin, 1995.

[SW92] G. J. Sussman and J. Wisdom. Chaotic evolution of the solar system. *Science*, 257:56–62, 1992.

[Tre04] D. Treschev. Evolution of slow variables in a priori unstable hamiltonian systems. *Nonlinearity*, 17(5):1803–1841, 2004.

[Wis82] J. Wisdom. The origin of the Kirkwood gaps: a mapping for asteroidal motion near the 3/1 commensurability. *Astronom. J.*, 87(3):577–593, 1982.

[WZ03] D. Wilczak and P. Zgliczynski. Heteroclinic connections between periodic orbits in planar restricted circular three-body problem—a computer assisted proof. *Comm. Math. Phys.*, 234(1):37–75, 2003.

[Xue10] J. Xue. Continuous averaging proof of the nekhoroshev theorem with sharp stability constant c_2. Preprint, Penn State University, 43 pp, 2010.

[Zhe10] Y. Zheng. Arnold diffusion for a priori unstable systems and a five-body problem. Preprint, Penn State University, 51 pp, 2010.